Modelling of a Stand-alone Photovoltaic System with Dedicated Hybrid Battery Energy Storage System

Department of Electrical Engineering
University of Cape Town

Prepared by:

Nicholas Vanden Eynde

A thesis submitted to the Department of Electrical Engineering at the University of Cape Town, in fulfilment of the requirements for the degree of Masters of Science in Electrical Engineering.

March 2012.

Declaration

I declare that this dissertation is my own, unaided work. It is being submitted for the degree of Masters of Science in Electrical Engineering in the University of Cape Town. It has not been submitted before for any degree or examination in any other university.

Signature of Author . . . . . .

Cape Town
10 March 2012

Abstract

The purpose of this thesis project was to model and simulate a stand-alone photovoltaic (PV) plant that utilized the maximum power point tracking (MPPT) technique and included a hybrid battery energy storage system (BESS). The model consisted of five main components namely; the photovoltaic module, maximum power point tracking technique, hybrid battery energy storage system, controller and load. The thesis project had five major sections to be conducted:

- To develop a model for the stand-alone photovoltaic system
- To develop a model for the hybrid battery energy storage system
- Implement the model in Matlab
- Obtain results and validations for the model components
- Draw conclusions and recommendations for improvements

The stand-alone system consisting of the photovoltaic and battery module was constructed in Matlab using m-file's. Each component was designed and modelled to form a library in the simulation software.

The model was tested and validated to the results. DC load studies were conducted using the simulated model of the stand-alone system and results were obtained. The results were then analysed and conclusions were drawn. Recommendations based on the conclusions were made concerning future improvements to the system.

Terms of Reference

This thesis project, “Modelling of a stand-alone photovoltaic system with dedicated hybrid battery energy storage system“, was initiated by Prof. S.P Chowdhury, of the department of electrical engineering at the University of Cape Town.

The World Bank estimated that approximately 40 percent of the world’s population live in areas not supplied by a utility grid. The task of connecting these areas to the national grid by adding additional transmission lines is both an expensive and difficult undertaking. It was decided that the most feasible solutions to this problem would be to supply these areas with their own independent source of power.

The stand-alone system would be ideal for a situation like this as it is capable of providing power over 24 hours.

As a result, Prof. S.P Chowdhury has recommended that the research for the project focuses on the following points:

- To perform a comprehensive literature review on the subject matter
- To develop a concept stand-alone system comprising of the PV and BESS module
- To develop a model for the proposed stand-alone system
- To computer-simulate the stand-alone system
- To conduct load studies on the stand-alone system
- To draw conclusions and make recommendations for improvements

Acknowledgements

I would like to thank the following people for assisting and supporting me through me thesis project and undergraduate degree:

Dr. S. Chowdhury and Dr. S. P Chowdhury, the supervisor of my thesis for their guidance and assistance throughout my thesis project as well as giving me the opportunity to do all of this.

My family whose continuing love and support made this all possible for me.

My girlfriend, Tarryn Clarke, for her love and understanding throughout my degree.

God for His love and care without which none of this would have been possible.

Contents

List of Figures

Nomenclature

BESS – Battery Energy Storage System

CC – Constant Current

CC-CV – Constant Current – Constant Voltage

CV – Constant Voltage

CVT – Constant Voltage Tracking

DOD – Depth of Discharge

E – Irradiance

IncCond – Incremental Conductance

KiBaM – Kinetic Battery Model

MPP – Maximum Power Point

MPPT – Maximum Power Point Tracking

P&O – Perturb-and-observe

PV – Photovoltaic

SOC – State of Discharge

T – Temperature

1 Introduction

1.1 *Subject of the thesis*

The subject of the thesis was an investigation of a stand-alone photovoltaic (PV) system with a dedicated hybrid battery energy storage system (BESS). The investigation required that the PV system as well as the BESS were to be modelled and simulated to form the basis of a concept stand-alone system. A mathematical model for a polycrystalline PV plant would need to be developed and incorporated together with an effective maximum power point tracking (MPPT) technique. A model of the hybrid battery energy storage system (BESS) for three different battery chemistries, namely lithium-ion, nickel-cadmium and lead-acid, and a super-capacitor was also needed for the complete model. The DC PV system and BESS need to be modelled against a realistic load form. The performance of the stand-alone system would be simulated and recommendations for further study made.

1.2 *Background*

Photovoltaic and renewable energies are growing at a much faster pace than the rest of the economy in Europe and the rest of the world. In [3] it was noted that the photovoltaic world market has grown tremendously by 58.5% in 2004 alone. This and the dramatic oil price increases in 2005 have led to a remarkable re-evaluation of the renewable energy sector by politics and financing institutions. [3]

Almost half of this growth was due to the exorbitant growth of the market in Germany who has increased their installed solar system capacity from 153MW in 2003 to 363MW in 2004. The new Feed-in Law has been said to be the main driver of this growth with the European PV production growing by 50% and Europe becoming a net importer of photovoltaic again. Spain and Austria have also doubled their installed PV power whereas Luxembourg propelled itself to World Champion and leads statistics in terms of installed PV per capita. [3]

Photovoltaic systems have become widespread in Korea [4]; this is due to government policies for renewable energy sources which include a very large photovoltaic house dissemination project by 2012 which will involve over one hundred thousand households.

Most of the small villages of southern Morocco [5] are not yet connected to the conventional electric network. Construction of autonomous photovoltaic systems will be a good solution

to supple electric power to these isolated villages. The Iberoamerica-Europe Foundation (CIPIE) and ISOFOTON S.A. have carried out work in the development of a photovoltaic system to be implemented in this region. Many rewards have already been achieved by the objectives reached. These can be summarized into technological development of photovoltaic energy, social improvement for poor rural zones and international cooperation between Spain and developing countries.

With this rapid growth and interest in renewable energies both in Africa and the rest of the world, the development of stand-alone Photovoltaic system are becoming a must.

1.3 *Objectives of thesis*

The aim of this thesis is to model and simulate the stand-alone system using Matlab. An MPPT technique must be implemented in order to provide the load with the maximum power and corresponding voltage and current. A hybrid battery energy storage system (BESS) must also be modelled and simulated and the two power sources must be controlled by a controller. A simulated load will enable load studies to be done.

1.3.1 Find and model the most applicable model for a PV cell

Various PV cell models must be critically reviewed in order to determine the most suitable model for the stand-alone system. The mathematical model must then be simulated in Matlab as a component of the combined system.

1.3.2 Implement an effective MPPT technique

An effective MPPT technique must be applied to the PV module in order to produce the maximum power output for various values of irradiance and temperature.

1.3.3 Find and model a suitable hybrid BESS

A battery source must be incorporated with the PV module in order for the system to provide power in conditions of zero irradiance, allowing the system to provide power over 24 hours. The battery will also absorb excess power from the PV module and provide power to the load when the PV is unavailable or the load demand is more than the PV power provided. Different battery chemistries must be investigated for the use in the BESS as well as a suitable super-capacitor.

1.3.4 Design and implement a controller

The controller will be used to manage the power flow of the system by comparing the power required for the load and BESS charging and the power provided by the PV and the BESS

discharging. The controller will control when the BESS is charged by the PV and discharged to the load. A suitable controller algorithm must be designed and implemented.

1.3.5 Conduct load studies on a realistic load form

A load that is realistic in terms of a small rural community must be modelled in order for load studies to be conducted

1.4 *Scope and limitations of thesis*

This thesis investigates the characteristics and performance of a stand-alone PV system with hybrid battery energy storage system (BESS), with respect to varying environmental conditions. It was required to design and simulate the system in order to perform load studies.

In this thesis, rapidly changing solar irradiations and temperatures were not considered and the BESS was assumed to be housed at a controlled, constant temperature. The actual temperature of the system was not accounted for. Consideration was not given to completely minimise the error in every component due to the limited time available.

Due to the expenses of solar panels and BESS batteries, they could not be provided to obtain test data and results from.

1.5 *Plan of development*

A short description of the various sections and stages of this thesis is as follows:

1.5.1 Literature review

A literature review of reviewed theories and existing methods that are applicable to this thesis are presented in this section. Different methods derived for problems encountered as well as various techniques are discussed. The advantages and disadvantages of the findings are stated.

1.5.2 System design

In this section, mathematical models provided for the various components along with specific designs for each component in the stand-alone PV system with hybrid BESS in order to understand the workings and capabilities of the stand-alone system.

1.5.3 Simulation in Matlab

The components designed in the previous section are implemented Matlab in this section. Detailed diagrams and descriptions of the simulation structures are included.

1.5.4 Analysis of results and model validation

Results from the simulations are displayed and analysed, and the models are validated to the theory.

1.5.5 Conclusions

Based on the results obtained, conclusions are drawn. Limitations in the designs and simulations are discussed.

1.5.6 Recommendations

Recommendations are provided and they are based on the limitations discussed in the conclusions.

1.6 *Methodology*

Findings of studies conducted into stand-alone photovoltaic systems and hybrid battery energy storage system (BESS) and published papers, textbooks, conference papers and manufacturer's data were used as the theoretical information. The theoretical information was used to form the basis of understanding needed to conduct the thesis project while the findings of studies were used in order for designs and models.

A model for the components of the stand-alone photovoltaic system were developed and simulated in Matlab. The simulation was done by modelling each component in an m-file and then incorporated together to form the complete system. Results from the simulations were acquired and analysed and conclusions about the performance and viability the stand-alone photovoltaic system with hybrid battery energy storage system (BESS) were drawn. Recommendations based on the conclusions were then made on possible future improvements ion bettering the system.

2 Literature Review

2.1 *Introduction*

Solar energy is a clean, maintenance-free and abundant source of energy. The increased interest in environmental issues as well as the rapid trend of industrialization of nations has recently led to the consideration of the use of renewable energy forms such as solar power. The many advantages that photovoltaic (PV) generation possesses are rendering it increasingly important as a renewable source. These advantages include amongst others no fuel costs, a lack of pollution, little maintenance, and no emission of noise. [1]

Photovoltaic (PV) systems directly convert sunlight into electricity. The basic device of the PV system is the PV cell which may be grouped together to form panels or arrays. The current and voltage available at the terminals of the PV device can be used to directly feed small loads such as lighting systems and DC motors. Electronic controllers that are used to process the electricity from the PV device are required in more sophisticated applications. The controllers may be used to regulate both the current and the voltage at the load, in order to control power flow in the grid-connected systems, but is mainly used to track the maximum power point (MPP) of the device. This process of tracking the maximum power point is known as maximum power point tracking (MPPT) [2]. The following diagram Figure 1 shows a basic setup of a photovoltaic system.

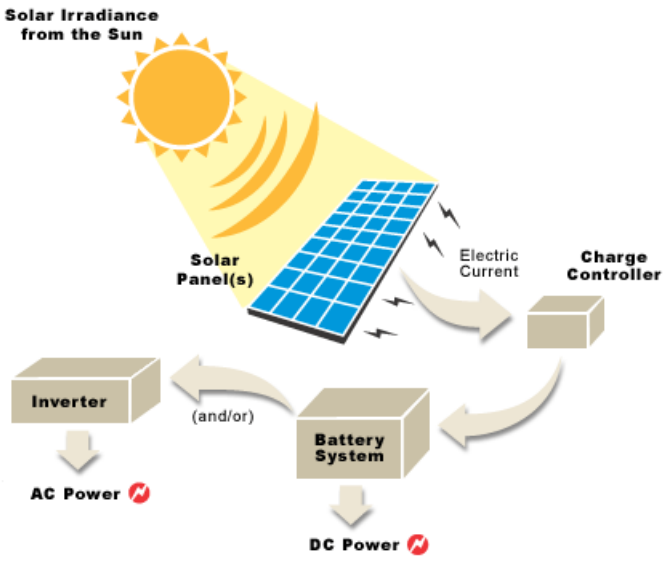

Figure 1: A simple photovoltaic system [19]

2.2 *Photovoltaic (PV) system*

2.2.1 How a PV cell works

A photovoltaic cell is a semiconductor whose P-N junction is exposed to light. These cells are made of several different types of semiconductors each using a different manufacturing process. The more popular monocrystalline and polycrystalline silicon cells can only be found at commercial scale at the present time. The silicon photovoltaic cells are made of either a thin silicon film or a thin layer of bulk silicon, which is then connected to the terminals. Doping of one of the sides of the silicon layer is important in order to form the P-N junction. Once the P-N junction is formed, a thin metallic grid is placed on the sun-facing surface of the semiconductor. The following diagram Figure 2 shows the physical structure of a PV cell. [2]

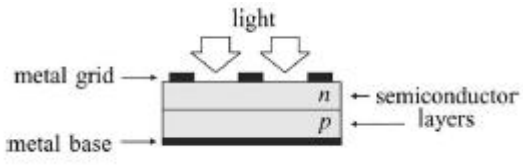

Figure 2: Physical structure of a photovoltaic cell [20]

In [2], it was explained that the incidence of light on the cell generates charge carriers, which can produce a current if the cell is short-circuited. The charges are generated when the incident solar photon is able to overcome the energy of the covalent bonds possessed by the electron and the semiconductor and detach the electrons from the semiconductor. This is highly dependent on the material of the semiconductor used and the wavelength of the incident light. This can basically be described as the absorption of solar radiation, the generation and transportation of free carriers at the P-N junction and the collection of these electric charges at the terminals of the photovoltaic device.

The rate at which the electric charge carriers can be generated is dependent on the absorption capacity of the semiconductor as well as the flux of the incident light. The absorption capacity mainly depends on the semiconductor's band gap, the shape and treatment of the surface, the temperature and several other factors.

Solar irradiation consists of photons which have different energies. If the energy possessed by the photon is less than that of the energy required to overcome the band gap of the PV cell, no voltage or current will be generated. However, if the energy of the photon is greater than the energy required to overcome the band gap, electricity will be generated.

Semiconductor materials that can achieve better conversion efficiency then silicon are available but this comes at higher and commercially unfeasible costs. Silicon therefore is the only one whose fabrication process is economically feasible in large scale. [2]

2.2.2 Factors affecting the model

Temperature

Temperature has an effect on the output of a photovoltaic cell. By increasing the temperature at high voltages the voltage may be susceptible to drop. Operating the cell in this high-voltage high-temperature region of the curve will lead to significant power reductions in the output. This is a particularly severe problem since the cell is mainly operated at its maximum power point, which falls into this region. The effect of temperature on short-circuit current is small but increases with irradiance growth. The following graph Figure 3 displays the effects of temperature on the I-V curve. [6]

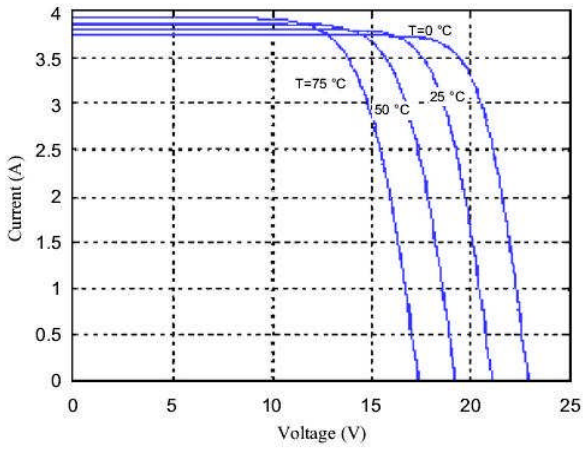

Figure 3: Effect of temperature on the I-V curve [4]

Solar irradiation

The intensity as well as spectral distribution of the solar radiation experienced will be a factor of geographic position, time day of the year, climate conditions, composition of the atmosphere, altitude, and several other factors. The AM 1.5 spectral distributions, which is used as the industry standard in photovoltaic systems, are only average estimates that serve as references for the evaluation and comparison of the photovoltaic device. This is due to the factors influencing solar radiation. [2]

In [6], they noted that the solar irradiance has a large effect on the short-circuit current, which can be thought of as the relatively horizontal arm of the I-V curve, while the effect on the open-circuit voltage, i.e. the relatively vertical arm of the I-V curve, is rather weak.

Regarding the maximum power output (MPP) of the photovoltaic cell, it is clear that when the irradiance is higher, the cell generates more power. The following graph Figure 4 demonstrates the effects of irradiance on the I-V curve.

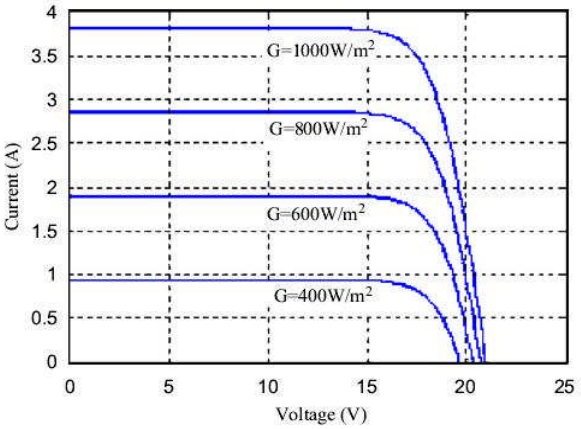

Figure 4: Effects of irradiance on the I-V curve [4]

Series and parallel resistances

The practical photovoltaic device has a series resistance R_s whose influence is stronger when the device operates in the voltage source region while the parallel resistance R_p is has a stronger influence in the current source region. The series resistance is a sum of the structural resistances of the device [2], which are shown in Figure 2. The I-V characteristics of the photovoltaic device depend on the internal characteristics of the device such as the series and parallel resistances and also the external influences such as irradiation level and temperature.

The series resistance basically depends on the contact resistance of the metal base with the p semiconductor layer, the resistances of the p and n bodies, the contact resistance of the n layer with the top metal grid, as well as the resistance of the grid. The value of the series resistance is very low and is sometimes neglected to simplify the model.

The parallel resistance exists mainly due to the leakage current of the p-n junction and depends on the fabrication method of the photovoltaic cell. The value of the parallel resistance is generally high and some authors choose to neglect this resistance in order to simplify the model, as stated in [2].

In [6], they found that the series resistance term proved to be an important parameter, especially for irradiances and cell temperatures far from the reference conditions. Given the same set of reference conditions, each I-V model traces I-V curves that are very similar, but only near the reference conditions. Away from the reference conditions, I-V models,

including a series resistance term, describe I-V curves that are quite different than the curves described by those neglecting this term. Over a full range of operating conditions, such as in an annual simulation, the predicted output (for maximum power tracked systems), when series resistance is neglected ranges from 5% to 8% lower than if the "correct" series resistance is used.

Diode saturation currents

The diode saturation currents of the photovoltaic cells that compose the device depend on the saturation current density of the semiconductor and on the effective area of the cells. The current density depends on the intrinsic characteristics of the photovoltaic cell, which in turn depend on several physical parameters such as the coefficient of diffusion of electrons in the semiconductor, the lifetime of minority carriers, the intrinsic carrier density and so on. This kind of information is not normally available for commercial photovoltaic arrays and is therefore indirectly obtained from experimental data which is obtained by evaluating the model at the nominal open circuit conditions.

Diode constant

The value of the diode constant may be arbitrarily chosen. Many authors [2] and [7] discuss ways to estimate the correct value of this constant and usually ranges between 1 and 2 depending on the parameters of the I-V model. Some values are found on empirical analyses. Due to diode constant expressing the degree of ideality of the diode, it is totally empirical and any initial value can be altered in order to adjust the model and improve the model fitting. This constant affects the curvature of the I-V curve and varying the constant can slightly improve the model accuracy.

2.2.3 Models of stand-alone photovoltaic devices

Photovoltaic cell

The performance of a solar photovoltaic cell or array is strongly dependent on operating conditions and field factors, such as the geometric location and irradiation levels of the sun and the ambient temperature [8]. Each individual array comprises of a matrix of cells interconnected in series and parallel. However, the performance of the array greatly depends on the behaviour of each individual solar cell

The circuit equivalent of the photovoltaic cell can be modelled through the following circuits shown in Figures 5, 6, 7 and 8. The PV cell can be modelled by the light generated source

I_{ph}. The photocurrent I_{ph} generated in the PV cell is proportional to the level of solar illumination. The intrinsic p-n junction characteristics are modelled as a diode in the equivalent circuit. Current I is the output current of the photovoltaic cell while the current I_d through the bypass diode varies with the junction voltage as well as the reverse saturation currents I_s. The voltage V is the output of the photovoltaic cell while R_p and R_s are the parallel and series resistances, respectively. [1]

Many authors [2], [9], [10] and [11] have proposed numerous sophisticated models for photovoltaic cells which represent various levels of accuracy and serve different purposes. The single diode model is a very popular way of modelling the cell due to it offering a good compromise between accuracy and simplicity. An extra diode is added in the Double Exponential Model [10] and is used to represent the effect of the recombination of carriers. A three-diode model has been proposed in [11] to include the influence of effects that are not considered by the previous models. Keating and Enebish et al in [10] developed an analytical approach using iteration and curve fitting using a very limited number of points. We shall examine some of the models proposed for single diode and double diode photovoltaic cell models.

Single diode model

A model was proposed in [9] that consisted of a single diode as the model for the photovoltaic cell. It is also known as the ideal model for a PV cell. The PV array used in this model consisted of 72 cells in series. The model neglected the series and parallel resistances. A change in irradiance will cause a change in the operating temperature but due to this change being much slower than the other effects considered, it was not considered explicitly in the proposed model.

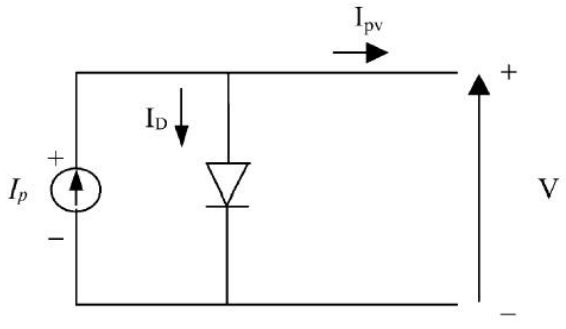

Figure 5: Single diode model [9]

The overall volt-ampere characteristics of the model are given by the following equation

$$I_{pv} = I_p - I_D - N_p I_{sc}\left(\frac{I_r}{100}\right) - N_p I_0\left[e^{\left(\frac{qV_{pv}}{akTN_s}\right)} - 1\right] \quad (1)$$

The model used algebraic and differential equations to express the relationship between variables. It was capable of representing the system's response to both small and large changes in irradiance and ac grid voltage. However, the model was very simplistic resulting in a degradation of accuracy.

Single diode with series resistance model

Lorenzo [12] proposed a model that involved the one-diode model and a series resistance. The solar cell can be represented by an electrical equivalent one-diode model, as shown in Figure 6.

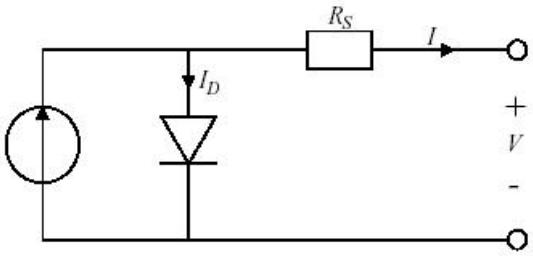

Figure 6: Single diode model with series resistance [6]

The model contains a current source I_{ph}, one diode and a series resistance R_s, which represents the resistance inside each cell and in the connection between the cells. The net current is the difference between the photocurrent I_{ph} and the normal diode current I_d.

$$I_{pv} = I_{ph} - I_0\left[e^{\left(\frac{q(V+IR_s)}{mkT_c}\right)} - 1\right] \quad (2)$$

The model [7] takes into account the idealising factor m, the Boltzmann's gas constant k, the absolute temperature T_c, the electronic charge q and the voltage V imposed across the cell. The dark saturation current is strongly dependent on the temperature.

The model reflects properly the influence of the irradiation and of the cell temperature on the I-V characteristics of the PV module [12]. This model must be cautiously used for the case of extremely high irradiation, high ambient temperature and high operating temperature. It was noted to be more accurate than the one diode model omitting the series resistance in [9].

Single diode with series and parallel resistance

In [2], a model consisting of one diode and parallel and series resistances was proposed. The circuit equivalent shows the ideal model of a PV cell in Figure 7a, and this was said to not properly represent the I-V characteristics of a practical PV array. Practical arrays are composed of several connected PV cells and the observation of the characteristics at the terminals of the PV array requires the inclusion of additional parameters to the basic equation. Hence, the addition of the parallel R_p and series R_s resistances into the array which are seen in Figure 7b.

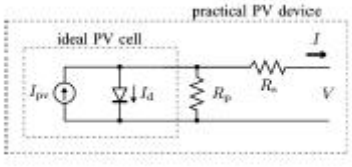

Figure 7: Model for the ideal PV cell (a) and for the containing series and parallel resistances (b) [7]

The circuit equivalent can be represented by the following algebraic difference equation.

$$I_{pv} = I_{ph} - I_0\left[e^{\left(\frac{V+IR_s}{vtA}\right)} - 1\right] - \frac{V + IR_s}{R_p} \qquad (3)$$

The equation (3) displays the relationship of the output current at the terminals I with the photocurrents I_{ph} and the saturation currents I_o of the array. An equation to express the dependence of the diode saturation current on the temperature was proposed and used in the model. The thermal voltage of the array with N_s cells connected in series is introduced as vt, where $vt = N_s kT/q$. This includes Boltzmann's constant k, the temperature T and the electrical charge q.

This model offers a good comprise between simplicity and accuracy and has been used by several authors in previous works [2]. The addition of the parallel and series resistances has increases the accuracy of the model and has made sure that the maximum power of the model is equal to the maximum power of the practical array.

Double exponential model

J.A Gow and C.D Manning [10] sought to develop a cheap, but effective system to characterize existing cells and generate the device-dependent data that provides the link between the environmental variables irradiance and temperature, and the electrical characteristics of the device. This was due to the majority of PV models that have been

developed are either those of complete systems, or are the model of a specific system. Bosch et al [13] described a complete modelling tool to aid the design of PV plants; this however is not a universal electrical simulation model of a PV array. Figure 8 displays the circuit equivalent of the double exponential model.

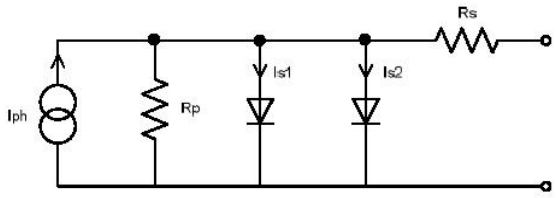

Figure 8: The double exponential model [17]

The electrical characteristics of a polycrystalline PV cell are given by the familiar double-exponential model,

$$I = I_{ph} - I_{s1}\left[e^{\left(\frac{V+IR_s}{vt}\right)} - 1\right] - I_{s2}\left[e^{\left(\frac{V+IR_s}{Avt}\right)}\right] - \frac{V+IR_s}{R_p} \qquad (4)$$

This model takes into account the photocurrent I_{ph}, the saturation currents of the two diode terms I_{s1} and I_{s2} as well as the series and parallel resistance R_s and R_p, respectively. These are known as the five parameters of the model. The Boltzmann's constant k, the temperature T and the electrical charge q are present in vt where $vt = kT/q$.

The equation (4) clearly shows that the electrical characteristics are dependent upon the values of the five parameters. These parameters are, in turn, dependent on the two environmental variables solar irradiance E and absolute temperature T. This model further went to relate the five parameters to the two environmental variables E and T.

So far, this model has been used to considerable success in the development of an advance photovoltaic converter system. The model is able to characterise any polycrystalline cell as all cells will possess the same device physics. It has been noted to be the more accurate than any of the one-diode models and has been found to be robust, efficient and of low computational burden. The results from [17] have clearly shown that this model can be well utilised for detailed load performance analysis of PV arrays as well as for representing PV-based DER's for studying the performances of distributed power systems and micro-grids with hybrid types of sources. The model has been vindicated by researchers too numerous to cite and is accepted as valid for all examples of polycrystalline cells. [10]

2.3 *Battery energy storage system (BESS)*

The BESS is an important part of the stand-alone photovoltaic system. The BESS stores energy at lower demand and sends saved energy back to the system during peak load. It thus represents a good solution for daily load levelling [21]. It is necessary in such a system due to the fluctuating nature of the output delivered by the photovoltaic arrays. During night-time, or a period of low solar irradiation, energy is supplied to the load from the battery.

Under the electricity market conditions, it is found that the viability assessment of an investment in BESS is much more complex, especially with respect to load levelling. At this stage, it is important to point out the other possibilities of battery system usage and related savings, in particular for solving different problems in utility and industry distribution systems, as well as in railway supply [21].

A number of models have been proposed by authors such as Facinelli, Hyman et al [14] and Manwell and McGowan [7]. Most of these models have been defined as phenomenological which means they are based on observable quantities such as voltage , current and time and therefore do not depend on the internal structure of the system such as the model proposed by Manwell et al. Other models have been noted to be based on the physical or electrochemical processes.

2.3.1 General characteristics and applications of secondary batteries

It is stated in [26] that secondary batteries, also known as rechargeable batteries, are found to be used in many applications. The most familiar being starting, lighting and ignition (SLI) automotive applications as well as emergency and standby power. Smaller secondary batteries are being used in increasing numbers to power portable devices such as toys, lighting and consumer electronic devices. Secondary batteries have more recently received renewed interest as power sources for electrical and hybrid electric vehicles. This has led to the initiating of programs aimed towards improving performance of existing battery systems and developing new systems to meet the stringent specifications of these new applications.

There are found to be two major categories for the use of secondary batteries:

1. Applications where the battery is used as an energy storage device. This application results in the battery being charged by a prime energy source and delivering its energy to the load demand when the prime energy source is not available or

adequate to handle the load requirements. Examples of this application include automotive and aircraft systems and standby power sources.

2. Applications where the battery is discharged similarly to that of the primary battery and recharged after use, either in the equipment it was discharged or separately. This application yields the benefit of convenience and cost saving and also for power drains beyond the capability of primary batteries. Most consumer electronics and electric-vehicle applications fall into this category.

2.3.2 History of secondary batteries

Secondary batteries have been used in applications for over 100 years with the lead-acid battery being first developed in 1859 by Plante' [26]. Lead-acid is still found to be the most widely used battery chemistry and has experienced many design changes and improvements. The automotive SLI battery is by far the most dominant one.

The nickel-iron alkaline battery was introduced by Edison in 1908 and was used as power source for early electric automobile. Its advantages included durability and long life but lost most of its market share over time due to high costs, maintenance requirements and lower specific energy.

In 1909 the pocket-plate nickel-cadmium chemistry was introduced and primarily used for heavy-duty industrial applications while, during the 1950's the sintered-plate design led to increased power capacity and energy density. The development of the sealed nickel-cadmium battery led to its widespread use in portable and other applications. The specific energy and energy density of rechargeable nickel-cadmium batteries have not made any significant improvements in the past decade and are now being surpassed initially by nickel-metal hydride and more recently the lithium-ion battery which are capable of exhibiting higher specific energy and energy density [26].

2.3.3 Battery chemistry types

A few battery chemistries have been investigated in the following section. The table below displays a summary of characteristics of a number of battery chemistries.

Table 1: Summary of battery technologies used in PV battery systems [29]

Table 1
Description of the batteries used in the PV-battery system

Technology	Abbreviation	Model	Description	Positive electrode or catholyte	Electrolyte	Negative electrode or anolyte
Li-ion	Li-ion	SAFT Li-ion VL 50 E Mixed oxide: LiNi0.8(Co+M) 0.2 O_2[a]	Cylindrical, sealed maintenance free cells	$Li_{1-x}MeO_2$/ $LiMeO_2$[a]	PC, $LiPF_6$	Li_xC/C
Sodium–sulphur	NaS	NGK-TEPCO E50 module, 50 kW, 430 kWh/module	384 T5 cells (8 serial × 6 parallel) × 8 serial, 128 V	xS/S_x^{2-} $(x = 5 - 3)$	β-Al_2O_3	Na/Na^+
Nickel–cadmium	NiCd	SAFT Sunica.plus 1110	Pocket plate, thick electrodes, felt-isolated, vented, flooded electrolyte	$NiOOH/Ni(OH)_2$	20% KOH (1.2 kg/dm^3)	$Cd/Cd(OH)_2$
Nickel–metal hydride	NiMH	SAFT NH12.3, 12 V module	EV battery plates, foam electrodes, sealed maintenance free	$NiOOH/Ni(OH)_2$	KOH	MmH/Mm[b]
Lead–acid	PbA	Tudor Exide 16OGi 1260	Vented, pasted flat plates, flooded electrolyte[c]	$PbO_2/PbSO_4$	1.3 kg/dm^3 H_2SO_4	$Pb/PbSO_4$
Polysulfide-bromide	PSB	Regenesys	Redox flow	$NaBr_3$(aq)/ 3 NaBr(aq)	H_2SO_4	2 Na_2S_2(aq)/ Na_2S_4(aq)
Vanadium	VRB	Sumitomo Electric Industries	Redox flow, 4 stacks × 80 cells (serial)	$VO_2^+(aq)/VO^{2+}(aq)$	1.8 M V in 4.2 M H_2SO_4	$V^{2+}(aq)/V^{3+}(aq)$
Zinc–bromine	ZnBr	ZBB research	Redox flow	$Br_2(aq)/2\ Br^-(aq)$	2.25 M $ZnBr_2$	$Zn/Zn^{2+}(aq)$

Lithium-Ion

It is noted in [26] that lithium-ion batteries have captured over half of the sales value of the secondary consumer market in the last decade. The “Three-C” market for laptop computers; cell phones and camcorders are found to be major applications of lithium-ion batteries.

These cells are found to provide high energy density and specific energy as well as long cycle life, typically greater than 1000 cycles at 80% depth of discharge and operate in a broad temperature range. It is stated in [25] that lithium-ion batteries are suitable as BESS because of these properties. Moreover, they have the advantage of being low maintenance batteries, a property most chemistries can’t claim. They also experience no memory effect and no scheduled cycling is required to prolong the battery’s life. The self-discharge rate is also found to be less than half that when compared to nickel-cadmium.

Nickel-Cadmium

The nickel-cadmium chemistry is found to be the most popular alkaline secondary battery and is available in a number of cell designs and in a wide range of sizes. The original cell design was that of the pocket-plate construction [26].

The vented pocket-plate cells are found to be very rugged and can withstand both mechanical and electrical abuse. They have very long life cycles and require little maintenance. This type of battery is used in heavy-duty industrial applications such as emergency or standby power.

The sintered-plate construction is a more recent development than the pocket-plate construction and has higher energy density. The performance at high temperatures and low temperatures, albeit more expensive, is better than that of the pocket-plate. This construction is used in aircraft engine starting and communications and electronics equipment. This is due to their lighter weight and superior performance characteristics.

The sealed cell uses an oxygen-recombination feature similar to that of the sealed lead-acid batteries which prevents the build-up of pressure cause by gassing during charge. The sealed cells are available in a variety of shapes and sizes and are predominantly used in consumer and small industrial applications [26].

Lead-acid

The lead-acid battery is found to have a number of advantages such as the charge-discharge process being essentially reversible, the system not suffering from deleterious chemical action. Although the lead-acid exhibits low specific energy and energy density, they are found to perform reliably over a wide range of temperatures. It's low cost and good performance as well as cycle life are the key factors for its popularity and dominant position.

Lead-acid batteries have many different configurations such as the small sealed cells having a capacity of 1Ah to large cells with capacity of 12 000Ah [26]. Automotive SLI batteries are by far the most popular and in the widest use. The most significant advancement in the SLI battery design include using lighter-weight plastic containers, the improvement in shelf life, the dry-charge process and the maintenance-free design.

Lead-acid industrial storage devices are generally larger than the SLI batteries and exhibit a stronger, higher quality construction. The valve-regulated lead-acid battery (VRLA) is found to be an important development which operates on the principle of oxygen recombination, using an immobilized or "starved" electrolyte.

Smaller sealed lead-acid batteries are used in emergency lighting and devices requiring back up power in the event of a utility power failure and various consumer-type applications. Two configurations are available namely prismatic cells with parallel plates with a capacity ranging from 1 to 30Ah and cylindrical cells which are similar in appearance to the alkaline cells and range up to 25Ah capacity.

New applications, to take advantage of the cost effectiveness of this battery, include load levelling for utilities and solar photovoltaic systems. Improvements in the energy and power density properties are required for these applications.

2.3.4 BESS models

Several battery models have been proposed for use in computer simulation. [27] Proposed that the major issues in generating an appropriate and feasible battery model are due to complex inter-related battery electrical parameters exhibited by the battery. These need to be considered together for accuracy in modelling. The challenge presented is obtaining a not-too-complex battery model but is still able to depict the battery terminal voltage and the internal resistances which are seen as a function of several inter-related variables such as the battery state of charge (SOC).

Kinetic battery model (KiBaM)

The Kinetic Battery Model (KiBaM) was developed at the University of Massachusetts in order to predict the performance of the battery and was based on the manufacturer's data and the published papers of Manwell & McGowan [14]. The main aim of the KiBaM model is to represent the sensitivity of storage capacity to the rate of discharge; no extensive measurements of voltage or current are required.

The model developed in [14] composed of two major parts describing:

1. Capacity Model
2. Voltage Model

The basis of the capacity model is the assumption that some of the capacity in the battery is immediately available for the load, while the rest is chemically bound. The model is characterised by the constants k, c and q_{max}. In order to simplify the equations obtained in [7], it was assumed that in both charging and discharging, the same constants were applied.

The voltage model proposed in [7] provides the magnitude of the terminal voltage, as affected by charging and discharging to different depths at different current rates. The voltage model was able to predict that the battery voltage drops slowly and linearly during the first part of the discharge and rapidly at the end, when the battery is nearly empty. The model was characterised.

Universal lithium-ion model

The authors in [22] proposed a universal modelling and simulation approach for rechargeable lithium batteries as a practical method to conduct battery pack simulations from accurate cell models that can account for cell imbalance. The model was based on an equivalent circuit technique commonly used in electrochemical impedance characterizations and used parameters deduced directly from cell testing.

The modelling approach was said to be simple yet practical as it allows accurate prediction of battery performance using data collected in the laboratory at present time, but with an expectation that it will be performed in the future with in-line cell monitoring. Attention was paid to the analysis of rate and SOC dependence of the polarization resistance in individual cells; this was thought to be critical to an improved prediction at the pack level when intrinsic imbalance among cells is considered.

The model offered high fidelity simulation of the battery performance and was found to be a simple, general purpose but effective battery modelling approach.

Dynamic lithium-ion model in SIMPLORER

In [25], a lithium-ion battery model was devised using SIMPLORER simulation software. The model simulated the behaviour of the battery under dynamic conditions. A mathematical model of the battery was developed based on measured battery data. The model took the battery operating temperature and the rates of the battery charge/discharge current into account. The thermal characteristics of the battery where also considered.

It was found in [25] that the equilibrium potential of the battery was dependant on the temperature and the amount of active material available in the electrodes. The state of discharge (SOD) was able to specify this and it was found that in general, the discharge capacity of the battery is also dependant on the discharge current, temperature and lifecycle. This led the authors to seek a general expression for the potential *E* where *T(t)* represented the battery temperature, *i(t)* the discharge current and *l* the lifecycle of the lithium-ion battery.

The equilibrium potential *E* was modelled as follows:

$$E[i(t),T(t),t,l] = v[i(t),T(t),t,l] + R_{int}i_r(t) \quad (5)$$

$$v[i(t),T(t),t,l] = \sum c_k SOD^k[i(t),T(t),t,l] \quad (6)$$

$$SOD[i(t),T(t),t,l] = 1/Q\int i(t)dt \quad (7)$$

$$R_{int} = R_1 + R_2 \quad (8)$$

The model was formulated in a general sense, but specifically for use in the SIMPLORER simulation software. The method accounted for the current rate and the temperature dependence of the capacity and thermal dependence of the equilibrium potential. The

modelling procedure, which was based on experimental data, allowed the model to possess good accuracy and the flexibility to represent other battery types.

Dynamic lithium-ion model in VTB

The model proposed by [23] was found to be a complete dynamic model of a lithium-ion battery that is suitable for virtual-prototyping of portable battery-powered systems. It accounted for nonlinear equilibrium potentials, rate- and temperature-dependency, thermal effects and response to transient power demand.

The model was based on publicly available manufacturer's data obtained from data sheets and coded according to the resistive companion method, allowing systematic handling of nonlinearities in the model equations and easy connection to other objects in a system-level simulation.

The authors [23] attempted to replicate the electrical and thermal properties of the battery as it interacts with the external world. The equilibrium potential *E* was modelled as follows:

$$E[i(t),T(t),t] = v[i(t),T(t),t] - R_{int}i_r(t) \quad (9)$$

$$v[i(t),T(t),t] = \sum c_k SOD^k[i(t),T(t),t] + \Delta E(T) \quad (10)$$

$$SOD[i(t),T(t),t] = 1/Q_r \int \alpha[i(t)].\beta[T(t)].i(t)dt \quad (11)$$

The described model was found to be suitable for portable power systems. It was formulated in the general sense, but was coded specifically for use in the Virtual Test Bed (VTB) computational environment. The method consisted of a 4-step modelling procedure which accounted for rate- and temperature-dependency, thermal dependence of the equilibrium potential and transient response. The model primarily used simple representations for the potential loss and transient process modelling and was found to deviate from the experimental data at low temperatures and high discharge rates. The internal losses found were the result of many intricate processes.

Impedance based lithium-ion model

The work in [24] employs the method of electrochemical impedance spectroscope (EIS) to extend the physics-based, nonlinear equivalent circuit models of super-capacitors to describe lithium-ion batteries.

The authors in [24] where able to relate the impedance *Z* and current *I* to a potential *U* of the following form:

$$U = \int Z(I_{dc}) dI_{dc} \qquad (12)$$

It was stated that due to mass transport phenomena, dynamic battery performance during continuous discharging or charging of batteries differs significantly from that during dynamic micro-cycling with frequent changes between charging and discharging. As this is seen typical for many practical battery applications, the EIS on lithium-ion batteries was performed using a specific micro-cycle technique.

The nonlinear, lumped-element equivalent circuit model was found to meet the accuracy requirements for simulation models of energy storage devices. The model presented an "excellent" agreement of simulated and measured voltage data and was able to be employed to other storage technologies due to its versatility.

Capacity based lead-acid model

It is stated in [21] that the evaluation of the Ampere-hour capacity of the battery needed for load levelling during a period of several hours is of great importance when using BESS as an active power peaking station. The simulation model was developed for this purpose. The model takes into account the battery voltage dependency on the capacity and current, and is based on the performed battery measurements at constant discharging currents. The simulation was performed in the stability mode of the NETOMAC digital program system.

The model derived used a direct approach based on the interpolation among lead-acid battery characteristics obtained by measurements during the discharging process. The BESS and load model where represented as controllable impedances and the development of the BESS model was based on the fact that the Ah of the battery are constant, irrespective of which trajectory of the battery cell voltage characteristic is followed during discharge. The temperature effect was not included as the battery system was taken as installed inside a production hall where the ambient temperatures don't vary significantly. Voltage characteristics at constant discharging current were interpolated by third-order polynomials and used to determine the power of discharge and conduct load studies.

The model was validated by a comparison of simulated and measured results. The model was found to exhibit a very good agreement between both sets of results achieved.

2.3.5 Super-capacitor

It was seen in [28] that large busts of current, such as those of a motor start up, supplied by the battery will degrade the battery plates. This ultimately leads to the destruction of the battery. An alternative method of supplying these large bursts of current would be to incorporate a super-capacitor into the BESS in order to deal with this high current, short period bursts. The battery will provide the continuous energy while the super-capacitor will provide the instantaneous power to the load.

The super-capacitor in [28] was combined with a lead-acid battery in order to form a hybrid BESS. It was noted that by utilizing a battery super-capacitor hybrid energy storage system, the battery size can be reduced and a higher state of charge can be maintained. The super-capacitor has a notable higher power density than the battery and therefore can provide more power over a short period of time. However, the battery has a much higher energy density when compared to the super-capacitor which results in the battery being able to store more energy and release the energy over a long period of time.

Table 2: Lead-acid and super-capacitor performances [28]

	Lead Acid Battery	Supercapacitor
Specific Energy Density (Wh/kg)	10-100	1 – 10
Specific Power Density (W/kg)	<1000	<10,000
Cycle Life	1,000	> 500,000
Charge/Discharge Efficiency	70 – 85%	85 - 98%
Fast Charge Time	1 - 5h	0.3 – 30 sec
Discharge Time	0.3 – 3h	0.3 – 30s

2.4 *Controller*

All power systems must include a control strategy that describes the interactions between its components. Due to the use of a battery as a storage form implies that a charge controller will be needed. In [7] a method was proposed to model the controller. The charge controller is used to manage the energy flow to photovoltaic systems, batteries as well as loads. The controller collects information on the battery voltage and by knowing the maximum and minimum values acceptable for the battery voltage; it is able to control the energy flow.

There are two main operating modes for the controller:

1. Normal Operating Condition, where the battery voltage fluctuates between the maximum and minimum voltages
2. Overcharge or Over-Discharge Condition, which occurs when the battery voltage reaches some critical value.

The method described introduced a way of protecting the battery against an excessive charge; the photovoltaic arrays are disconnected from the system when the terminal voltage increases above a certain threshold known as $V_{max,off}$ and when the current required by the load is less than the current delivered by the photovoltaic arrays. The photovoltaic arrays will be again connected when the terminal voltage decreases below a certain value $V_{max,on}$. This can be done using a switch hysteresis cycle which is illustrated in Figure 9.

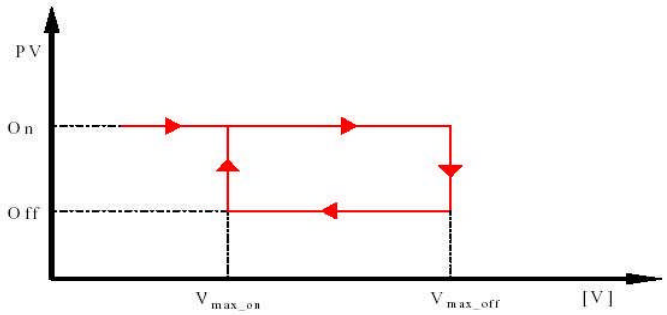

Figure 9: Overcharge protector operating principles [7]

In order to protect the battery against excessive discharge, the load is disconnected when the terminal voltage falls below the certain threshold $V_{min,off}$ and when the current required by the load is bigger than the current delivered by the photovoltaic arrays. The load is then reconnected to the system when the terminal voltage is above a certain value $V_{min,on}$. This also uses a switch hysteresis cycle as shown in the following Figure 10.

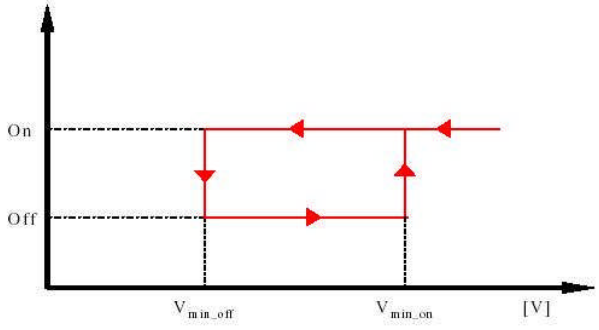

Figure 10: Discharge protector operating principles [7]

The switches can either be electromechanical, such as relays and contactors, or solid state, such as the bipolar transistors and MOSFET's. [12]

The steps of modelling the controller process as proposed by [7] are summarised in the following table.

Table 3: Control process summary [7]

	Constraint	*Command*
(1)	If $V>V_{max\_off}$ and $I_{load}<I_{pv}$	Disconnect PV arrays from the system
(2)	If command (1) is done and $V<V_{max\_on}$	Reconnect PV arrays to the system
(3)	If $V<V_{min\_off}$ and $I_{load}>I_{pv}$	Disconnect the load from the system
(4)	If command (3) is done and $V>V_{min\_on}$	Reconnect the load to the system

2.5 *Load*

2.5.1 Resistive load

Hansen, Sorensen and Binder [7] proposed the following model for a load. The load that exists in a stand-alone photovoltaic system can be of many types. Both DC, such as television and lighting, and AC, such as electrical motors and heaters, are examples of the loads endured by the photovoltaic system.

They modelled the load as an electrical heater which is actually a simple resistance controlled by a thermostat. This led to the formation of the following equations for the load model.

Where I_{ac} and V_{ac} are the AC-current and AC-voltage, respectively. R_{heater} is the resistance of the heater, which can easily be determined by the rated power P_{heater} and the rated voltage V_{heater} of the heater.

$$R_{heater} = \frac{(V_{heater})^2}{P_{heater}} \qquad (13)$$

This model for the load was seen to be favourable as it is simple and an accurate representation of the loads experienced.

2.5.2 Load Profile

The authors in [30] modelled the load over 24 hours for a rural location in Kerala, India. The load profile shows a varying demand pattern over the day with two load peaks centred around 06h00 and 20h00 while the load drops off in between. Figure 11 below depicts the load.

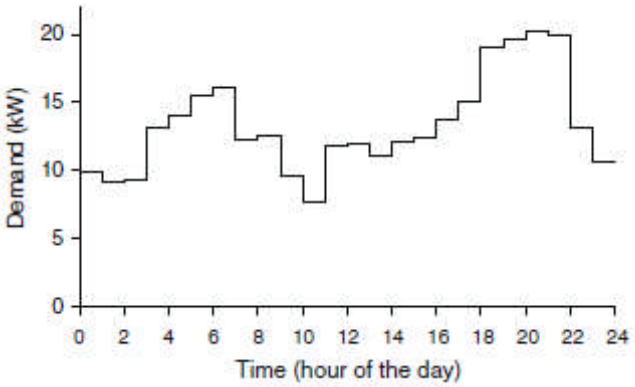

Figure 11: Load profile for Kerala, India

2.6 *Maximum power point tracking (MPPT)*

The power that is available at the photovoltaic cells output keeps changing due to changes in solar irradiation and ambient temperature. This is due to the photovoltaic cells exhibiting a nonlinear current-voltage characteristic [1]. Therefore, the maximum power point (MPP) of the photovoltaic cells also varies with solar irradiation and ambient temperature. Maximum power point tracking (MPPT) techniques are used to make full utilization of photovoltaic array output power, which depends on the solar irradiation and the ambient temperature.

Due to the nonlinear relationship between the current and the voltage of the photovoltaic cell, it was noted that there is a unique maximum power point (MPP) at a particular environment. This peak power changes with respect to solar irradiation and ambient temperature.

An important consideration for photovoltaic generation in achieving a high efficiency is to match the photovoltaic source and load impedances properly for any weather conditions [1], thus obtaining the maximum power generation. The technique used to do this task is known as maximum power point tracking (MPPT). In recent years, many authors have proposed techniques for maximum power point tracking (MPPT). Enrique et al [15] investigated four main techniques namely the perturb-and-observe (P&O or hill climbing) method, the incremental conductance (IncCond) method and Neutral networks and curve fitting. Hohm and Ropp [16] investigated the constant voltage tracking (CVT) algorithm. The main methods of maximum power point tracking (MPPT) will now be revised.

2.6.1 Constant voltage tracking and algorithm (CVT)

In [16] it was explained that the maximum power point (MPP) voltage is proportional to the open circuit voltage and that the proportional constant of 0.76 is generally used. The maximum power point (MPP) is then calculated by measuring the open circuit voltage of the panel and then multiplying it by the proportional constant. The converter sets the panel output voltage to the calculated maximum power point (MPP) voltage for a fixed length of time before recalculating the open circuit voltage and resetting the output voltage to the new maximum power point (MPP) voltage value. This step is the continuously repeated in order to track the maximum power point.

Hohm and Ropp [16] noted two flaws in this method, which are:

1. There is a loss of energy while measuring the open circuit voltage.
2. The maximum power point (MPP) is not always found at 76% of the open circuit voltage.

The constant voltage tracking (CVT) method is very simple and easily implemented. But the constant voltage can't track the maximum power point (MPP) when the solar illumination varies. Therefore the constant voltage tracking (CVT) method is not often used in true maximum power point tracking (MPPT) strategies. [1]

2.6.2 Perturb-and-observe (P&O)

The perturb-and-observe technique (P&O) is widely used due to simplicity, only requiring measurements of V_{PV} & I_{PV}, and it is capable of tracking the maximum power point (MPP) rather accurately even through variations of solar irradiance and ambient temperature.

The method works by perturbing the voltage V_{PV} and observing the impact of the change on the output power of the photovoltaic array. At each cycle this voltage and current are measured to calculate the power. The algorithm works by trying to find the optimum voltage and current values in order to obtain the maximum power point (MPP). If however, the power has decreased from the previous cycle, the voltage will be adjusted in the opposite direction to the previous cycle. The voltage is thus perturbed at every maximum power point tracking (MPPT) cycle. When the maximum power point has been reached, the voltage will oscillate around the optimal voltage value. This causes a loss in power that increases with the step size of the perturbation. If this step size is large, the algorithm will respond quickly to sudden changes in operating conditions. If the step size is small, the losses under stable or slowly changing conditions will be lower but the system will not respond quickly to rapid changes in temperature or irradiance. [4]

Enrique et al [15] was found to prefer this method due to its simplicity and easy implementation. However, this method has several drawbacks such as slow tracking speed and oscillations about the maximum power point when a high standard of accuracy is needed, making it less favourable for rapidly changing environments.

2.6.3 Incremental conductance method (IncCond)

Li and Wang [1] applied the incremental conductance with a variable step size in a photovoltaic power system in this paper. The incremental conductance method (IncCond) is based on the fact that the slope of the photovoltaic array power curve is zero at the maximum power point (MPP), positive on the left and negative on the right of the maximum power point (MPP). The INC algorithm decrements or increments V_{ref} to reach the new maximum power point when the atmospheric conditions change.

It was said that at the maximum power point, V_{ref} is equal to V_{MPP}. Once the maximum power point is reached, the photovoltaic array is maintained at this point unless a change in current is noted. The algorithm increments or decrements V_{ref} to track the new maximum power point when the weather conditions change. [1]

The incremental conductance method was able to improve the dynamic and steady state performance of the photovoltaic system due to the introduction of the variable step size. This method is accurate under changing weather conditions but much more complex than the other methods proposed.

The power value obtained is compared to the power value obtained in the previous cycle. If the output power has increased, then the voltage is adjusted further in the same direction as in the previous cycle.

3 Design of stand alone Photovoltaic System

The main purpose of the following section is to describe the models of the elements of the stand-alone photovoltaic system. The major components of the system are the photovoltaic (PV) system, maximum power point tracker (MPPT), battery energy storage system (BESS), controller and load. Modelling of the stand-alone system has been based on modular blocks and simplifies the modelling of the other system structures and replacing of the elements. This can be seen in Figure 12.

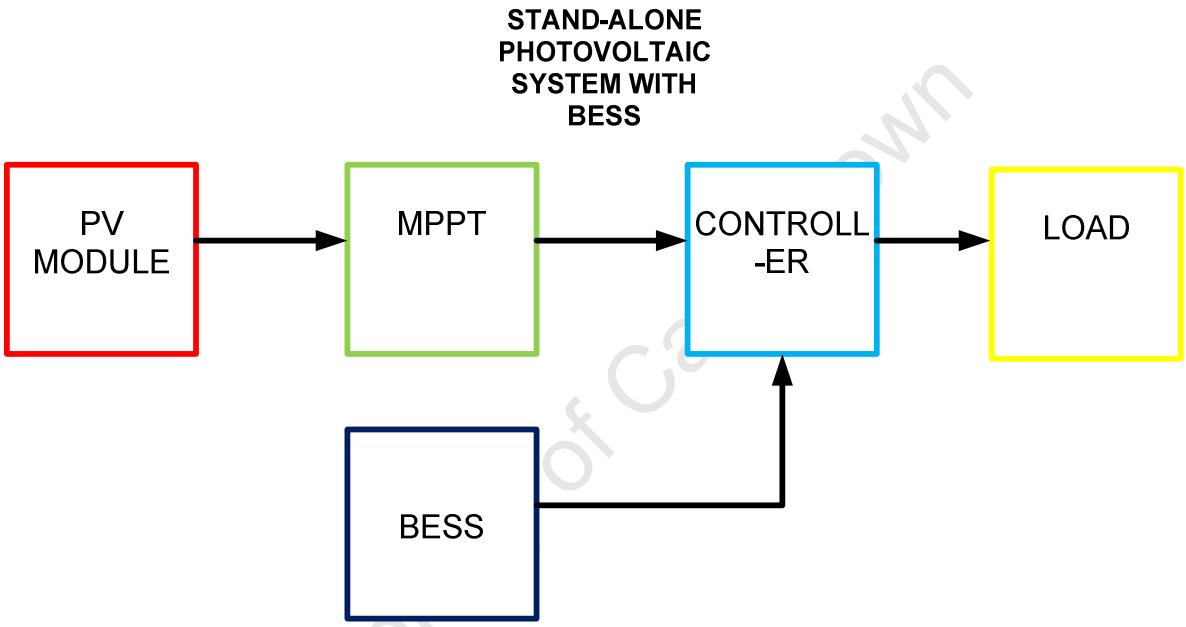

Figure 12: Block diagram for the stand-alone system

The figure show how the various components of the stand-alone PV system interrelate. An in-depth investigation into the requirements and characteristics of the components of the system is conducted in this section. The design of the stand-alone system required consideration of the interaction between both the major component and the sub-components. The flowchart below Figure 13, illustrates the considerations on which the design decision-making was based. It must be noted that this work was done from a theoretical view point.

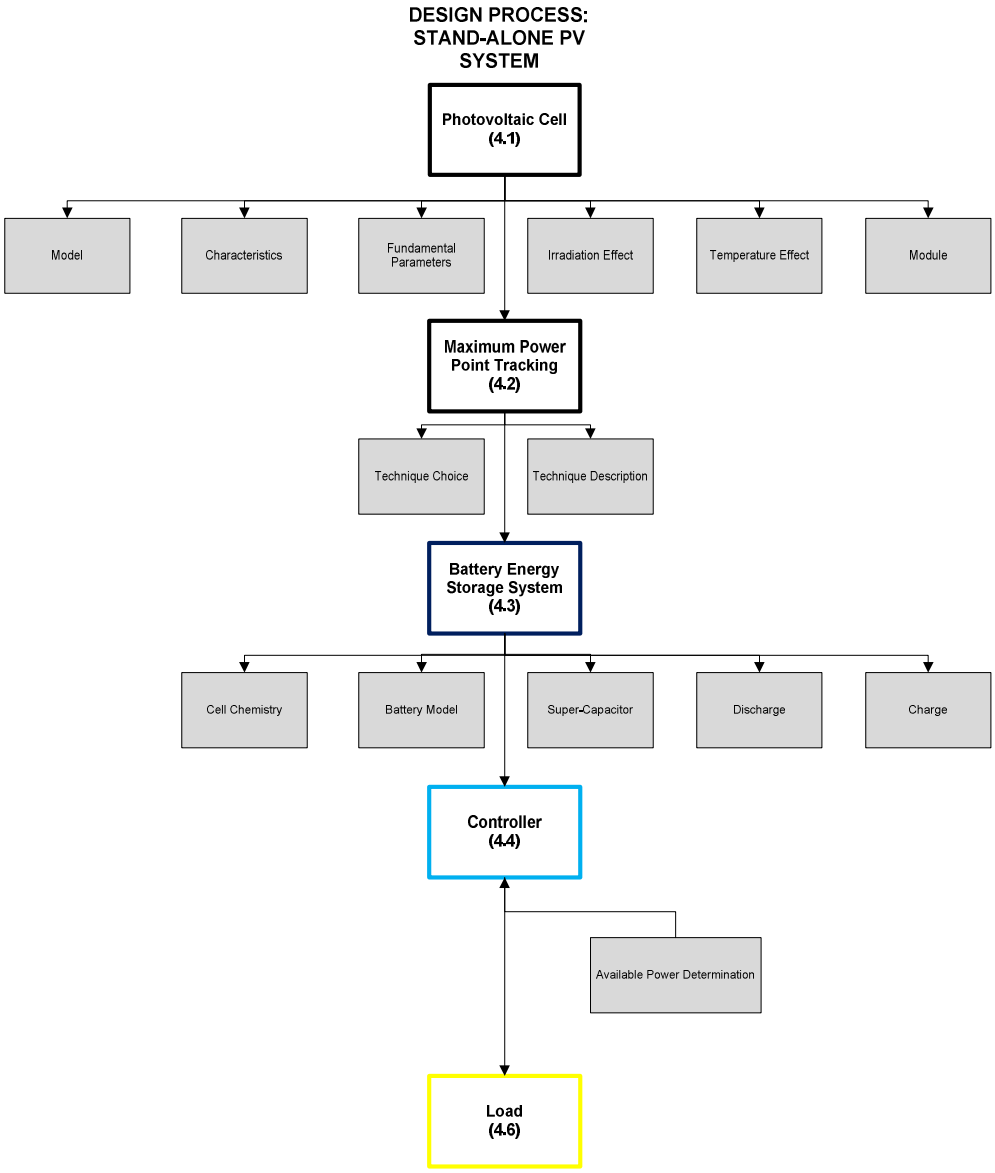

Figure 13: Flow chart of the design of the stand-alone system

3.1 *Photovoltaic cell*

3.1.1 Model of the photovoltaic cell

The double exponential model was used to model the photovoltaic cell and is shown below in the equivalent circuit diagram Figure 14. This model takes into account the irradiance, ambient temperature, series resistance and the parallel resistance, all of which have a large impact on the I-V curve as well as the accuracy of the model.

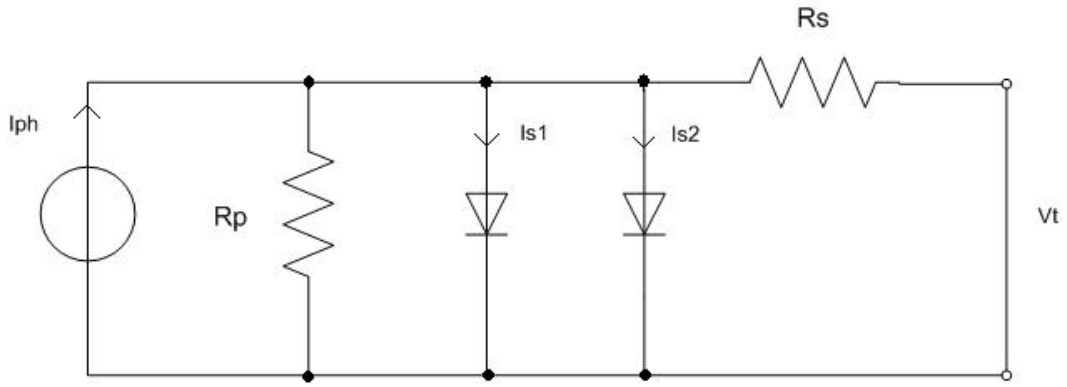

Figure 14: Circuit diagram of the double exponential model

3.1.2 Characteristics of the photovoltaic cell

The model expresses the I-V characteristics of the cell by the following equation:

$$I = I_{ph} - I_{s1}\left[e^{\left(\frac{V+IR_s}{vt}\right)} - 1\right] - I_{s2}\left[e^{\left(\frac{V+IR_s}{Avt}\right)}\right] - \frac{V+IR_s}{R_p} \qquad (14)$$

where,

$$vt = kT/e \qquad (15)$$

In this model *I* and *V* represent the terminal current and voltage respectively. The Boltzmann constant *k*, the absolute temperature T and the electronic charge *q* are also present. The five parameters $I_{ph}, I_{s1}, I_{s2}, R_s, R_p$ are the photocurrent, the two diode saturation currents and the series and parallel resistances respectively.

Equation (14) and (15) show that the electrical characteristics of the model are dependent upon the five parameters which are in turn dependent upon two variables. These variables are known as the environmental variables and are the ambient temperature *T* (^{0}K) and the solar irradiance *E* (watts/m^2).

In order to be able to run simulations and determine the efficiency of the maximum power point trackers, it would be ideal to relate the electric parameters $I_{ph}, I_{s1}, I_{s2}, R_s, R_p$ to the environmental variables *E* and *T* directly. This would allow us to be able to see the different output responses for the model by varying the solar irradiation and the temperature. To complete the model, it was necessary to determine what relationship existed between each of the five parameters and the environmental variables.

Veissid et al [18] published work on the relations between the parameters and temperature. A method was devised in [10] which related the parameters to the environmental variables *E* and *T*. The method made use of curve fitting to determine the initial sets of double-exponential model parameters from experiment data. A complete characterisation system was based around a standard PC with cheap acquisition hardware and is used in this thesis.

Photocurrent (I_{ph})

In [10], the initial photocurrent was plotted against temperature. The photocurrent varies linearly with irradiance and [18] suggested a linear relationship with temperature. At absolute zero or in the dark there can be no offset term and combining the irradiance and temperature relations give the desired relation between environmental variable (*E* and *T*) and the photocurrent parameter. This is shown in the following equation:

$$I_{ph} = K_0 E(1 + K_1 T) \qquad (16)$$

By applying a linear fit, the values of K_0 and K_1 can be found.

First diode saturation current (I_{s1})

It was suggest in [18] that the first saturation current was to take the form of the following equation and was obtained by the device physics;

$$I_{s1} = KT^3 e^{\frac{qvt}{kT}} \qquad (17)$$

K was a constant to be found while *k* was the Boltzmann's constant. Seeing that (17) contains an exponential, it was linearized by taking logarithms and plotting $\ln(I_{s1}/T^3)$. There was little deviation of the curve with irradiation found and all the points lay along a single line. By putting $K = K_2$ and $K_3 = (qV_g / k)$ then using a linear curve fit, the values of K_4 & K_5 where found. This is now substituted into (17) to from the new equation (18).

$$I_{s1} = K_2 T^3 e^{\frac{K_3}{T}} \qquad (18)$$

Second saturation current (I_{s2})

A very similar procedure was taken in obtaining the second diode saturation current involving device physics. The equation (19) shows the relationship between I_{s2} and the environmental variable of temperature (*T*).

$$I_{s2} = KT^{\frac{3}{2}} e^{\left(\frac{qV_g}{kT}\right)} \quad (19)$$

Since this equation also contains an exponential it was linearized with $K_4 = K$ and $K_5 = (qV_g / k)$. The value for the second diode saturation current can be obtained by using the values of K_4 & K_5. These new values substituted into (19) form the new equation (20).

$$I_{s2} = K_4 T^{\frac{3}{2}} e^{\frac{k_5}{T}} \quad (20)$$

Diode parameter (A)

In order to approximate the Shockley-Read-Hall recombination in the space-charge layer, the diode parameter is normally set to 2. However, for the amorphous cells it is suggested that the parameter varies linearly with temperature which altered the equation to the following form:

$$A = K_6 + K_7 T \quad (21)$$

In this model the value of *A* is set to 2, therefore the values of K_6 and K_7 are set accordingly.

Series resistance (R_s)

The series resistance exhibits a dependence upon temperature, which is effectively a fixed 'bulk' resistance. The behaviour with respect to irradiance is unknown. The series resistance was plotted against *E* and *T* and from this plot it was noted that R_s is linear in *T* but nonlinear in *E*. The relationship with *E* was found to be inversely proportional and plotting $1/R_s$ confirmed this. Combining the two dependencies gave the relation:

$$R_s = K_8 + \frac{K_9}{E} + K_{10} T \quad (22)$$

A linear curve fit can then return the values for K_8, K_9 and K_{10}.

Parallel resistance (R_p)

The parallel resistance forms the last parameter to be fitted and it was suggested that the relationship with respect to temperature was given by (15). Its dependence upon irradiance was unknown and highly unlikely.

$$R_p = K_{11} e^{K_{12} T} \tag{23}$$

The final constant K_{11} and K_{12} can be found by performing a linear curve fit.

It can be seen from the double exponential model equation (7) that the values of *I* and *V* are the terminal current and voltage, respectively. Due to the terminal current being present on both sides of the equation, a tiresome iterative method would be needed to predict the final terminal current of the PV cell. This was overcome by the fact that $(V + IR_s)$ is in fact equal to the voltage of the diode.

$$V_d = V + IR_s \tag{24}$$

This easily removed the iteration problem as well as the potential problem of having to know the terminal voltage of the PV cell.

A summary of the constants and the five parameters are shown in the following table.

Table 4: Values of input coefficients and parameters

Parameter	Coefficient Value	Coefficient Value
$I_{ph} = K_0 E(1 + K_1 T)$	K_0 = -5.729e-7	K_1 = -0.1098
$I_{s1} = K_2 T^3 e^{\frac{K_3}{T}}$	K_2 = 44.5355	K_3 = -1.2640e4
$I_{s2} = K_4 T^{\frac{3}{2}} e^{\frac{k_5}{T}}$	K_4 = 11.8003	K_5 = -7.3174e3
$A = K_6 + K_7 T$	K_6 = 2	K_7 = 0
$R_s = K_8 + \frac{K_9}{E} + K_{10} T$	K_8 = 1.47 K_{10} = -4.47e3	K_9 = 1.6126e3
$R_p = K_{11} e^{K_{12} T}$	K_{11} = 2.3034e6	K_{12} = -2.8122e-2

These coefficient values can now be substituted into the relevant parameters which in turn are substituted into the initial I-V characteristic equation (14). The output of the I-V characteristic equation (14) is the output current of a single photovoltaic cell.

3.1.3 Fundamental parameters of the photovoltaic cell

As noted in [7], a sign convention is used in the representation of I-V characteristics. The current generated by a cell due to irradiance is taken as positive and the voltage applied on the cell's terminals is also taken as positive.

If the cell's terminals are connected to a variable resistance *R*, which simulates the load, the operating point is determined by the intersection of the I-V characteristic of the solar cell with the load I-V characteristic. This is shown in Figure 15. The power delivered to the load depends solely on the resistance.

For a resistive load, the load characteristic is a straight line with a slope *I/V = 1/R*. For a small load *R*, the cell will operate in the region MN of the curve. Here the cell behaves as a constant current source, almost equal to the short-circuit current. For a large load *R*, the cell will operate on the region PS of the curve. Here the cell behaves more as a constant voltage source, almost equal to the open-circuit voltage. [7]

A real solar cell can be characterized by the following four fundamental parameters, also present on the sketch in Figure 15.

- Short Circuit Current: $I_{sc} = I_{ph}$. The short circuit current is the greatest value of current produced by the cell. Short circuit conditions can be found at V=0.

- Open Circuit Voltage: The open circuit voltage corresponds to the voltage drop across the two saturation diodes (I_{s1} *and* I_{s2}) when the photocurrent (I_{ph}) passes through it. This is when the generated current is equal to zero. For open circuit voltage conditions, $I = 0$. This simulates the cell in zero irradiance such as night time.

  It can be worked out by solving the following equation:

$$V_{OC} = V_t \ln\left(\frac{I_{ph}}{I_0}\right) \qquad (25)$$

- Maximum Power Point: The maximum power point is the operating point A(V_{max}, I_{max}) in Figure 15. The power dissipated in the resistive load, when operating at this point, is at a maximum.

$$P_{\max} = V_{\max} * I_{\max} \tag{26}$$

- Fill Factor: This is the ratio of the maximum power that can be delivered to a load and the product of the short circuit current and open circuit voltage.

$$FF = \frac{P_{\max}}{V_{OC} * I_{SC}} \tag{27}$$

Fill factor is a measure of the real I-V characteristics with good cells having a value higher than 0.7. As cell temperature increases, the fill factor decreases.

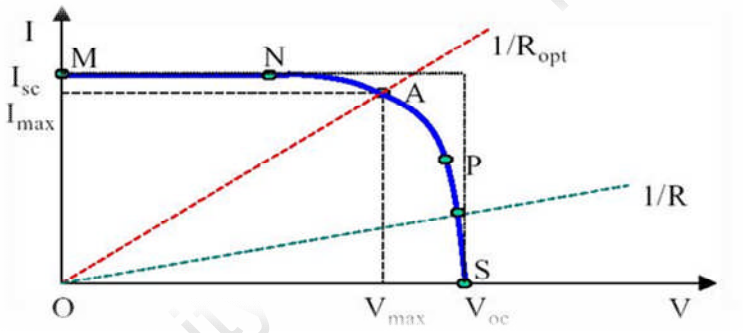

Figure 15: A typical I-V characteristic curve for a PV cell [7]

3.1.4 Irradiation effect

The influence of the ambient irradiation E on the cell's I-V characteristic is shown in the following Figure 16.

The figure shows that the short circuit current is linear with respect to changes in irradiation while the open circuit voltage increases logarithmically with irradiation.

The arrow shows which way the irradiation of the cell increases.

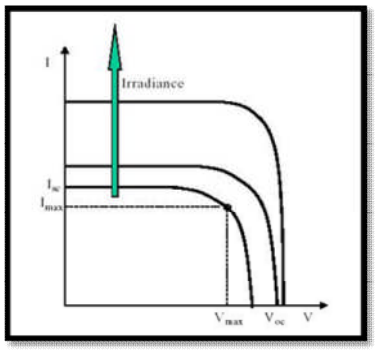

Figure 16: Irradiation effect on the PV cell

3.1.5 Temperature effect

The influence of the cell's temperature on the I-V characteristic curve of the cell is illustrated in the following Figure 17.

The short circuit current of the photovoltaic cell, increases slightly with an increase in cell temperature. The dominant effect is the linear decrease in open circuit voltage with increasing cell temperature.

The arrow indicates the direction of increasing cell temperature.

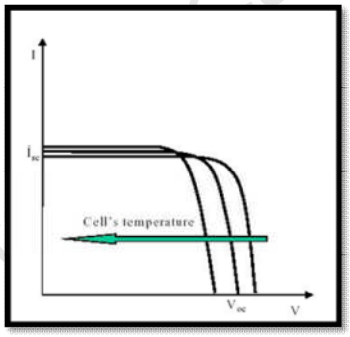

Figure 17: Temperature effect on the PV cell [7]

3.1.6 Photovoltaic module

The photovoltaic solar cells are usually grouped into modules. These consist of solar cells connected in series and/or parallel. The following Figure 18 shows the effects of connecting cells in series or parallel.

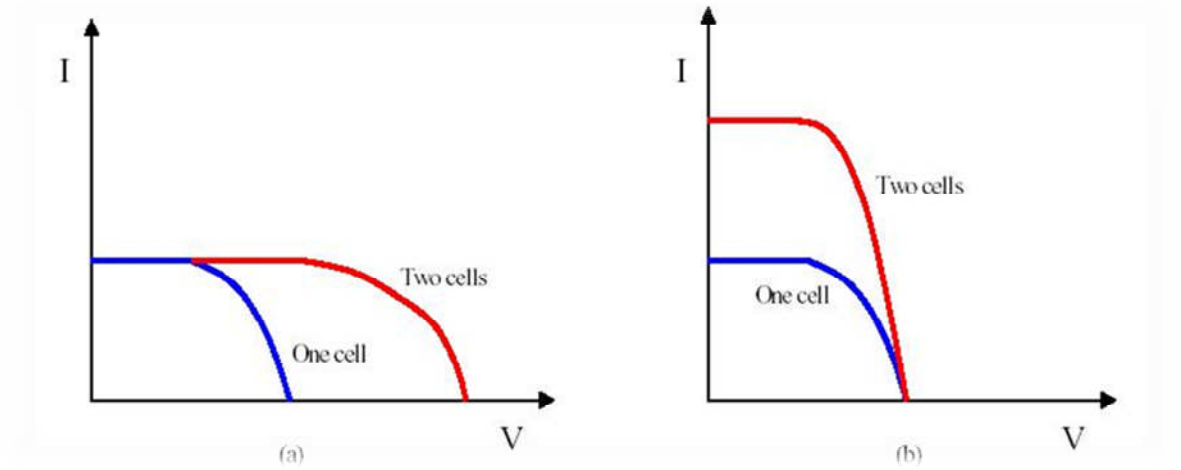

Figure 18: Identical PV cells connected in series (a) and parallel (b) [12]

It can be seen from (a) that by connecting the identical cells in series, their individual voltages have been added together while their currents remain unchanged. In (b) where the identical cells have been connected in parallel, their individual currents have been added together while their voltages remain unchanged.

This leads to the following equations where the parameters with subscript "m" are referring to the PV module, while the parameters with subscript "c" refer to the solar cell. The number of parallel branches is given by $N_{p,}$ while the number of series cells in the branches is given by N_s.

$$V_{OC,n} = V_{OC,c} * N_s \quad (28)$$

$$I_{SC,m} = I_{SC,c} * N_p \quad (29)$$

$$R_m = \frac{N_s}{N_p} * R_c \quad (30)$$

$$P_m = P_c * N_s * N_p \quad (31)$$

These configurations are shown in the following Figure 19:

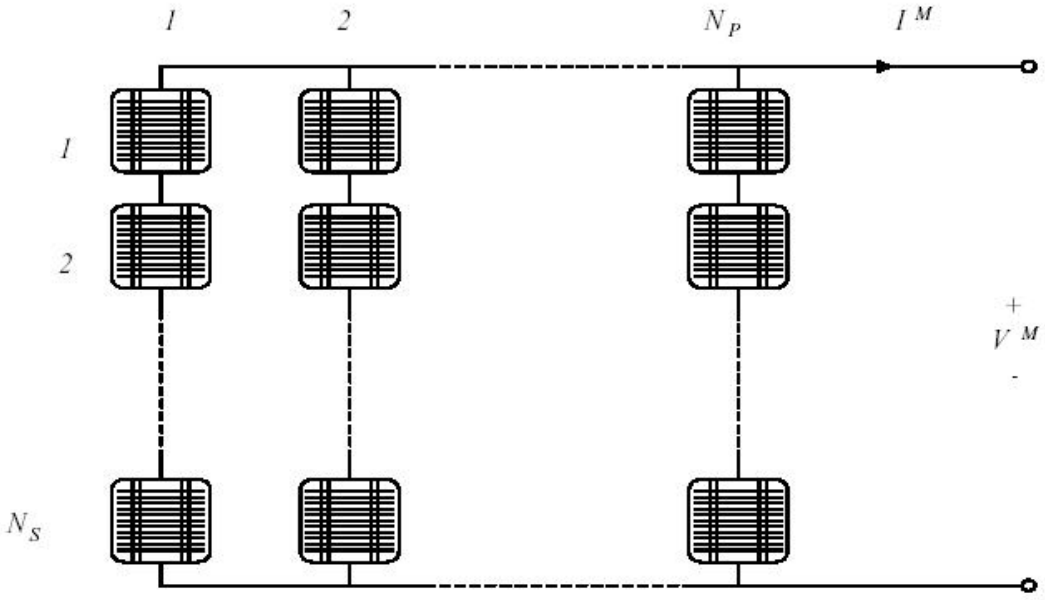

Figure 19: PV module consisting of Np branches, each of Ns series cells [7]

We want to create a PV module that has an output power of about 9kW. In order to achieve this, we will need to create parallel branches with series connected cells.

The number of parallel branches and series connected cells in the module used for this design were:

$N_s = 3900$

$N_p = 450$

3.2 *Maximum Power Point Tracking*

3.2.1 Technique choice

When considering methods for finding the maximum power point, the speed and accuracy at which the MPPT algorithm operates was a main concern. The methods described in Section 2.6 had been critically reviewed with the perturb-and-observe (P&O) technique in Section 2.6.2 proving to be the most efficient with respect to speed and time.

This method was implemented in Matlab and the simulation proved to be rather complex with difficulties encountered. Thus, an alternative method was devised which proved to be faster and more accurate. This method was of a search form, utilizing an m-file that had inputs for power and the corresponding voltage and current matrices, and is explained in the following section.

3.2.2 Description of Technique

The MPP technique used in this design performed a search for the maximum power point. The flowchart below outlines the steps in the method for finding the maximum power point and outputs the values of the power, voltage and current at the MPP.

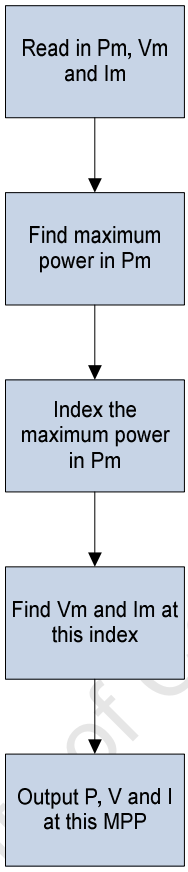

Figure 20: Flows chart of the MPP technique

From the above Figure 20, the steps in the process can easily be seen. The first step in obtaining the MPP is reading in the arrays of power, voltage and current. These values come from the output of the PV array and are all of the same length.

$$P_i = V_i * I_i \quad (32)$$

where "i" denotes the row in the array,

Once these values have been read in, a search is performed on the power array for the maximum power value. This is the maximum power that the PV module can provide to a load and corresponds with the maximum peak value of the P-V characteristic curve of the PV module.

The next step finds the point in the array, the row "i", at which the maximum power is found and sets this point as the index for MPPT. Once the MPP has been indexed, the corresponding values of voltage and current are found and are then outputted together with the maximum power as the MPP for power, voltage and current.

This proved to be an easier alternative to the perturb-and-observe technique.

3.3 *Battery energy storage system (BESS)*

The BESS system will be used to provide power to the load when the PV system is unavailable or doesn't meet the load requirement.

The discharge characteristics of the BESS are described by mathematical equations for the three types of battery chemistries. A battery cell was chosen for each of the battery types.

The modelling technique in [21] was used to determine the battery characteristics. However, this technique was modified in order to simulate and model all three chemistries for their discharging characteristics as well as their charging characteristics.

Experimental data of voltage discharge curves against the depth of discharge for various discharge rates for each of the chemistries was used. The experimental data was interpolated into a 3rd order mathematical equation for the various discharge rates with the cut-off voltage and actual rates of discharge being taken into account during the simulation.

The 3rd order mathematical equations relating the voltage of the cell to the depth of discharge were determined in Matlab using the curve fitting tool.

The current is discharged at a constant rate and therefore the power equations and its profile are easily determined and will follow the form of the determined voltage profile.

The charging characteristics of the three chemistries were determined using the same method applied to obtain the discharging characteristic.

Since the discharge rate and time was known from the cell specifications as well as the publicly available manufacturer's data, the discharge voltage and power characteristics could be plotted against time.

With this mathematical model it was possible to determine electrical equations for equilibrium potential, terminal voltage and state of charge (SOC).

3.3.1 Design Considerations

In this work, the emphasis was on the comparison study between the performances of the different battery chemistries used in a BESS. All values used were obtained from

manufacturer's data sheets specific to the chemistry. Sizing of the batteries were determined for a specific condition and they were designed to be modular in order to be able to supply systems of various voltages, currents and powers. This enables us to investigate various scenarios of configurations and sizes tailored to the need of the industry.

In order to compare the BESS chemistries a scenario was chosen where the output voltages of the lithium-ion and the nickel-cadmium batteries where based on the output current of the PV module. It was thought that keeping one characteristic constant throughout the system, in this case the current, would ease the comparison study and hence current source inverters (CSI) would be used. The work done with the lead-acid chemistry in [21] was found to be good practical work and therefore it was decided to use a similar larger cell, opposed to the lithium-ion and nickel-cadmium, of 2500Ah in order to ease the validation of the modelling technique.

It was decided to rate the batteries at 2.5kWh with the single cell chemistries as follows:

Lithium-ion : 2500mAh;

Nickel-cadmium : 2500mAh;

Lead-acid : 2500Ah

A comparison of three charging techniques was performed and in order to ease the comparison, the charging protocols of the three chemistries all apply to a 2.5Ah cell. It must be noted that the BESS is modular and the various configurations will result in various BESS sizings.

The temperature effect is seen as being a major factor influencing the characteristics of the batteries. The battery bank was designed for a set temperature as the BESS can be housed in a controlled temperature environment, for this reason the temperature effect was not considered in the model. The BESS was held at the same temperature as the PV system in order for continuity.

3.3.2 Lithium-ion

This section depicts how the lithium-ion BESS model was obtained. A lithium-ion battery cell was chosen as the basis of the study. The cell had the following properties:

Table 5: Lithium-ion cell properties

Lithium-Ion Cell Specification	
Maximum Voltage	4.2V
Nominal Capacity	2500mAh

Charge	Method	CC-CV (2.5h)
	Max. Current	1C
	Max. Voltage	4.2V
Discharge	Max. Current	2C
	Termination	3.0V
Operating Temperature	Charge	25°C
	Discharge	25°C

Discharge characteristics

The interpolated 3rd order equations representing the battery cell voltages for different discharge rates as a function of the depth of discharge (DOD) are displayed below.

$$U_{0.2C} = 4.2 - 0.0136\, C_{DOD} + 2.6162x10^{-4}\, C_{DOD}^{2} - 2.6995x10^{-6}\, C_{DOD}^{3} \quad (33)$$

$$U_{0.5C} = 4.118 - 0.0151\, C_{DOD} + 3.3495x10^{-4}\, C_{DOD}^{2} - 3.3963x10^{-6}\, C_{DOD}^{3} \quad (34)$$

$$U_{1C} = 4.0029 - 0.0164\, C_{DOD} + 3.8172x10^{-4}\, C_{DOD}^{2} - 3.8226x10^{-6}\, C_{DOD}^{3} \quad (35)$$

$$U_{2C} = 3.88 - 0.0234\, C_{DOD} + 5.6646x10^{-4}\, C_{DOD}^{2} - 5.1646x10^{-6}\, C_{DOD}^{3} \quad (36)$$

Where:

C_{DOD} depth of discharge (DOD), 0% is equal to 2500mAh;

$U_{0.2C}$ V_{batt} at a constant discharging current of 0.47 A and 5-h discharging time as a function of the depth of discharge (DOD);

$U_{0.5C}$ V_{batt} at a constant discharging current of 1.125 A and 2-h discharging time as a function of the depth of discharge (DOD);

U_{1C} V_{batt} at a constant discharging current of 2.175 A and 1-h discharging time as a function of the depth of discharge (DOD);

U_{2C} V_{batt} at a constant discharging current of 4 A and 0.5-h discharging time as a function of the depth of discharge (DOD);

The power provided by the BESS for different discharge rates can be calculated as follows. The discharge voltage and discharge current are multiplied by the amount of series connected lithium ion cells for that specific BESS sizing, respectively.

$$P_{0.2C} = N_s * U_{0.1C} * N_p * I_{0.1C} \quad (37)$$

$$P_{0.5C} = N_s * U_{0.5C} * N_p * I_{0.5C} \quad (38)$$

$$P_{1C} = N_s * U_{1C} * N_p * I_{1C} \quad (39)$$

$$P_{2C} = N_s * U_{2C} * N_p * I_{2C} \quad (40)$$

The discharge voltage and discharge current are multiplied by the amount of series connected lithium ion cells for that specific BESS sizing, respectively.

Charging characteristics

The charging protocol chosen for the lithium-ion cell was the 2.5h CC-CV (constant current – constant voltage) charging protocol. The protocol consists of two stages:

1. *Constant Current*: The cell is taken as completely discharged (DOD = 100% and SOC = 0%) at the beginning of the simulation where t = 0.A current of 1.4A is subjected to the cell and the voltage begins to rise until it reaches its V_{max} of 4.2V.
2. *Constant Voltage*: Once the V_{max} of 4.2 V is reached, we consider the charging protocol to now be in the constant voltage stage. The voltage is held at V_{max} of 4.2 V while the current drops from 1.4 A exponentially to zero.

The time taken to charge the cell from completely discharged (100% DOD and 0% SOC) to completely charged (0% DOD and 100% SOC) was modelled to be 2h30 hours. The cell was said to reach the 50% DOD and 50% SOC after a time of 0h28, the cell was found to be at a 30% DOD and 70% SOC at 0h19.

These charging characteristics were modelled using experimental data to obtain equations representing the charging currents and voltages and then interpolated as exponential functions as follows:

1. Constant Current: $V_{CC} = 3.994e^{0.11t} – 0.9933e^{-39.43t}$ V; (41)
   $I_{CC} = 1.4$ A;
   where $0 < t < 0.47$hours.

2. Constant Voltage: $V_{CV} = 4.2$V;
   $I_{CV} = 1.451e^{-1.161t}$ (42)
   where $0.47 < t < 2.5$ hours.

BESS sizing

By connecting cells in series and parallel we are able to increase the voltage and the current of the battery bank, respectively. This will allow us to determine the optimum configuration for a pre-determined BESS output power. The figure below shows how connecting cells in series and parallel affects the voltage and current of the BESS.

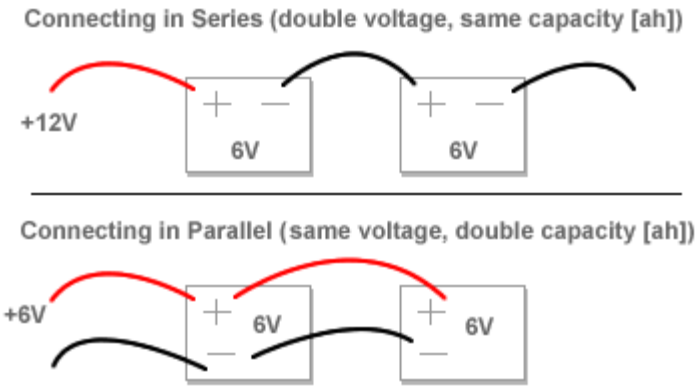

Figure 21: Series and parallel connected battery cells

The following equation shows the relationships between series and parallel connected cells and voltage and current.

$$V_{module} = N_s * V_{cell} \quad (43)$$

$$I_{module} = N_p * I_{cell} \quad (44)$$

This in turn results in an increase in the module power.

$$P_{module} = N_s * V_{cell} * N_p * I_{cell} \quad (45)$$

The lithium-ion BESS was calculated for discharge rates (C-rates) of 0.2C and 0.5C. We wanted an output power from the lithium-ion BESS of 2.5kWh. We also wanted to try keep the currents at 5 A for both discharge rates.

The BESS sizing was calculated as follows for the 0.2C discharge rate:

I_{cell} = 0.47 Ah;

V_{cell} = 4.2 V;

P_{cell} = 1.9790 Wh.

We want the BESS module to have an output power of 2.5kWh therefore;

P_{module} = 2.5kWh;

= $N_s * N_p * P_{cell}$

From this we can calculate the amount of cells in the bank ($N_s * N_p$).

$N_s * N_p$ = P_{module} / P_{cell};

= 2500 / 1.9790;

= 1266.46

We round the amount of 1266.46 cells to 1270 cells. A current of 5 A is needed therefore we can work out the amount of parallel branches (N_p) as follows:

I_{5A} = N_p*I_{cell};

By making Np the subject of the formulae:

N_p = 5 A / 0.47 A;

= 10.638 branches of parallel cells

We round the amount of 10.638 cells to 11 cells and can now determine the amount of series connected cells per parallel branch:

N_s = 1270 cells / 11 cells;

= 115.45 cells connected in series in each parallel branch.

We round the amount of 115.45 cells to 120 cells and can now determine the actual amount of cells.

N_s*N_p = 120*11;

= 1320 cells in the bank

We determine the BESS bank voltage, current and power with these values:

$V_{BESS,0.2C}$ = N_s*$V_{cel\ l}$ = 504 V;

$I_{BESS,0.2C}$ = N_p*I_{cell} = 5.17 Ah;

$P_{BESS,0.2C}$ = N_s*N_p*P_{cell} = 2605.68 Wh

With 1320 lithium-ion cells connected in the BESS we can provide a $P_{max,0.2C}$ of 2605.68 Wh.

3.3.3 Nickel-cadmium

This section explains how the lithium-ion BESS model was obtained. A lithium-ion battery cell was chosen as the basis of the study. The cell had the following properties:

Table 6: Nickel-cadmium cell properties

Nickel-Cadmium Cell Specification		
Maximum Voltage		1.3564V
Nominal Capacity		2500mAh
Charge	Method	CC (7h)
	Max. Current	1C
	Max. Voltage	1.68V
Discharge	Max. Current	1C

	Termination	1.0V
Operating Temperature	Charge	25°C
	Discharge	25°C

Discharge Characteristics

The interpolated 3rd order equations representing the battery cell voltages for different discharge rates are displayed below.

$$U_{0.1C} = 1.3564 - 0.0055\,C_{DOD} + 9.2373x10^{-5}\,C_{DOD}^2 - 5.5806x10^{-7}\,C_{DOD}^3 \quad (46)$$

$$U_{0.2C} = 1.3056 - 0.0051\,C_{DOD} + 1.1162x10^{-4}\,C_{DOD}^2 - 8.5209x10^{-7}\,C_{DOD}^3 \quad (47)$$

$$U_{0.5C} = 1.2610 - 0.0073\,C_{DOD} + 1.8814x10^{-4}\,C_{DOD}^2 - 1.633x10^{-6}\,C_{DOD}^3 \quad (48)$$

$$U_{1C} = 1.2084 - 0.0081\,C_{DOD} + 2.0579x10^{-4}\,C_{DOD}^2 - 2.0205x10^{-6}\,C_{DOD}^3 \quad (49)$$

Where:

C_{DOD} depth of discharge (DOD), 0% is equal to 2500mAh;

$U_{0.1C}$ V_{batt} at a constant discharging current of 0.5 A and 10-h discharging time as a function of the depth of discharge (DOD);

$U_{0.2C}$ V_{batt} at a constant discharging current of 1 A and 5-h discharging time as a function of the depth of discharge (DOD);

$U_{0.5C}$ V_{batt} at a constant discharging current of 2.125 A and 2-h discharging time as a function of the depth of discharge (DOD);

U_{1C} V_{batt} at a constant discharging current of 3.25 A and 1-h discharging time as a function of the depth of discharge (DOD);

$$P_{0.1C} = N_s * U_{0.1C} * N_p * I_{0.1C} \quad (50)$$

$$P_{0.2C} = N_s * U_{0.2C} * N_p * I_{0.2C} \quad (51)$$

$$P_{0.5C} = N_s * U_{0.5C} * N_p * I_{0.5C} \quad (52)$$

$$P_{1C} = N_s * U_{1C} * N_p * I_{1C} \quad (53)$$

Charging characteristics

The charging protocol investigated for the nickel-cadmium cell was the 7h CC (constant current) charging protocol.

The cell was subjected to a constant current of 20A/100Ah and was assumed to be fully discharged (0% DOD and 100% SOC). The cell was subjected to the constant current until the battery is fully charged (100%DODand 0% SOC).

These charging characteristics were modelled using experimental data to obtain equations representing the charging currents and voltages and then interpolated as a quadratic function over another quadratic function as follows:

V_{CC} = $(1.451t^2 – 15.61t + 52.64) / (t^2 – 11.12t + 37.44)$; *(54)*

I_{CC} = 20A/100Ah;

where $0 < t < 7$ hours.

BESS sizing

Using the same technique described for lithium-ion BESS sizing we were able to obtain the following results for nickel-cadmium discharge rates of 0.1C and 0.2C. Both BESS sizes for different discharge rates (C-rates) were designed to output a power of 2500 W at a current of 5 A. The results are as follows for the 0.1C charging rate:

$V_{BESS,0.1C}$ = 501.868 V;

$I_{BESS,0.1C}$ = 5 Ah;

$P_{BESS,0.1C}$ = 2509.34 Wh

where,

N_s = 370 cells connected in series in each parallel branch;

N_p = 10 parallel connected branches.

With 3700 nickel-cadmium cells connected in the BESS we can provide a $P_{max,0.1C}$ of 2509.3W.

The results are as follows for the 0.2C charging rate:

$V_{BESS,0.2C}$ = 500.04 V;

$I_{BESS,0.2C}$ = 5 Ah;

$P_{BESS,0.2C}$ = 2500.2 Wh

where,

N_s = 383 cells connected in series in each parallel branch;

N_p = 5 parallel connected branches.

With 1915 nickel-cadmium cells connected in the BESS we can provide a $P_{max,0.2C}$ of 2500.2Wh.

3.3.4 Lead-acid

This section explains how the lead-acid BESS model was obtained. A lead-acid battery cell was chosen as the basis of the study. The cell had the following properties:

Table 7: Lead-acid cell properties

Lead-Acid Cell Specification		
Maximum Voltage		2.01V
Nominal Capacity		2500Ah
Charge	Method	CV (7h)
	Max. Current	1C
	Max. Voltage	2.45V
Discharge	Max. Current	1C
	Termination	1.82V
Operating Temperature	Charge	25°C
	Discharge	25°C

Discharge characteristics

The interpolated 3rd order equations representing the battery cell voltages for different discharge rates are displayed below.

$$U_{0.1C} = 2.01 - 0.00145\,C_{DOD} + 2.38\times10^{-5}\,C_{DOD}^2 - 2.54\times10^{-7}\,C_{DOD}^3 \quad (55)$$

$$U_{0.2C} = 2 - 9.46\times10\text{-}4\,C_{DOD} + 1.39\times10^{-5}\,C_{DOD}^2 - 3.03\times10^{-7}\,C_{DOD}^3 \quad (56)$$

$$U_{0.3C} = 1.99 - 8.81\times10\text{-}4\,C_{DOD} + 1.97\times10^{-5}\,C_{DOD}^2 - 5.05\times10^{-7}\,C_{DOD}^3 \quad (57)$$

$$U_{1C} = 1.94 - 0.00125\,C_{DOD} + 1.10\times10^{-5}\,C_{DOD}^2 - 4.16\times10^{-7}\,C_{DOD}^3 \quad (58)$$

Where:

C_{DOD} depth of discharge (DOD), 0% is equal to 2500Ah;

$U_{0.1C}$ V_{batt} at a constant discharging current of 250 A and 10-h discharging time as a function of the depth of discharge (DOD);

$U_{0.2C}$ V_{batt} at a constant discharging current of 430 A and 5-h discharging time as a function of the depth of discharge (DOD);

$U_{0.3C}$ V_{batt} at a constant discharging current of 625A and 3-h discharging time as a function of the depth of discharge (DOD);

U_{1C} V_{batt} at a constant discharging current of 1300 A and 1-h discharging time as a function of the depth of discharge (DOD);

$$P_{0.1C} = N_s*U_{0.1C}*N_p*I_{0.1C} \quad (59)$$

$$P_{0.2C} = N_s*U_{0.2C}*N_p*I_{0.2C} \quad (60)$$

$$P_{0.3C} = N_s*U_{0.3C}*N_p*I_{0.3C} \quad (61)$$

$$P_{1C} = N_s*U_{1C}*N_p*I_{1C} \quad (62)$$

Charging characteristics

The charging protocol chosen for the lead-acid cell was the 7h CV (constant voltage) charging protocol for a 2.5Ah lead-acid cell. The cells are modular and can form the 2500Ah lead-acid BESS.

The cell was subjected to a constant voltage of 2.45 V and was assumed to be fully discharged (100% DOD and 0% SOC). The cell was subjected to the constant voltage until the battery is fully charged (0%DOD and 100% SOC).

The current initially remained constant at 2 A until a time of 0h21. From here the current decreased exponentially to zero at which the lead-acid cell was taken as fully charged.

These charging characteristics were modelled using experimental data to obtain equations representing the charging currents and then interpolated as an exponential function as follows:

V_{CV} = 2.45 V;

I_{CV} = 2A;

where $0 < t < 0.35$ hours.

V_{CV} = 2.45 V;

I_{CV} = $2e^{-1.084t}$; (63)

where $0 < t < 7$ hours.

BESS sizing

Using the technique described for the lithium-ion 0.2C charge rate BESS sizing we are able to calculate the lead-acid 0.2C BESS sizing. We want the BESS power to be 2500 W but since the current of the 0.2C rate is 430 A, we won't connect anymore cells in parallel.

The results are as follows for the 0.2C charging rate:

$V_{BESS,0.2C}$ = 6 V;

$I_{BESS,0.2C}$ = 430 Ah;

$P_{BESS,0.2C}$ = 2580 Wh

where,

N_s = 3 cells connected in series in each parallel branch;

N_p = 1 parallel connected branches.

With 3 lead-acid cells connected in the BESS we can provide a $P_{max,0.2C}$ of 2580 Wh.

3.3.5 Super-Capacitor

The capacitor chosen for the super-capacitor section of the BESS was the Nesscap 600F/2.7V capacitor. A 600F capacitor rated at 2.7V was modelled based on the manufacturer's data presented below:

Table 8: Super-capacitor Specifications

Super-Capacitor Specification	
Capacitance	600F
Voltage Rated	2.7V
Tolerance	0% - 20%
ESR (Equivalent Series Resistance)	0.64mOhm
Charging Current	10A
Discharge Current	5A

The super capacitor was modelled for 10A charging and 5A discharges. It was modelled over time and can be described by the following equations:

$$U_c = -0.514t^2 + 0.8429t + 0.0153; \quad (64)$$

$$U_d = -0.1175t + 2.7; \quad (65)$$

3.4 *Controller*

A controller is used in all power systems to form a strategy that describes how certain components of the system interact together. In the case of the stand-alone PV system, the controller would be used to monitor the power of the load and the input voltages to the

inverter from the battery and the PV module. In essence, it would be used to manage the power flow to the load. When the load draws less power than the PV module produces, the excess power will go into charging the battery.

The controller would also be used for connecting the battery to the load when the power generated by the PV module is less than the power needed by the load.

The following flowchart describes the workings of the controller.

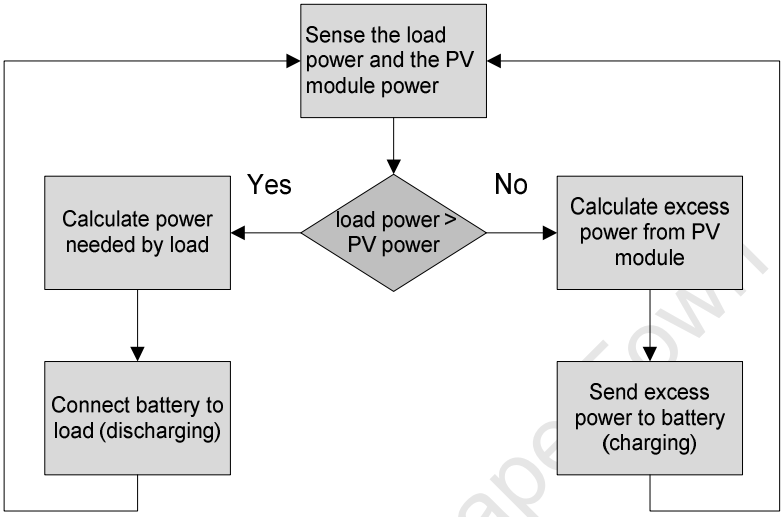

Figure 22: Flow chart of the controller

3.5 *Load*

The load was modelled based on the load profile presented in [23]. It was than adjusted to depict a load size that would be relevant to this stand-alone system.

The load was sized at 2.4kW and consisted of two peaks. These peaks represent times of the day when the most load power is drawn as a result. The peaks were found to be centred around 10h30 and 20h00. Either side of the peaks the load is found to drop at 15h00 to just above 2kW and at 05h00 to just below 1.5kW.

The load profile was modelled against time and can be characterised by the following equation as a sum of three sines:

$$Load(t) = 329.8\sin(0.07253t + 0.4902) + 265.8\sin(0.5251t - 0.2983) + 293.6\sin(0.5364t + 2.666) \quad (66)$$

4 Implementation of PV system in simulink

In this section the mathematical models of the components of the stand-alone PV system, which were described in Section 3, are implemented in Matlab.

The components of the stand-alone PV system where grouped into model blocks making it easier and more practical to understand and use. The system contains seven model blocks namely the environment, PV module, MPPT, BESS, controller, inverter and load. These models are then connected together to form the stand-alone PV system. The following figure demonstrates this:

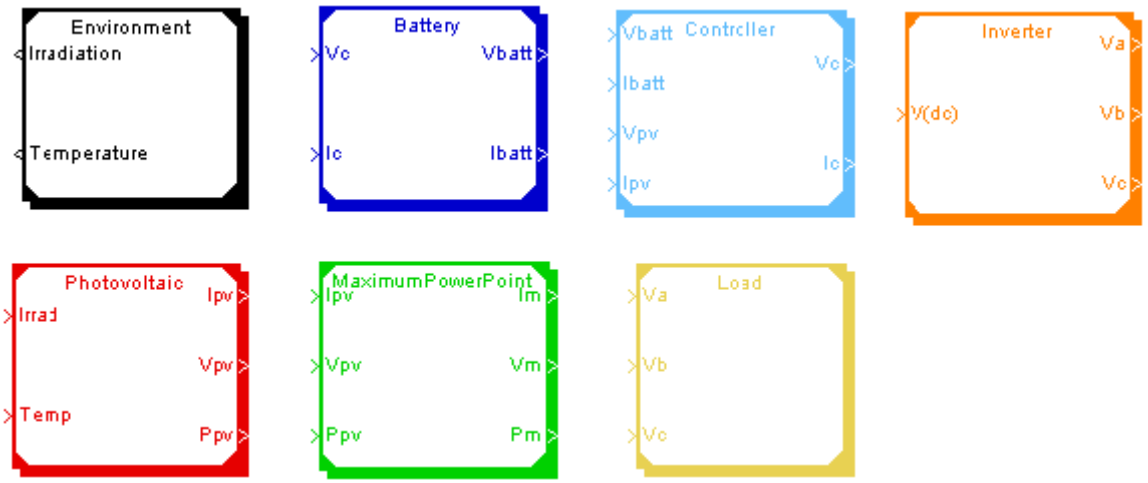

Figure 23: Model blocks for the stand-alone PV system

Advantages of using the model blocks are:

- It provides a quick overview of how the components are connected to each other.
- It is a simple way to present and understand the workings of the stand-alone PV system.
- It is an easy way to build more specific structures such as PV arrays and battery banks.

By connecting the model blocks together it is easy to see that the total system has only two input variables, temperature and irradiance, which are situated in the environment model block. These variables determine the output current, voltage and power of the PV module. The outputs of the PV module are then fed into the maximum power point tracking model block where the MPP values of the PV module are calculated. From here the MPP values are fed into the controller model block. The battery's voltages, current and resulting state of charge are inputted to the controller.

The controller block has another input in the form of the load and the controller then determines how much of the power produced by the PV module must go to either the BESS or the load. It also determines whether the BESS must supply the load. The output of the controller is connected to the DC/AC inverter. Here the power is converted from DC to AC and then delivered to the load where load studies can be performed. The inverter was included in this thesis in order to show where the output DC power of the system would be going. It had been simulated in Simulink in previous work but was not used in this thesis and was included merely for a greater understanding of the complete system. The DC power going to the DC to AC inverter is displayed in the final results of the section.

Figure 24 demonstrates how the model blocks are connected to form the stand-alone PV plant.

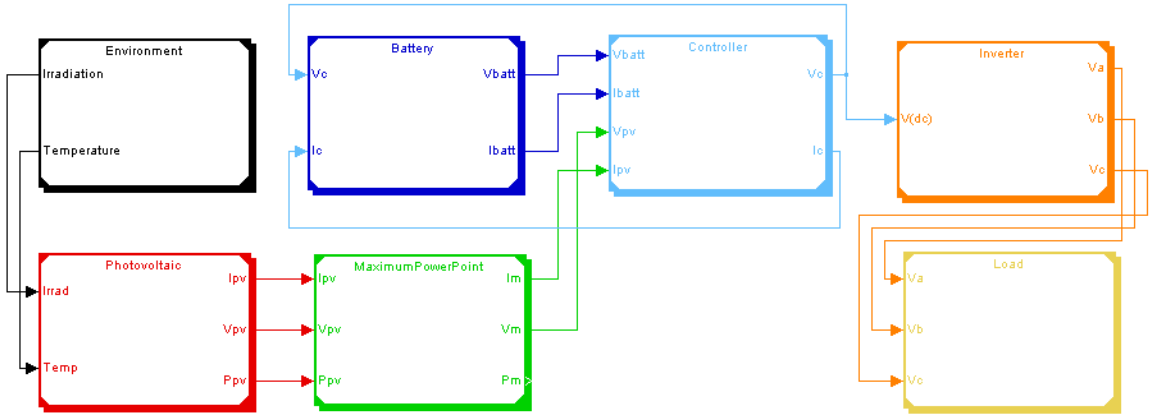

Figure 24: Stand-alone system structure

4.1 *Photovoltaic module model block*

The photovoltaic module was simulated having two input variables. The input variables irradiation and temperature were entered as matrices into the simulation. The irradiation matrix is the output of the irradiation profile for each time integration step. The temperature was chosen to be constant over the whole day and thus was entered as the constant scalar variable.

Having the environmental variables in the simulation we were able to calculate the PV cell currents. This required us to define variables for the coefficients used in formulating the PV cell current. The photocurrent and saturation current etc. were simulated as functions dependant on the coefficients as well as the irradiation and temperature. Due to the irradiance comprising of a matrix, the PV cell current became a matrix the same length as

the irradiation. This allowed us to be able to determine the I-V characteristics and P-V characteristics of the PV cell throughout the 24 hours.

In order to form the module, scalar variables for the number of series- and parallel-connected cells in the system were introduced. These were formulated into the corresponding power equations and adjusted the results obtained from the PV cell into the PV module.

It must be noted that the PV cell was simulated for irradiation values of winter and summer. The MPPT simulation shown in Section 4.2 was then run on the PV module matrices and the power against time was exported to the load.

4.2 *Maximum power point tracking model block*

The maximum power point tracking technique was simulated in a Matlab m-file. The method used to obtain the maximum power point voltage, current and power is shown in steps below:

- The matrix obtained from the PV for its voltage, current and power provided must be read into the simulation.
- The power matrix is searched for the maximum value of power. This power's row is then indexed as 'i'.
- The values of current (1, i) and voltage (1, i) are then found.
- These obtained values represent power, voltage and current at the maximum power point and are returned as outputs to the simulation.

4.3 *BESS model block*

The BESS consists of charging and discharging simulations. Both of these simulations are run in the same system. The controller determines when the battery is charging or discharging and this logic decides which corresponding m-file is to be used.

4.3.1 Discharge model

When the controller needs extra power from the BESS, its state becomes discharging. Its simulation is based on the design in Section 3.4.

The battery discharge characteristics were simulated in Matlab. An m-file was written which simulated the discharge curves over their capacity. The capacity was set up as a variable whose length corresponds to the total capacity discharged for the discharge rate. This was

entered into the discharge voltage characteristic equation, which resulted in a matrix whose rows ‘i’ contained the instantaneous value of the discharge voltage at capacity ‘i’.

This matrix coupled with the constant current variables allowed us to calculate the corresponding power at capacity ‘i’ over the discharge rates. The discharge voltage and power were then plotted against capacity as well as time.

4.3.2 Charge model

The charge model was simulated by an m-file for each charging protocol. The charging protocols are listed and explained below:

Constant Current - Constant Voltage:

This charging method was used for the lithium-ion chemistry. As stated, it consisted of two charging stages. The first, the constant current, was simulated with the constant scalar variable being the current. The voltage was simulated as an exponential function dependent on time.

The constant voltage allowed the constant scalar variable to be the voltage. The current was seen as exponentially decaying to zero and was simulated as an exponential function dependent on time.

The power required for this method of charge was easily obtainable in the simulation. A plot of power against time was then exported to the load required model.

Constant Current:

This charging method was used for the nickel-cadmium chemistry. The voltage was simulated as a quadratic function divided by another quadratic equation with the current being the constant scalar variable. The voltage was plotted against time. Power could also easily be determined.

Constant Voltage:

This resulted in two stages of simulation as the current is seen as constant for a short period. For this period of constant current we have to constant scalar variables in current and voltage. After said time the current is seen as decaying exponentially as a function of time. This was simulated and plotted against time. Power was easily determined and could be exported to the load required model.

4.4 *Load*

The load demand for a full day was simulated in Matlab. A simple m-file was created plotting the load equation, the sum of sines, as a function of time. This produced a load similar in form to the load in [30]. It also produced a matrix of length equal to 24 hours.

In order to simulate load studies, we would need to be able to determine the total power produced by the system and how much power the system and the load need.

The MPP power produced from the PV system and the power discharged by the BESS in are imported into the load m-file and summed. This represents the power provided by the stand-alone system.

The load profile demand, mentioned earlier, and the charging power requirements of the BESS are summed and considered to be the power required by the stand-alone system.

The power provided and the power required by the system is plotted against time on the same axis. Load studies can now be performed with the model.

The power availability is simulated as the difference between the provided and required power.

4.5 *Environment model block*

Matrices for the summer and winter irradiation over 24 hours were used as inputs into the model when investigating the power provided by a PV for irradiation levels over 24 hours. The temperatures were also modelled as matrices with different temperature values.

4.6 *Configuration parameters*

For the Matlab m-files, one hour was simulated over 100 steps resulting in a step size being 0.01. This resulted in the matrix lengths of the investigated characteristics being 1 by 2401 (Matlab begins at 1 not 0). It is of utmost importance to make sure that all the variables are of the same length when simulating the model.

5 analysis of results and model validation

The major findings for this thesis are as follows:

5.1 *PV module validation*

The aim of this section is to validate the PV model proposed in Section 3.1. This section contains an examination of results obtained from the PV cell model simulation. It explores the PV module's efficiency under varying conditions of irradiation E and temperature T as well as the relationship between the PV cell and PV module.

5.1.1 PV cell simulation results for the irradiance and temperature effect

The single PV cell model was tested with varying input conditions for irradiance E and temperature T. The model was subjected to a varying irradiance E while the temperature T was kept constant; then to a varying temperature T with the irradiance E being the constant.

The PV cell simulation showed these results for an irradiance of 200, 400, 600, 800 and 1000 W/m^2 at temperature T of 298^o F (25^o C)

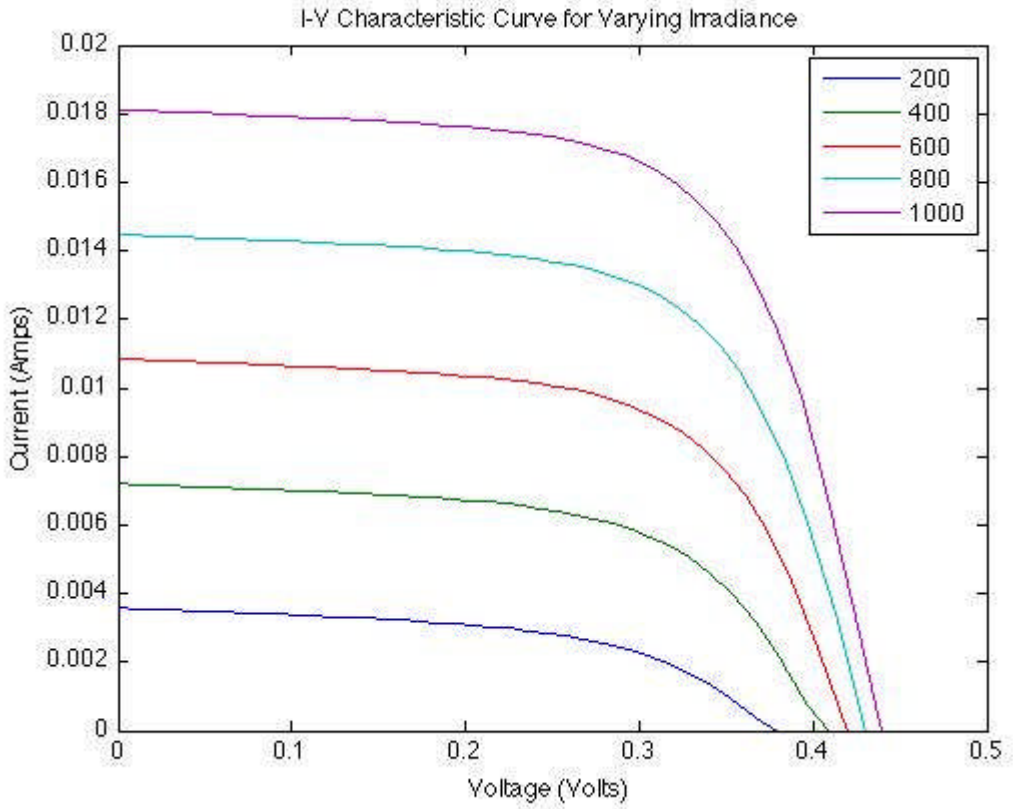

Figure 25: I-V Characteristics of the PV cell under varying irradiance E

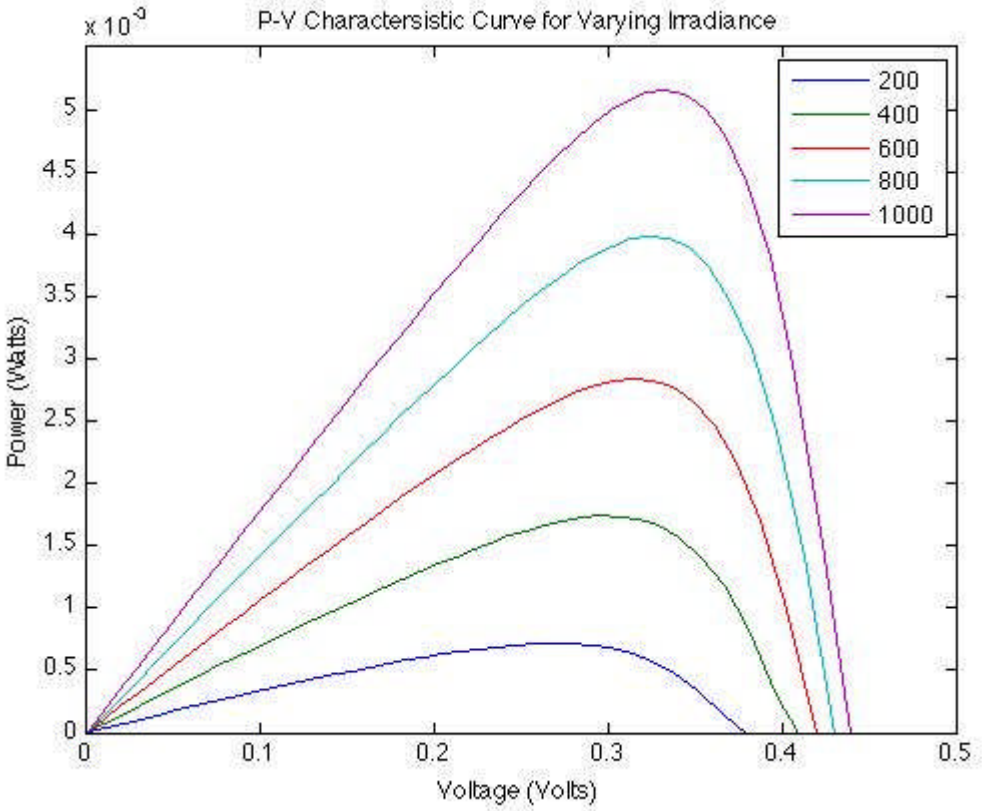

Figure 26: P-V Characteristics of the PV cell under varying irradiance E

The results of the simulation were summarised in the following table:

Table 9: Result summary of PV cell under varying irradiation E

Irradiance (W/m²)	Open Circuit Voltage (V)	Maximum Power Point			Short Circuit Current (A)
		Voltage (V)	Current (A)	Power (W)	
1000	0.439	0.3329	0.0156	0.0052	0.0181
800	0.432	0.3235	0.0123	0.004	0.0145
600	0.422	0.3145	0.009	0.0028	0.0108
400	0.4075	0.2955	0.0059	0.0017	0.0072
200	0.376	0.268	0.0027	0.0007	0.0036

The graphs obtained in Figure 25 and Figure 26 represents the I-V characteristic curve and the P-V characteristic curve of the simulated PV cell for a number of irradiances E, respectively. Table 9 gives the values for V_{oc}, V_{mpp}, I_{mpp}, P_{mpp} and I_{sc}. The open circuit voltage and short circuit current determined in Matlab correspond with the figures and the manufacturer's data.

The PV cell simulation showed these results for a temperature T of 278, 288, 298, 308 and 318°F at an irradiance E of 1000 W/m^2.

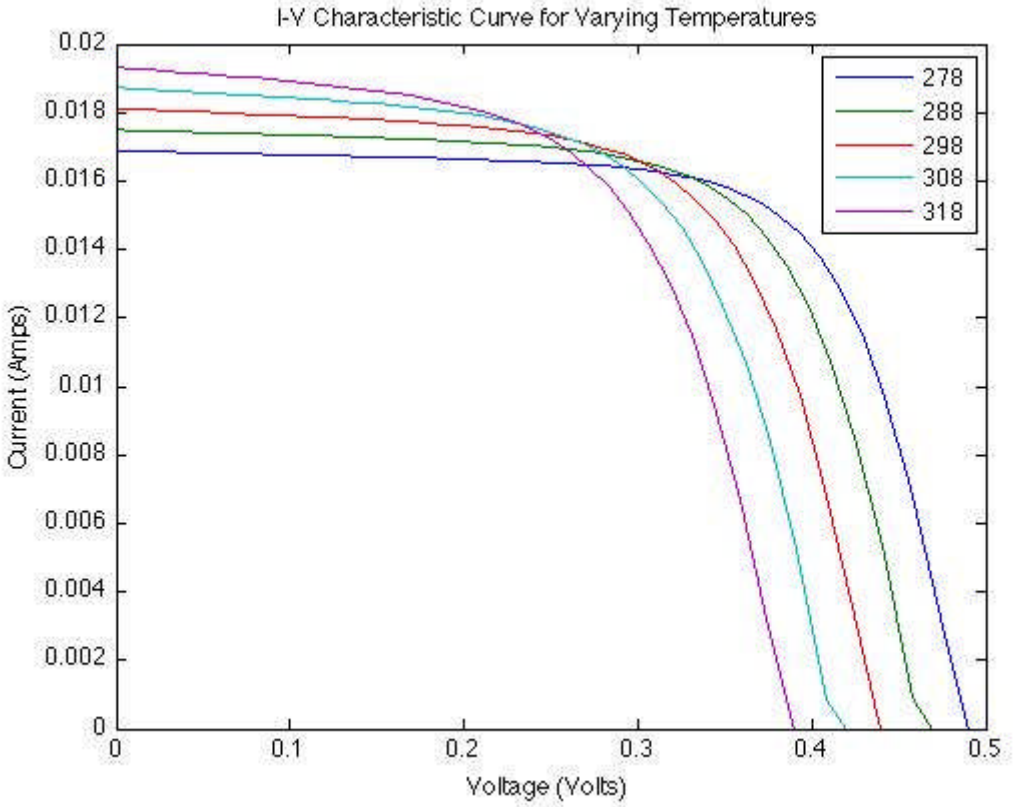

Figure 27: I-V Characteristics of the PV cell under varying temperature T

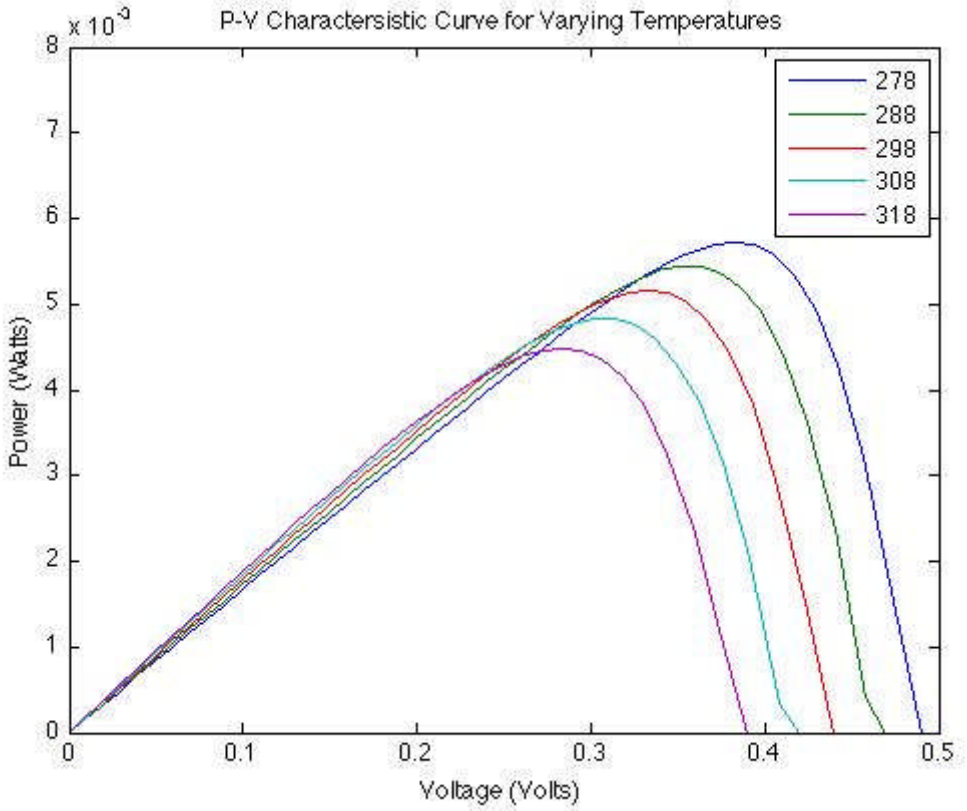

Figure 28: P-V Characteristics of the PV cell under varying temperature T

The results of the simulation were summarised in the following table:

Table 10: Result summary of PV cell under varying temperature T

Temperature (°K)	Open Circuit Voltage (V)	Maximum Power Point			Short Circuit Current (A)
		Voltage (V)	Current (A)	Power (W)	
318	0.39	0.2837	0.0159	0.0045	0.0193
308	0.415	0.3028	0.0158	0.0048	0.0187
298	0.439	0.3329	0.0156	0.0052	0.0181
288	0.464	0.3522	0.0153	0.0054	0.0175
278	0.488	0.3825	0.0149	0.0057	0.0169

The graphs obtained in Figure 27 and Figure 28 represents the I-V characteristic curve and the P-V characteristic curve of the simulated PV cell for a number of temperatures T, respectively. Table 10 gives the values for V_{oc}, V_{mpp}, I_{mpp}, P_{mpp} and I_{sc}. The open circuit voltage and short circuit current determined in Matlab correspond with the figures and the manufacturer's data.

5.1.2 Series and parallel connected PV cells

The PV cells were connected in series and parallel in order to test our model against the theories in Section 3.1.6. The results obtained for two PV cells connected in series are displayed below.

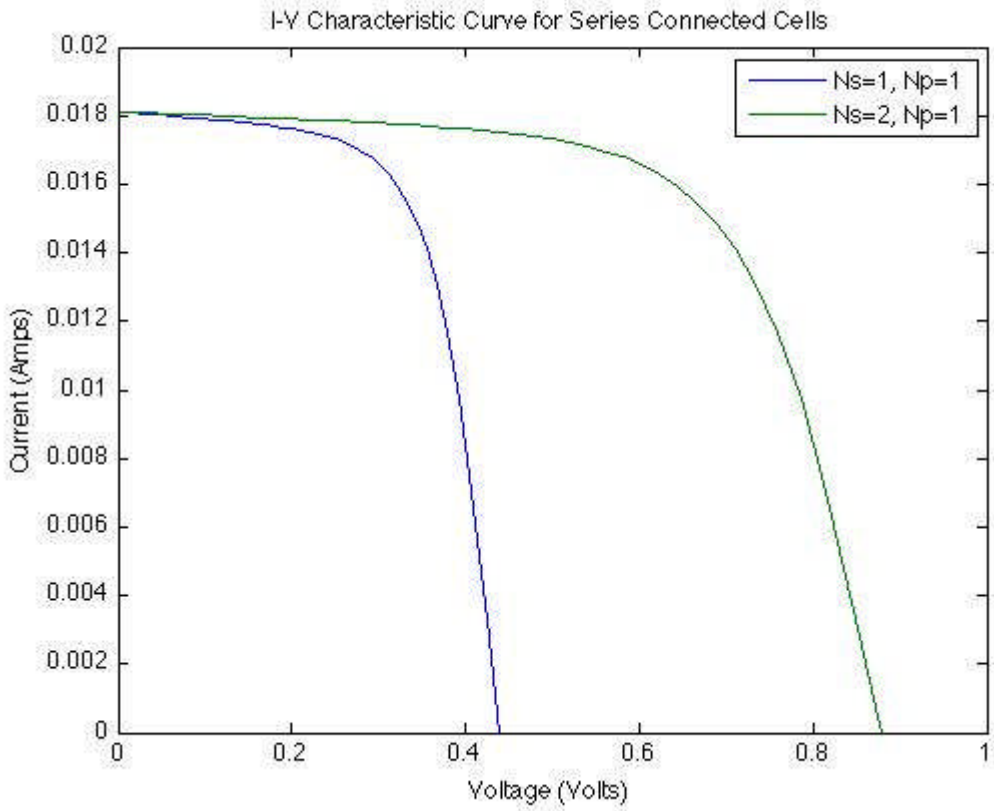

Figure 29: I-V Characteristics of series connected PV cells

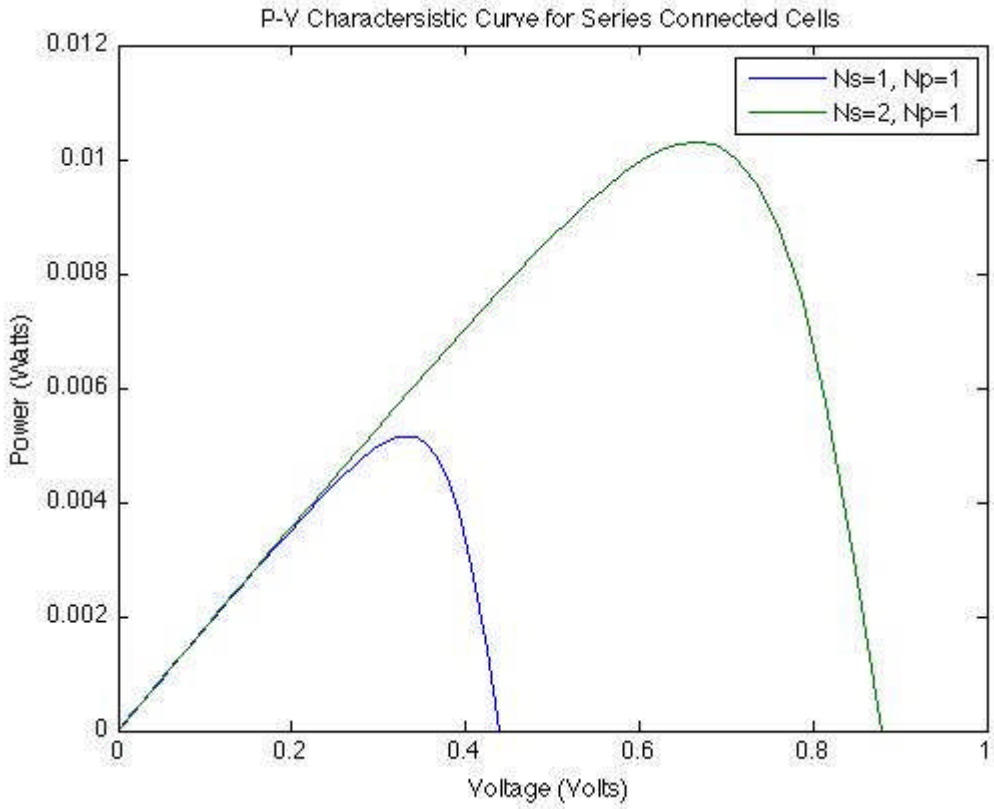

Figure 30: P-V Characteristics of series connected PV cells

The graphs obtained in Figure 29 and Figure 30 represents the I-V characteristic curve and the P-V characteristic curve of the simulated series connected PV cells, respectively.

The results obtained from the two PV cells connected in parallel are shown below.

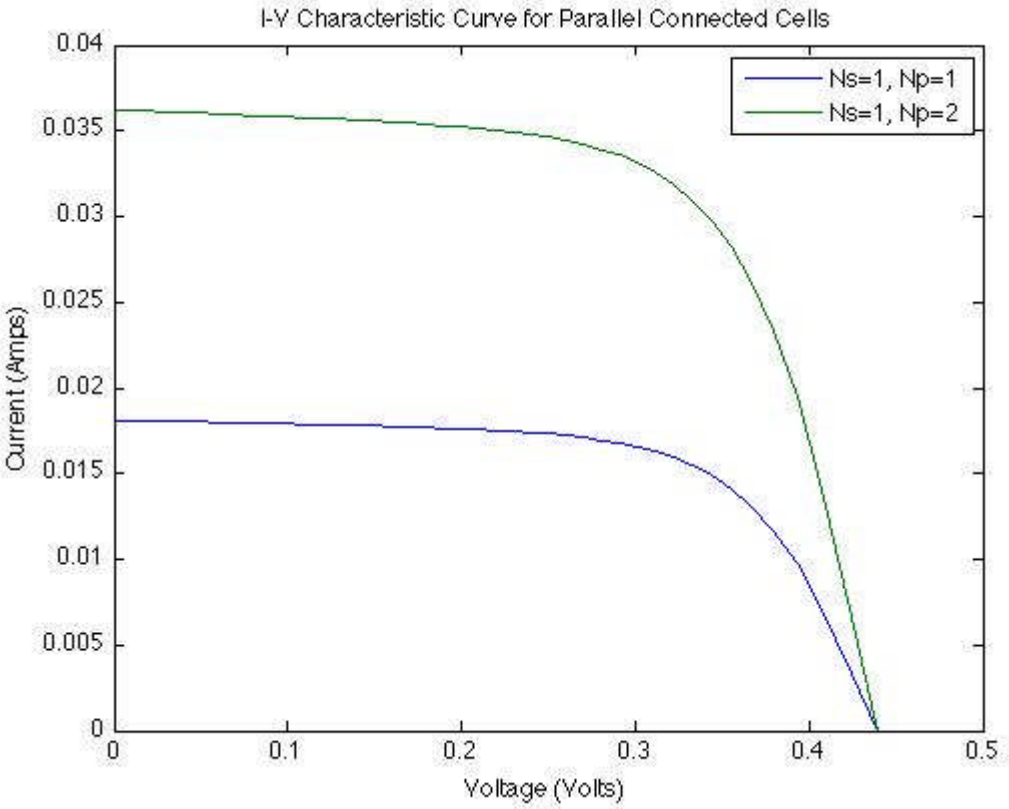

Figure 31: I-V Characteristics of the parallel connected PV cells

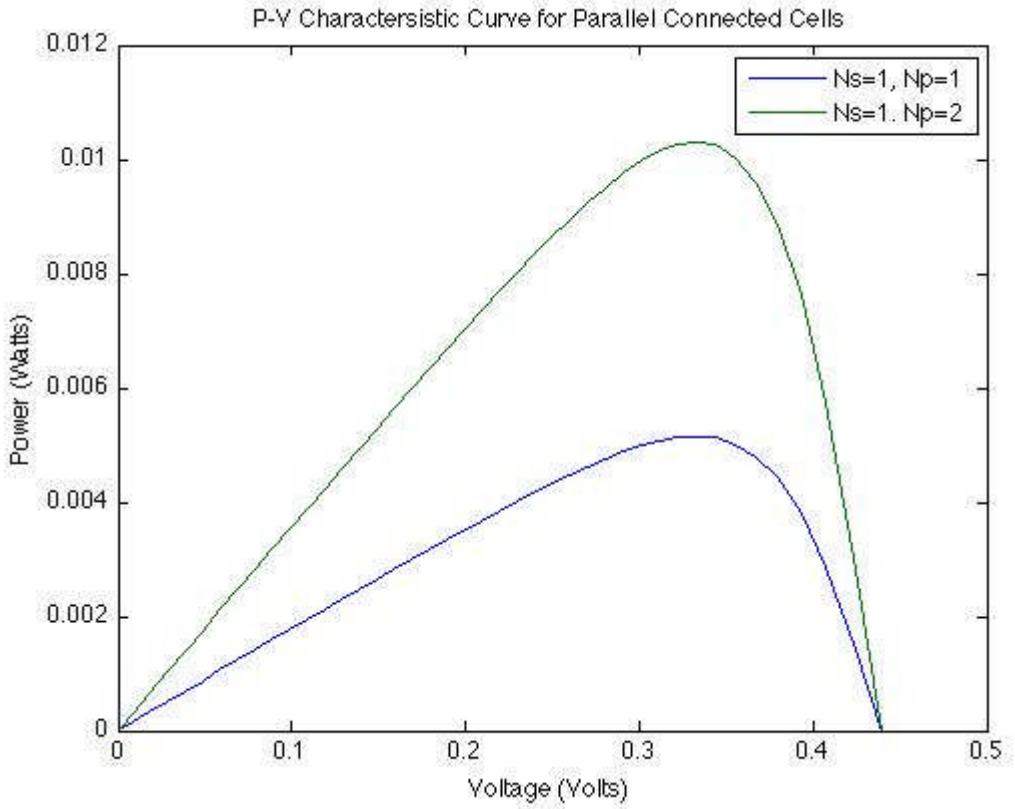

Figure 32: P-V Characteristics of the parallel connected PV cells

The graphs obtained in Figure 31 and Figure 32 represents the I-V characteristic curves and the P-V characteristic curves of the simulated parallel connected PV cells, respectively.

The results of the simulations were summarised in the following table:

Table 11: Result summary of series and parallel connected PV cells

Configuration	Open Circuit Voltage (V)	Maximum Power Point			Short Circuit Current (A)
		Voltage (V)	Current (A)	Power (W)	
Ns=1, Np=1	0.439	0.3329	0.0156	0.0052	0.0181
Ns=2, Np=1	0.878	0.6658	0.0156	0.0104	0.0181
Ns=1, Np=2	0.439	0.3329	0.0312	0.0104	0.0362

It can be seen from Table 11 that the Matlab simulation results in the table correspond with the figures.

The first row displays results for the PV cell, the second row displays results for the two series connected PV cells and the third row displays results for the parallel connected PV cells.

Section 3.1.6 states that with series connected cells, the open circuit voltage increases proportionally with the amount of cells connected in series. The open circuit voltage for the two series connected PV cells is double the open circuit voltage of the single PV cell. The current has only increased slightly and this may be due to the sample step size of the simulation not being perfectly accurate. The power has also doubled in value and from these results we can validate our method of connecting cells in series to increase the voltage alone.

It is stated that for parallel connected cells, the voltage remains the same while the current increases proportionally with the amount of parallel connected cells. It can be seen from the results that this is true with both the MPP current and the short circuit current doubling their values. The voltages have remained the same. This validates our model in the sense of increasing the current by connecting cells in parallel.

5.1.3 PV module results

The PV module consisted of 450 parallel branches of 2500 series connected cells. Results were obtained for various solar irradiances and temperatures in turn. The figure below shows the I-V and P-V characteristics of the simulated PV module at irradiances of 200, 400, 600, 800 and 1000 W/m^2 and temperature of 298^{o}F (25^{o}C).

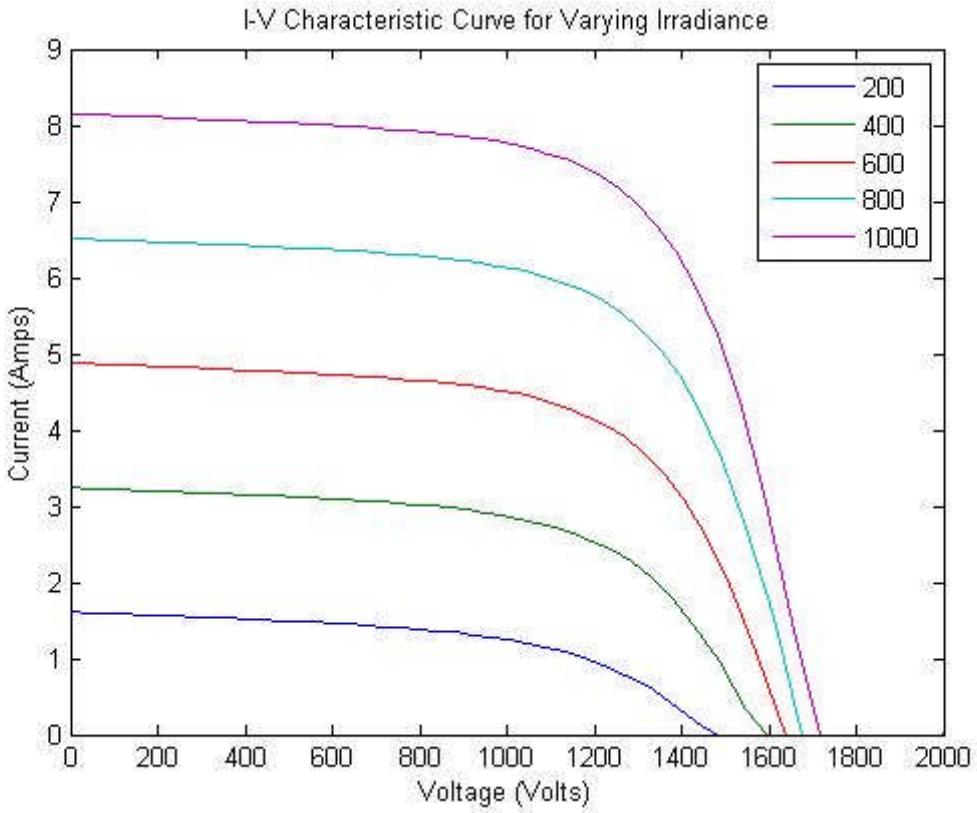

Figure 33: I-V Characteristic curve of the PV module under varying irradiation E

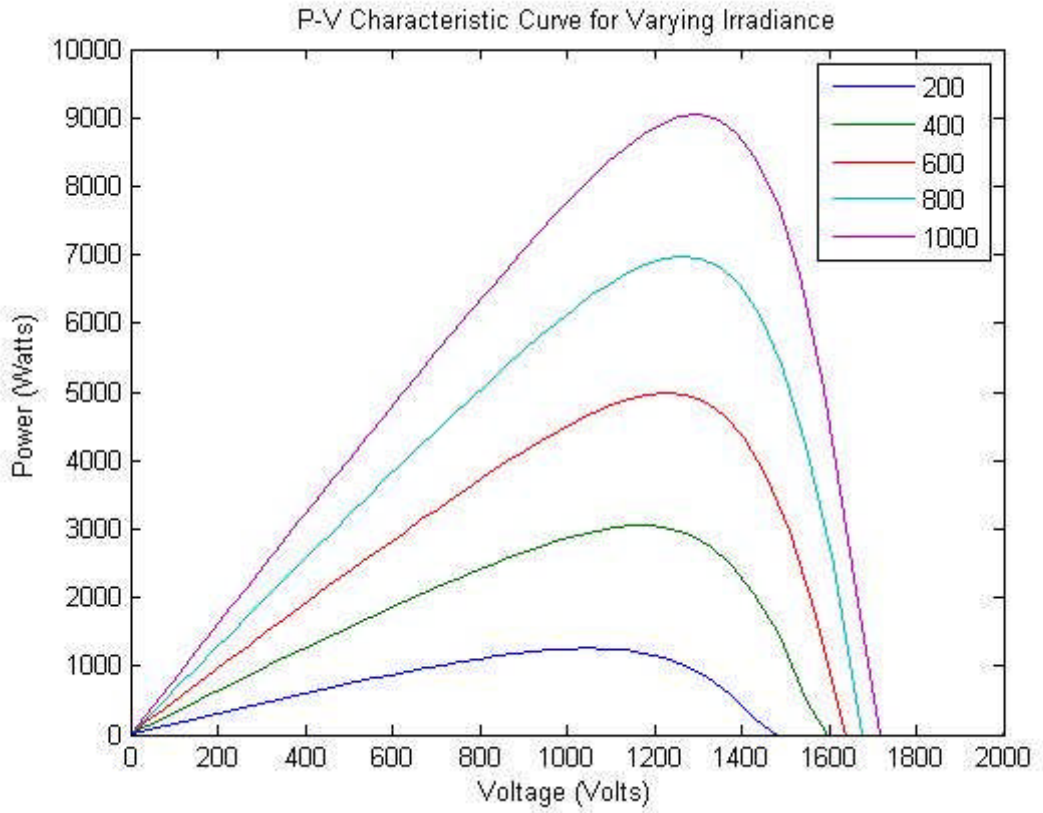

Figure 34: P-V Characteristic curve of the PV module under varying irradiation E

The graphs obtained in Figure 33 and Figure 34 represents the I-V characteristic curve and the P-V characteristic curve of the simulated PV module for a number of irradiances E, respectively. Table 12 displays the values for V_{oc}, V_{mpp}, I_{mpp}, P_{mpp} and I_{sc}. The open circuit voltage and short circuit current determined in Matlab correspond with the figures and the manufacturer's data.

Table 12: Result summary of PV module under varying irradiance E

Irradiance	Open Circuit Voltage	Maximum Power Point			Short Circuit Current
		Voltage	Current	Power	
(W/m²)	(V)	(V)	(A)	(W)	(A)
1000	1716	1298.3	6.97	9048.9	8.145
800	1677	1261.6	5.5382	6987.2	6.525
600	1638	1226.6	4.0604	4980.3	4.86
400	1587	1152.4	2.6461	3049.3	3.24
200	1466	1045.4	1.2048	1259.4	1.62

The PV cell simulation showed these results for a temperature T of 278, 288, 298, 308 and 318°F at an irradiance E of 1000 W/m^2.

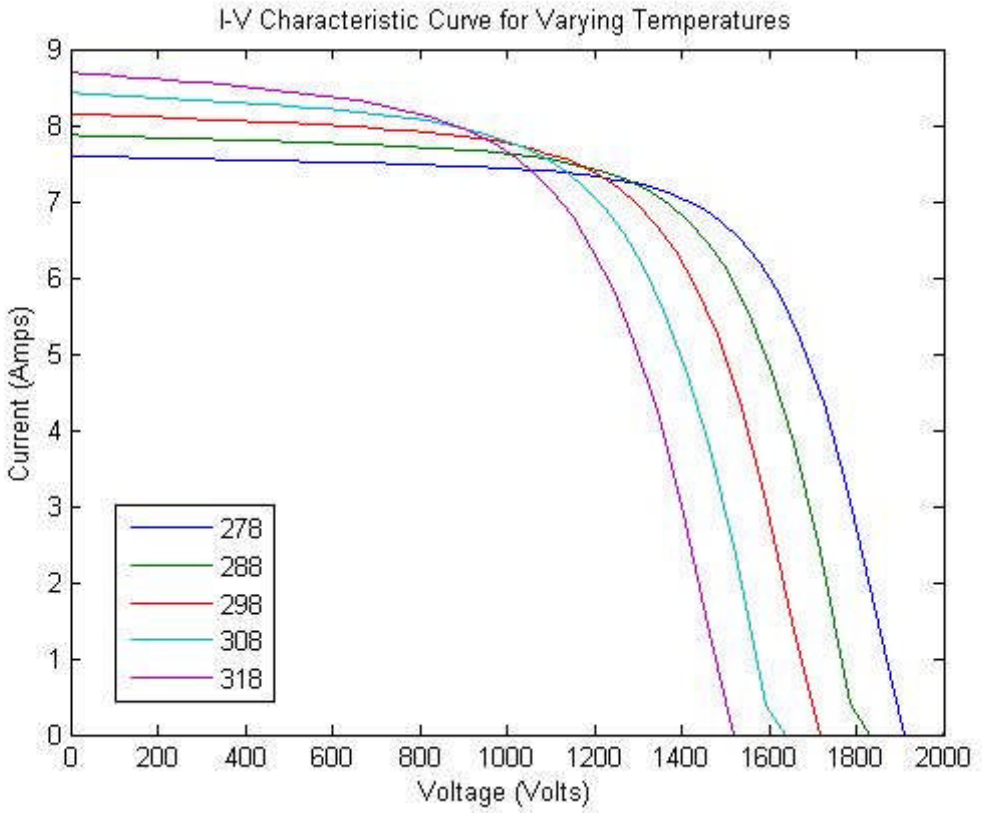

Figure 35: I-V Characteristic curve of the PV module under varying temperature T

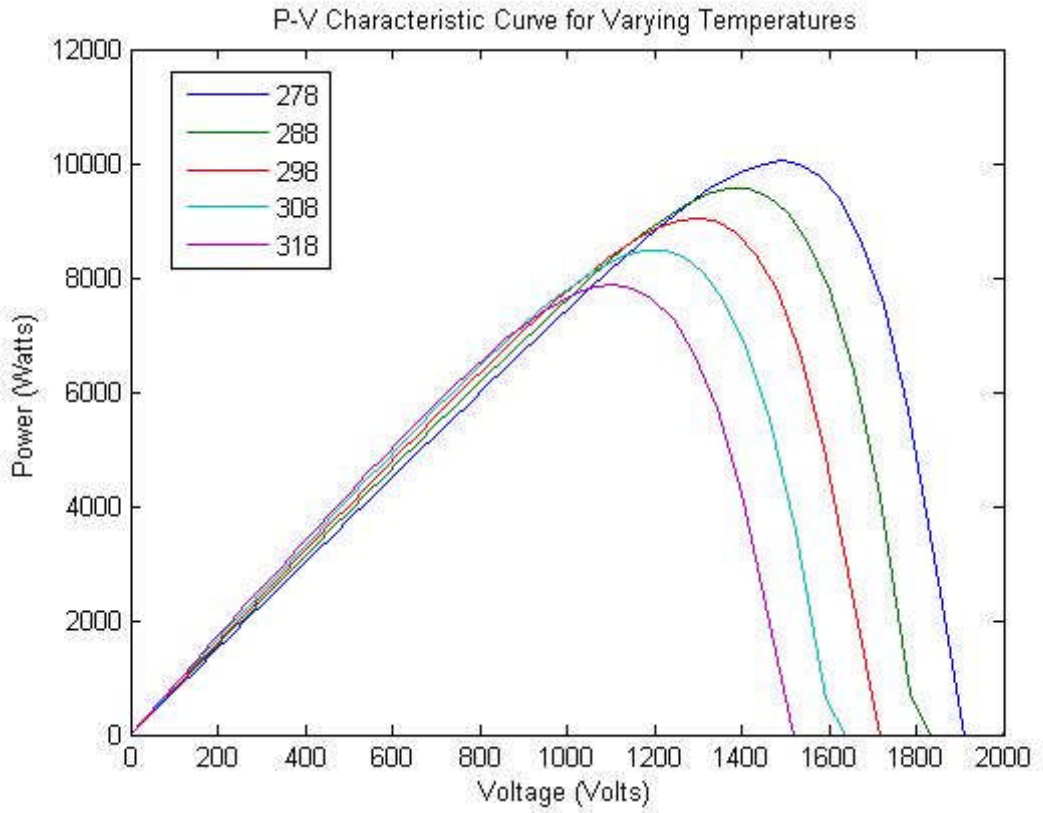

Figure 36: P-V Characteristic curve of the PV module under varying temperature T

The graphs obtained in Figure 35 and Figure 36 represent the I-V characteristic curve and the P-V characteristic curve of the simulated PV module for a number of temperatures T, respectively. Table13 displays the values for V_{oc}, V_{mpp}, I_{mpp}, P_{mpp} and I_{sc}. The open circuit voltage and short circuit current determined in Matlab correspond with the figures and the manufacturer's data.

Table 13: Result summary of PV module under varying temperature T

Temperature	Open Circuit Voltage	Maximum Power Point			Short Circuit Current
		Voltage	Current	Power	
(°K)	(V)	(V)	(A)	(W)	(A)
318	1521	1106.5	7.1185	7877	8.685
308	1618.5	1180.9	7.1764	8475	8.415
298	1712.1	1298.3	6.97	9049	8.145
288	1809.6	1373.7	6.9586	9559	7.875
278	1903.2	1491.7	6.7297	10039	7.605

The above simulated figures take the same form as the simulated I-V and P-V characteristic curves of the PV cell in Section 5.1.1.

5.1.4 Irradiance and temperature effect on voltage and current

In order to determine the relationship between the environmental parameters and the short circuit current and open circuit voltage, the varying irradiance and temperatures were plotted against the PV cell's respective current and voltage. The following figures display the results of the simulation for irradiance and temperature, respectively:

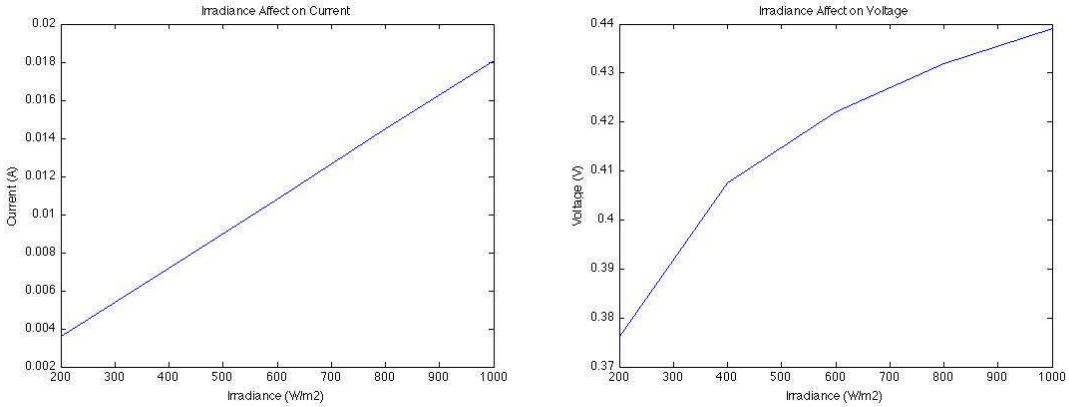

Figure 37: Effect of irradiance E on current and voltage

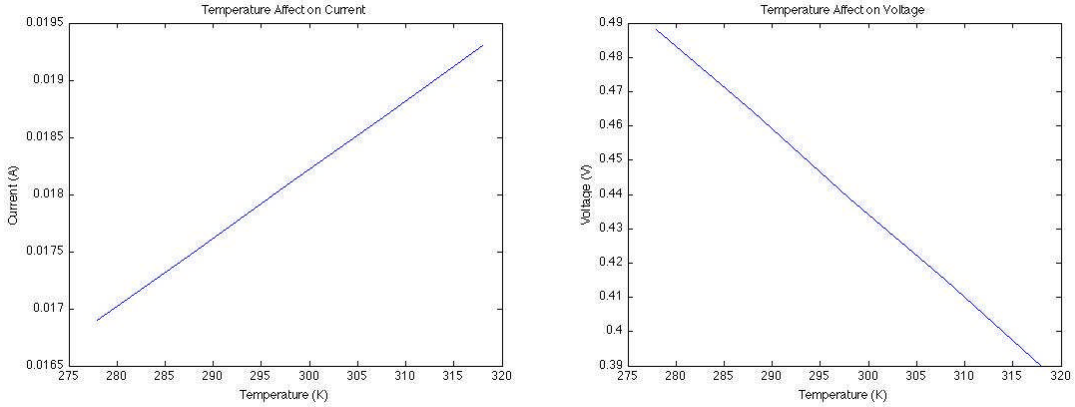

Figure 38: Effect of temperature T on current and voltage

It is observed from Figure 37 and Figure 38 that the PV module short circuit current is dependant and linear with respect to irradiation and temperature. The open circuit voltage can be seen to increase logarithmically with an increase in irradiation. It can also be noted that the open circuit voltage seemingly decreases linearly for an increase in temperature.

The results obtained from the simulation of the PV module are very similar to the results obtained for the validated PV module in [17].

5.2 *MPPT Validation*

The focus of this section is in validating the MPPT model simulations. The MPPT model is required to output the maximum power and the voltage and current at that point. The results obtained for the PV module in of the following design were used in validating the model. The results are presented below.

N_s = 2000;

N_p = 400;

The PV module P-V characteristic curve was modified to show the maximum power value and the corresponding MPP voltage on the x and y-axis respectively. From the value of voltage shown in the P-V characteristic curve, the current was found by performing the same method on the I-V characteristic curve of the PV module. The figures of the modified characteristic curves are shown below.

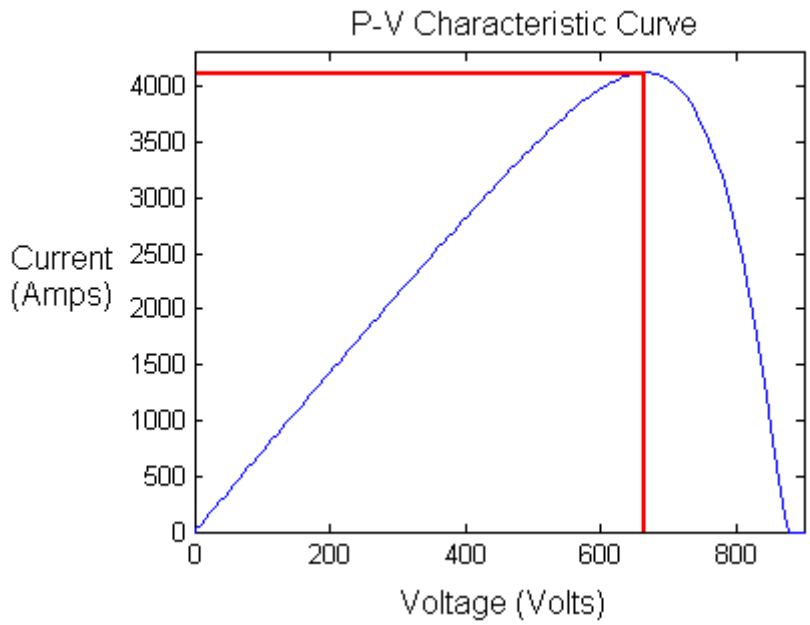

Figure 39: Modified P-V characteristic curve for the MPP model

As can be seen, the maximum power point is found in the region of 4100W on the y-axis. The corresponding voltage value on the x-axis is in the region of 660V.

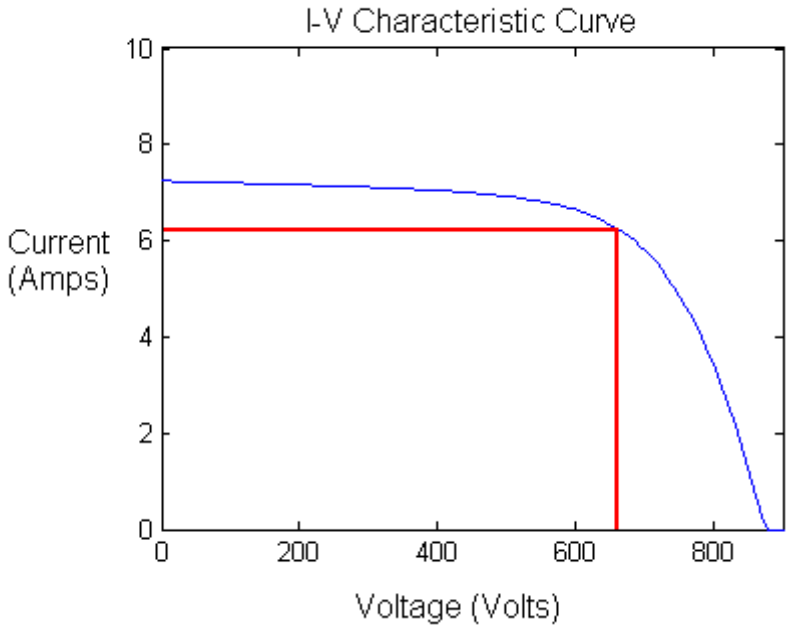

Figure 40: Modified I-V characteristic curve for the MPP model

The voltage value obtained from the modified P-V characteristic curve is superimposed on the I-V characteristic curve in order to find the corresponding MPP current. The MPP current is found to be in the region of 6.2A.

The simulated models for MPPT's results are displayed below in the following figure.

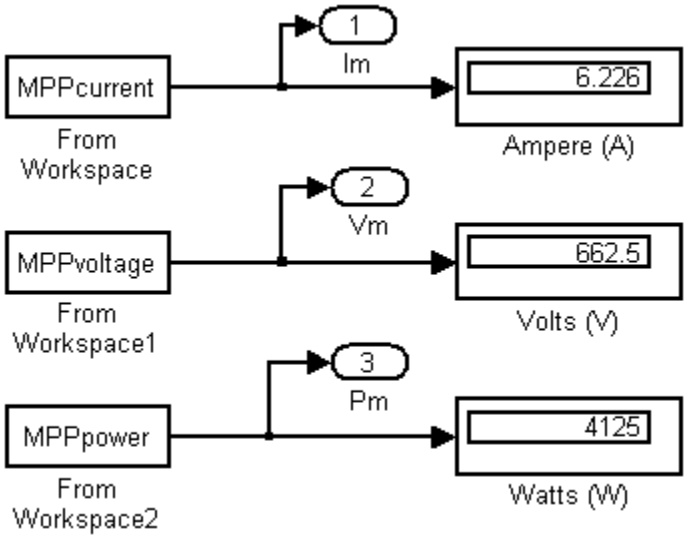

Figure 41: Simulated MPPT model results

The figure above displays the outputs of the MPPT model in the stand-alone PV model system. The results of the simulation agree with both the above figure's results as well as the search results. Therefore, the MPPT model that was simulated can be verified.

5.3 *Battery Energy Storage System (BESS) Validation*

The aim of this section is to validate the battery models proposed in Section 3.3.3. This section contains an examination of the results obtained from the battery model simulations of three different battery chemistries. The lithium-ion model was used to validate the modelling technique against manufacturer's data. Connecting cells in series and parallel and their influence on voltage and current are then investigated. Charging and discharging characteristics of the lithium-ion, nickel-cadmium and lead-acid chemistries were then explored as well as the relationship between the battery cell and the battery model.

5.3.1 Model validation

The lithium-ion model was used to validate the battery modelling technique. The simulation results of the battery cell voltage against the batteries capacity for various discharge and charging currents were compared to manufacturer's data.

The lithium-ion battery cell simulations as well as the manufacturer's data for current discharges of 0.5C, 1C and 2C are shown in Figure 42:

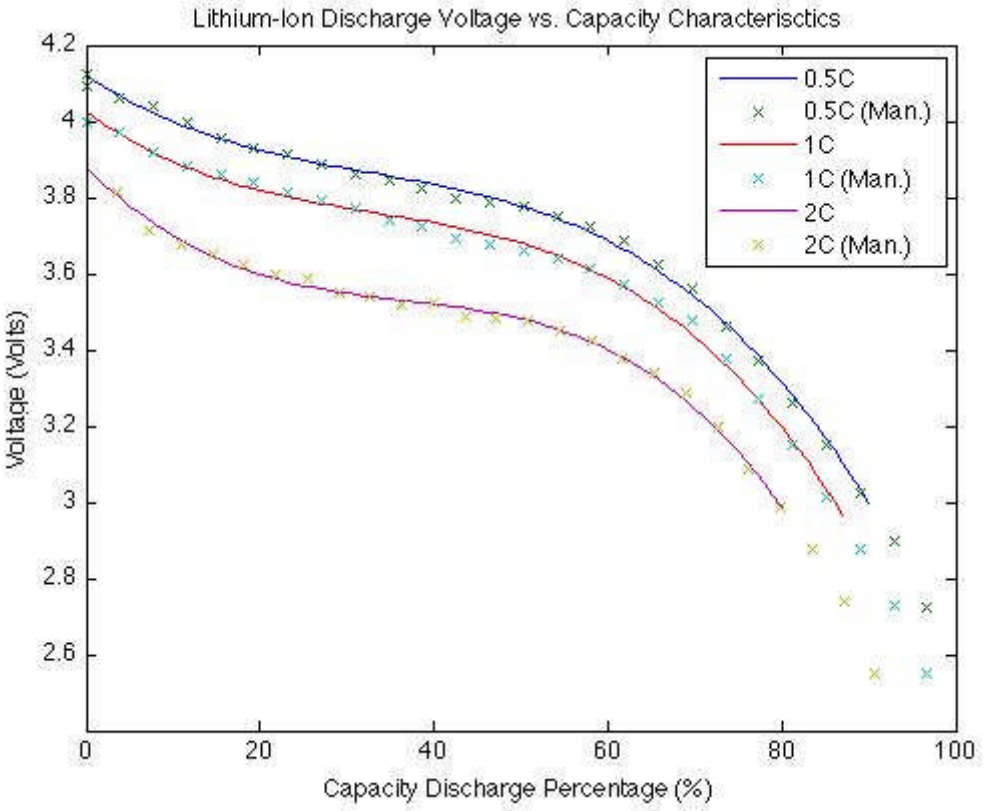

Figure 42: Lithium-Ion discharge voltage against capacity

The Figure 42 represents the lithium-ion batteries discharge curves against the depleted capacity percentage or depth of discharge (DOD). The battery was assumed to be fully charged at the start of the simulation. The simulated results, represented by the solid line, take the same form as the manufacturer's data, represented by the 'x' points.

5.3.2 Series and parallel connected battery cells

The lithium-ion model was used to test our model against the theories presented in Section 3.3.3. The battery cells were connected in series and parallel, respectively, and their voltages and power were then plotted against their depth of discharge (DOD) and voltage. The results were then examined where:

N_s = number of series connected cells;

N_p = number of parallel connected cells.

The results obtained for two lithium-ion battery cells connected in series are displayed in Figure 43 below.

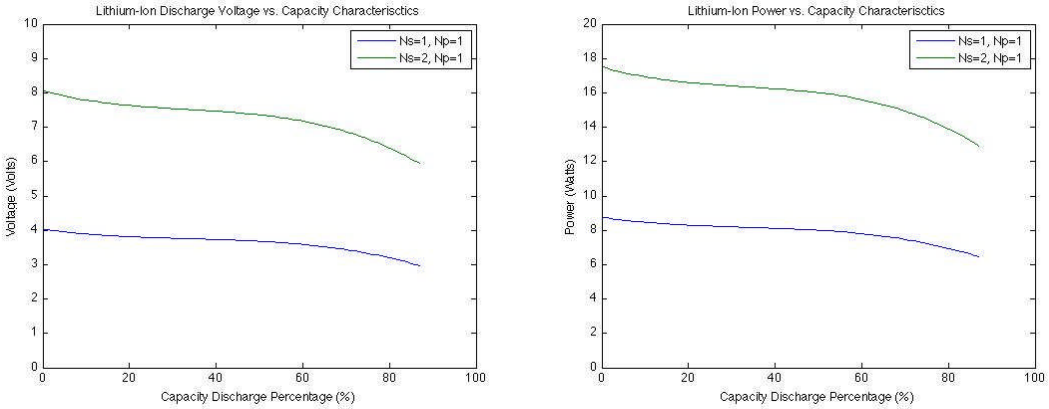

Figure 43: Lithium-Ion voltage and power against depth of discharge (DOD) for series connected cells

The results obtained from the simulation for cells connected in parallel are displayed in Figure 44 below.

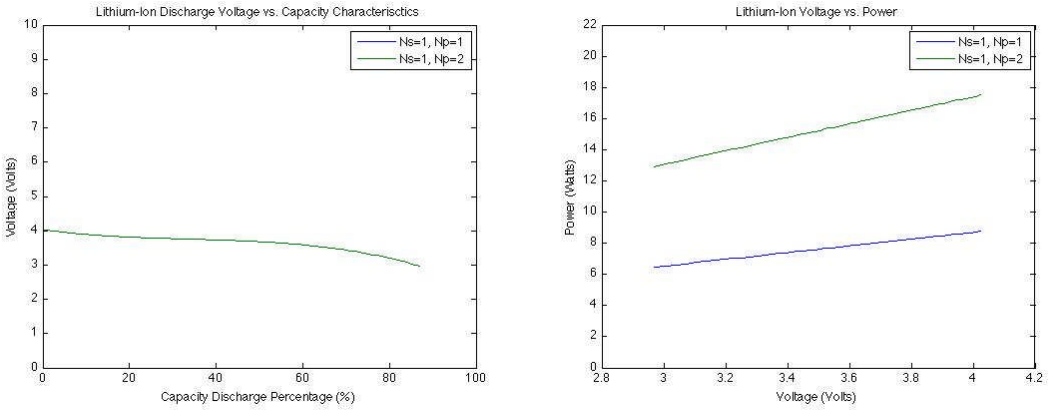

Figure 44: Lithium-Ion voltage against depth of discharge (DOD) and power against voltage for parallel connected cells

The results obtained from the simulations are summarised in the following table 14:

Table 14: Result Summary of series and parallel connected cells

Configuration	Voltage		Power		ΔPower (W)	Current (A)
	Start (V)	End (V)	Start (W)	End (W)		
Ns = 1, Np = 1	4.0229	2.9681	8.7498	6.4557	2.2941	2.175
Ns = 2, Np = 1	8.0458	5.9362	17.4996	12.9114	4.45882	2.175
Ns = 1, Np = 2	4.0229	2.9681	17.4996	12.9114	4.45882	4.35

It can be seen from Table 14, Figure 43 and Figure 44 that the Matlab simulation results correspond with the figures.

The first row displays the results for the lithium-ion cell, the second row displays results for two series connected cells and the third row displays results for the parallel connected cells.

It is stated in Section 3.3.3 that by connecting cells in series, the voltage increases proportionally to the amount of cells connected in series. A comparison of row 1 and row 2 of Table 14 that the voltages at the start time, fully charged cell, and at the end time, fully discharged cell, have doubled when the two cells have been connected in series however, the current has remained the same. The power has also doubled in value and from these results we can validate our method of connecting cells in series to increase the voltage and power alone.

It is also stated that by connecting cells in parallel, the current will increase in proportion to the amount of cells connected in parallel. By comparing row 1 and row 3 of Table 14 we can see that the voltages have remained the same however, the current and the power have doubled in value. From these results we can validate our model in the sense of increasing the current and power by connecting cells in parallel

5.3.3 Lithium-ion

In this section we will explore the discharge and charging characteristics that define the lithium-ion battery. The battery is modelled as a single cell and then as a module made up of cells connected in series and parallel.

Discharge Characteristics

The single lithium-ion cell was tested for various discharge rates (C-rates) and their influence on the discharge voltage, current and power was investigated. The cells were discharged until they reached their cut-off voltage of 3V.

The simulation results for cell voltage at discharge rates of 0.2C, 0.5C, 1C and 2C are plotted against depth of discharge (DOD) and displayed below in Figure 45.

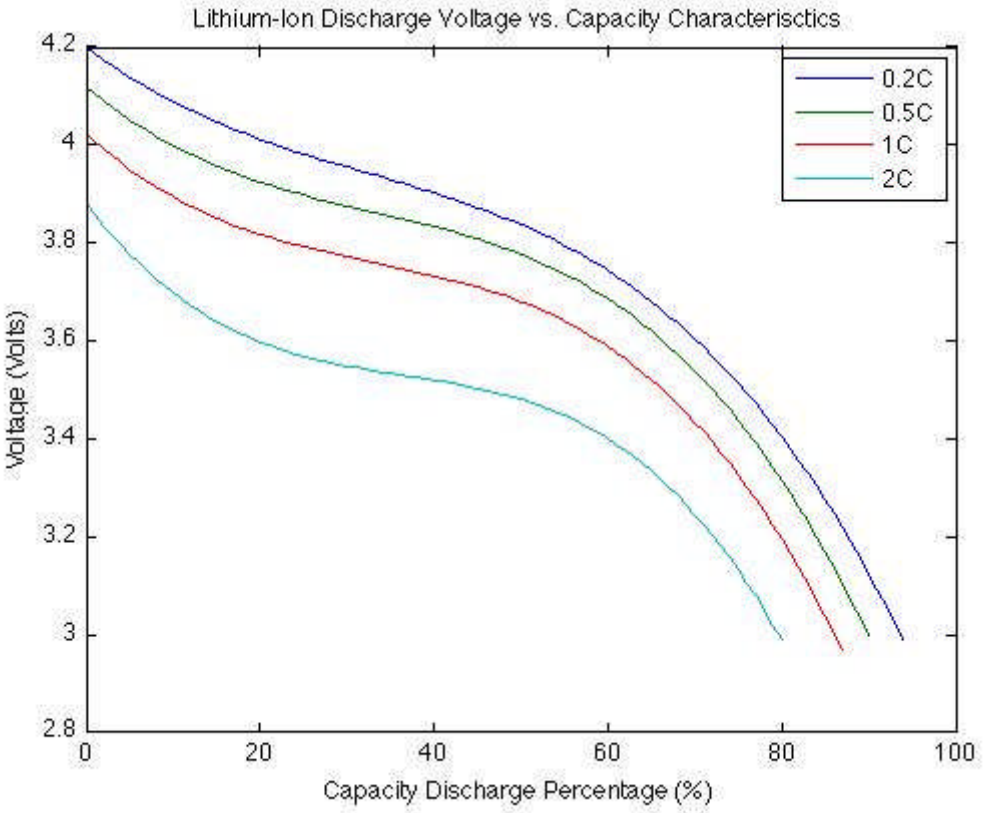

Figure 45: Lithium-Ion cell discharge voltage against depth of discharge (DOD)

The results of the simulations are summarised below in Table 15.

Table 15: Result summary of lithium-ion cell discharge voltage characteristics

C-Rate	Discharge Time (Hours)	Discharge Voltage at 0% DOD (Volts)	Discharge Current (Ampere)	Maximum Capacity at Cut-off (Ampere Hours)	Maximum Capacity (% of Full)
0.2	5	4.2	0.47	2.350	94
0.5	2	4.1188	1.125	2.250	90
1	1	4.0229	2.175	2.175	87
2	0.5	3.88	4	2.000	80

It can be seen that the results obtained for the Matlab simulations and from Figure 45 agree. It can be noted that as the C-rate increases, a decrease in the discharge voltage and the maximum capacity is experienced. The depth of discharge (DOD) of the battery is decreased as the discharge rate (C-rate) increases. However, the discharge current is increased with a faster C-rate. The decrease in maximum capacity with an increase in discharge current can be explained due to the cell not being able discharge these higher currents over the entire capacity of the battery. This results in a new maximum capacity, which can be seen in column 5 of Table 15, and decreases as the discharge current is

increased. This ultimately results in a new, practical C-rate which accurately accounts for the discharge time. The new C-rates of the cell under these conditions is summarised in the table below:

Table 16: Actual lithium-ion C-rate

Manufacturer's Data		Actual Data		ΔC-Rate (%)
C-Rate	Discharge Time (Hours)	C-Rate	Discharge Time (Hours)	
0.2	5	0.213	4.7	106.5
0.5	2	0.556	1.8	111.2
1	1	1.149	0.87	114.9
2	0.5	2.5	0.4	125

In Table 16 we can see the original manufacturer's discharge rates (C-rates) and compare them to the actual discharge rates (C-rates) experienced by the cell. The actual discharge rates are found to be larger than the manufacturer's discharge rates which results in a shorted discharge period.

The simulation results for the power discharged by the cell for discharge rates (C-rates) of 0.2C, 0.5C, 1C and 2C are displayed below in Figure 46.

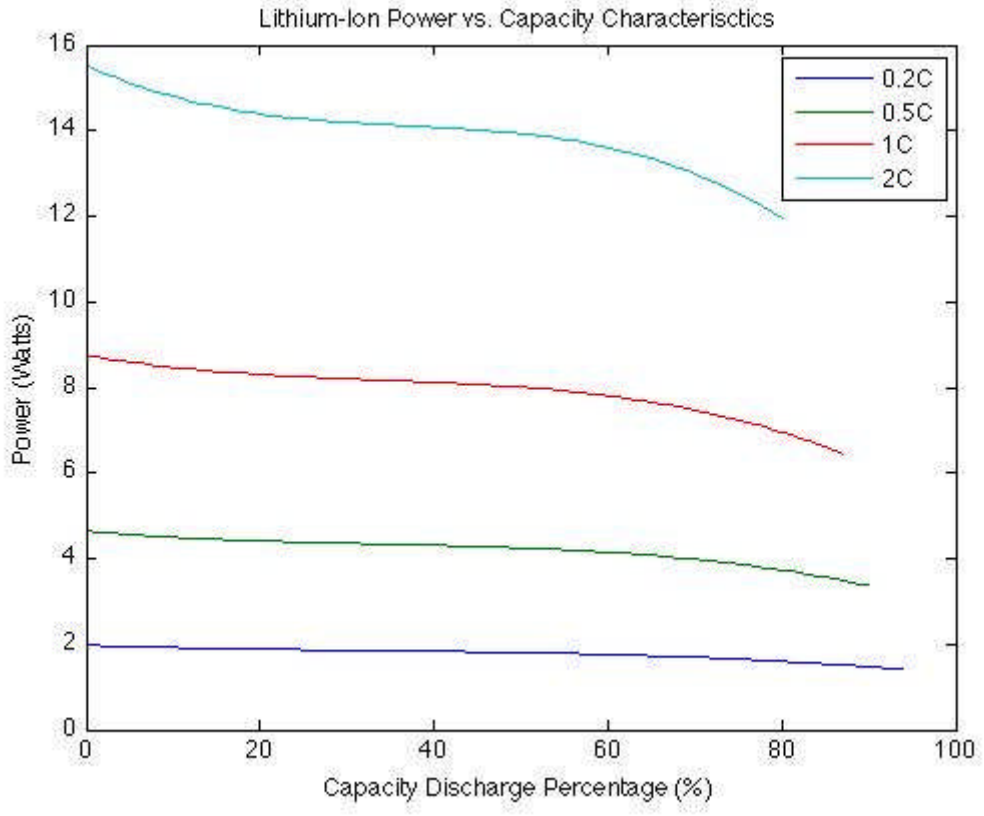

Figure 46: Lithium-Ion cell discharge power against depth of discharge (DOD)

The results of the simulation are summarised below in Table 17.

Table 17: Result summary of lithium-ion cell discharge power characteristics

C-Rate	Discharge Time (Hours)	Discharge Power at 0% DOD (Watts)	Discharge Power Final (Watts)	Δ Discharge Power (%)
0.2	5	1.974	1.4058	71.2
0.5	2	4.6337	3.3716	72.8
1	1	8.7498	6.4557	73.8
2	0.5	15.52	11.9563	77.1

It can be seen that the results obtained for the Matlab simulations and from Figure 46 agree. It is noted that the power discharged by the battery decreases as the depth of discharge (DOD) increases. The change in discharge power, represented in row 5 of Table 17, can also be seen increasing as the discharge rate (C-rate) increases. This leads us to believe that the smaller the rate of discharge, the bigger the difference in the power values obtained at 0% depth of discharge (DOD) and at final discharge. Hence, we can deduce that the smaller the rate of discharge (C-rate) exerted on the cell, the more 'unstable' the discharge power is. In reality this is not true as the higher the C-rate, the smaller the difference in powers is even though the change is larger. It is also noted that as the discharge rate (C-rate) increases, so does the power discharged. Another observation is that the current discharged remains constant for fluctuating values of voltage and power. This results in the power discharge curve taking the same form as that of the voltage discharge curve.

The lithium ion battery cell was simulated into a module by connecting cells in series and parallel to produce a desired output. The parameters were as follows:

Ns = 120 cells;

Np = 11 cells.

This resulted in the discharge curves shown in Figure 47 and Figure 48 for discharge rates (C-rates) of 0.2C, 0.5C, 1C and 2C.

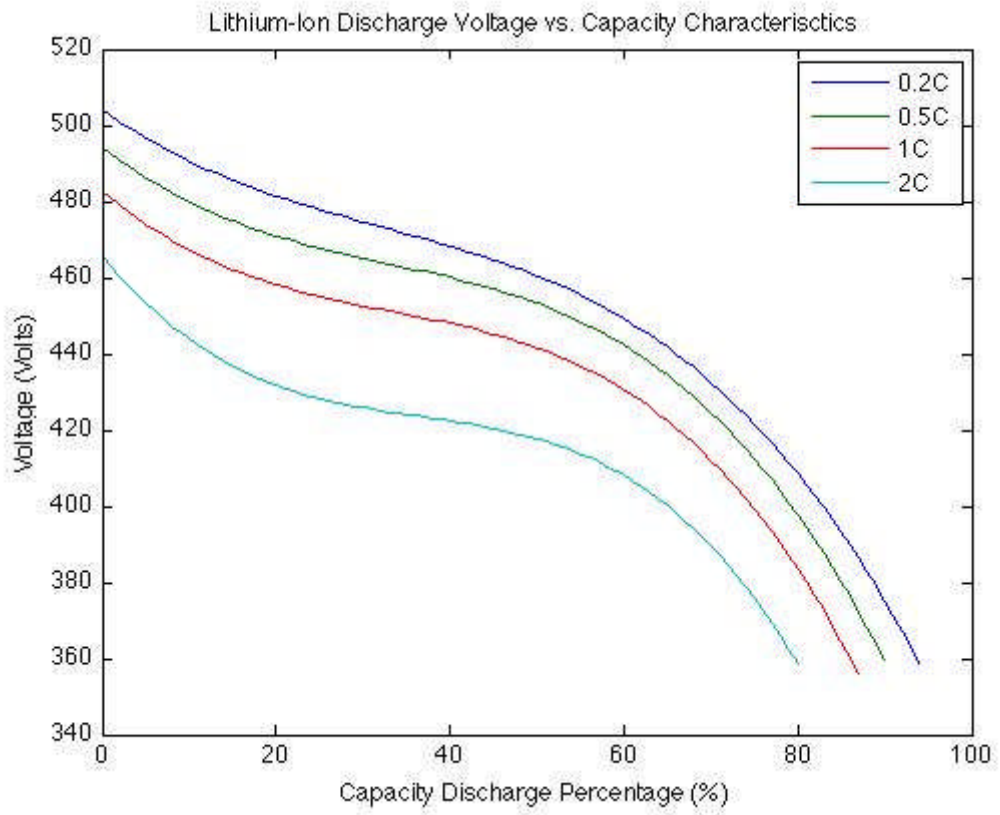

Figure 47: Lithium-Ion module discharge voltage against depth of discharge (DOD)

The results of the simulation were summarized in the following Table 18.

Table 18: Result summary of lithium-ion module discharge voltage characteristics

C-Rate	Discharge Time (Hours)	Discharge Voltage at 0% DOD (Volts)	Discharge Current (Ampere)	Maximum Capacity at Cut-off (Ampere Hours)	Maximum Capacity (% of Full)
0.2	5	504	11.47	25.850	94
0.5	2	494.3	12.38	24.750	90
1	1	482.7	23.93	23.925	87
2	0.5	465.6	44	22.000	80

It can be seen that the results obtained for the Matlab simulations and from figures agree. By comparing the results obtained for the cell and the module in, we can see that the theory of connecting cells in series and parallel has again been validated. The results for the module are scaled values of the results for the cell. The discharge voltage has increased in proportion to Ns (cells in series) and the discharge current and maximum capacity has increased in proportion to Np (cells in parallel). The new actual C-rates are found to be the same as those for the cell simulation.

The simulation results for the power discharged by the module for discharge rates (C-rates) of 0.2C, 0.5C, 1C and 2C are displayed below.

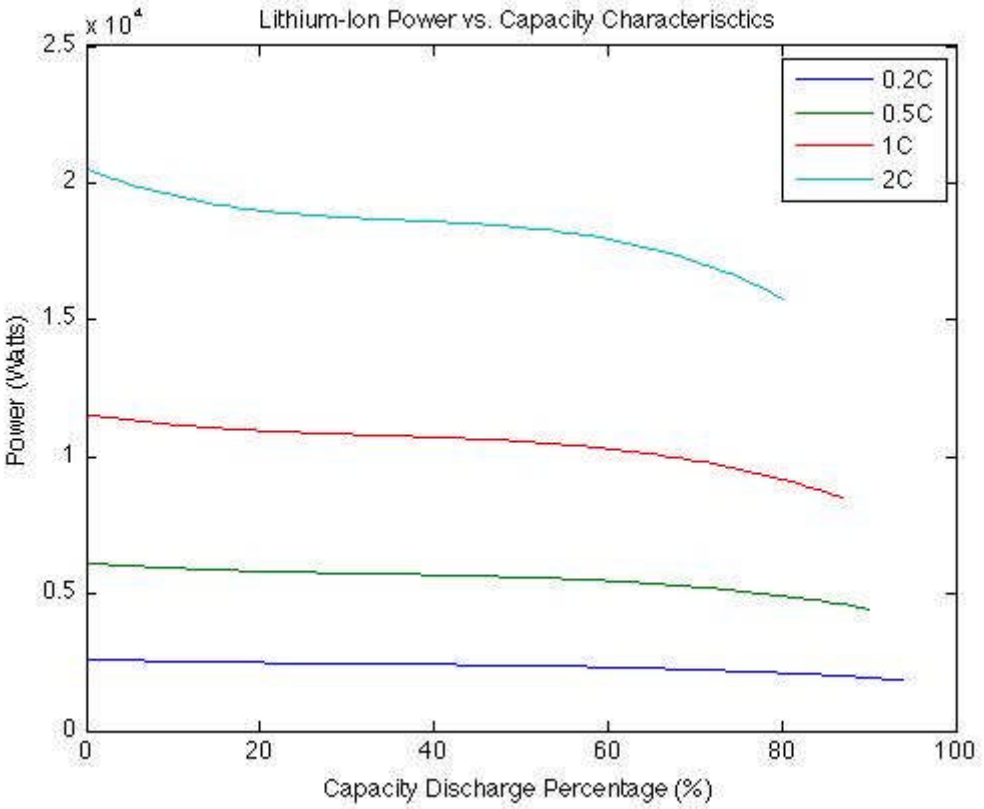

Figure 48: Lithium-Ion module discharge power against depth of discharge (DOD)

The results for the simulation have been summarized in Table 19.

Table 19: Result summary of lithium-ion module discharge power characteristics

C-Rate	Discharge Time (Hours)	Discharge Power at 0% DOD (Watts)	Discharge Power Final (Watts)	Δ Discharge Power (%)
0.2	5	2605.7	1855.7	71.2
0.5	2	6116.4	4450.5	72.8
1	1	11550	8521.5	73.8
2	0.5	20486	15782	77.1

By comparing Table 17 and Table 19, we can see that the power has increased in proportion to the product of the number of cells connected in series and parallel. The power discharged in 0.2C is seen as having the smallest actual power change (750W) for the different rates of discharge (C-rates) but produces the least quantity of instantaneous power to the system.

The lithium-ion module is seen as having the same characteristics as that of the lithium-ion cell, while increasing the voltage and currents discharged results in an increased power discharge.

Charge Characteristics

The lithium-ion charging characteristics were investigated for the charging protocol of CC-CV (constant current – constant voltage) charging. The influence charging has on the voltage and current of the cell are determined.

The CC-CV charging protocol consists of two phases. The first phase consists of charging the cell with a constant current of 1.4A until the cell voltage reaches its maximum voltage of 4.2V. The cell is then charged with a constant voltage of 4.2V until the cell is fully charged.

The results obtained for the simulation of a 2.5 hour CC-CV charging protocol on the lithium-ion cell are displayed below.

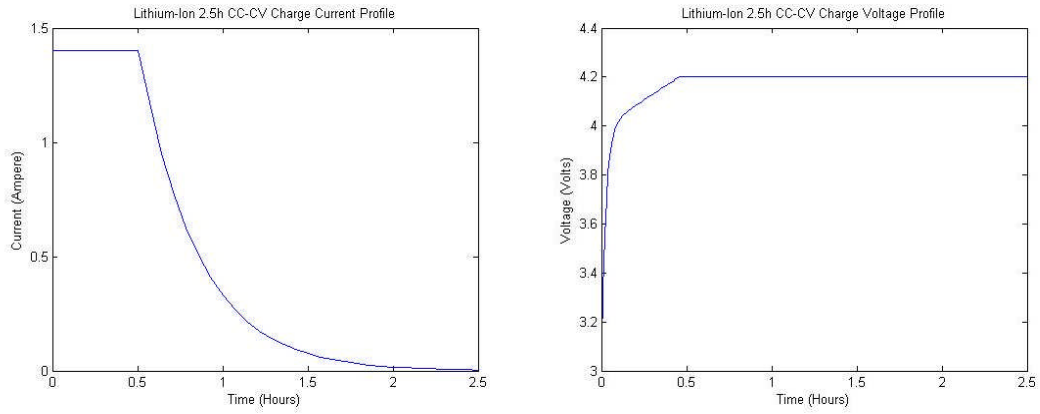

Figure 49: Lithium-Ion 2.5 hour CC-CV charging protocol for current and voltage

It can be seen from Figure 49 that the current is initially kept constant at 1.4A until the voltage reaches its maximum of 4.2V at 0.5 hours. The voltage then remains at 4.2V while the current decreases exponentially to 0A until the cell is fully charged. It is found that the cell reaches 50% fully charged at time 0.47 hours.

5.3.4 Nickel-cadmium

In this section we will explore the discharge and charging characteristics that define the nickel-cadmium battery. The battery is modelled as a single cell and then as a module made up of cells connected in series and parallel. The section takes the same form as that of the lithium-ion cell.

Discharge characteristics

The single nickel-cadmium cell was tested for various discharge rates (C-rates) and their influence on the discharge voltage, current and power was investigated. The cells were discharged until they reached their cut-off voltage of 1V.

The simulation results for cell voltage at discharge rates of 01.C, 0.2C, 0.5C and 1C are plotted against depth of discharge (DOD) and displayed below.

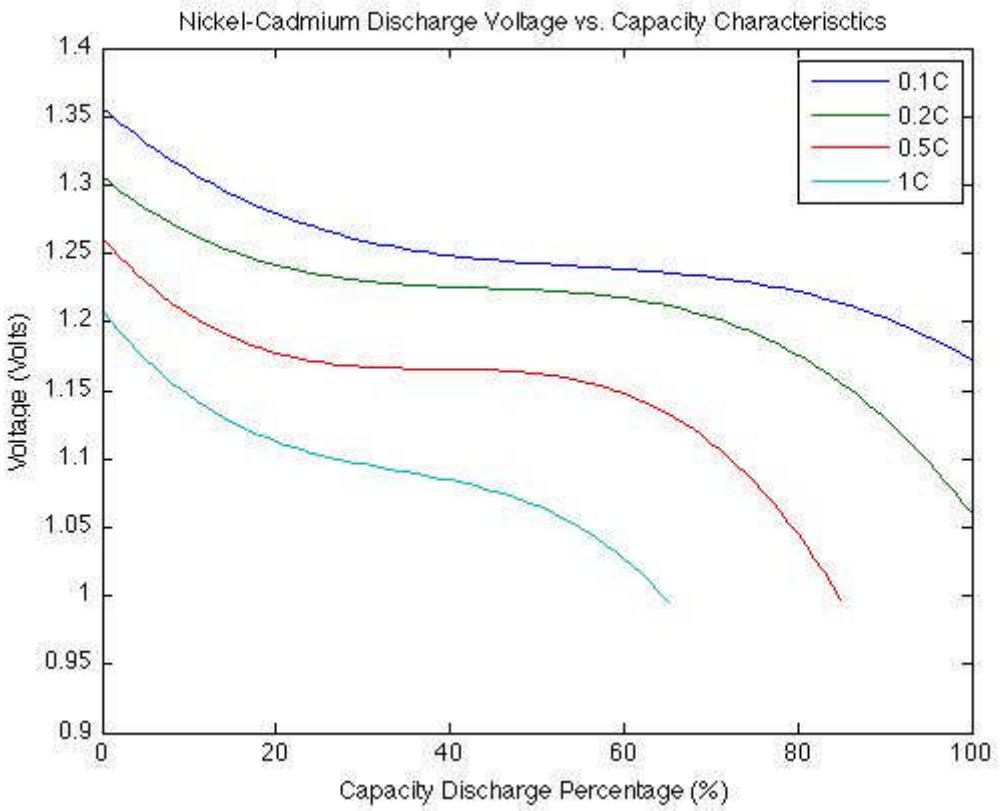

Figure 50: Nickel-Cadmium cell discharge voltage against depth of discharge (DOD)

The results of the simulations are summarised below in Table 20.

Table 20: Result summary of nickel-cadmium cell discharge voltage characteristics

C-Rate	Discharge Time (Hours)	Discharge Voltage at 0% DOD (Volts)	Discharge Current (Ampere)	Maximum Capacity at cut-off (Ampere Hours)	Maximum Capacity (% of Full)
0.1	10	1.3564	0.5	2.500	100
0.2	5	1.3056	1	2.375	95
0.5	2	1.261	2.125	2.125	85
1	1	1.2084	3.25	1.625	65

It can be seen that the results obtained for the Matlab simulations and from Figure 50 agree. With an increase in the C-rate, we can see a decrease in the discharge voltage and the maximum capacity. The depth of discharge (DOD) also decreases with an increase of discharge rate (C-rate), which is found to influence an increase in the discharge current. This is much like the discharge characteristics of the lithium-ion battery. The new actual discharge rates (C-rates) are summarized in the table 21 below.

Table 21: Actual nickel-cadmium C-rate

Original Data		New Data		ΔC-Rate (%)
C-Rate	Discharge Time (Hours)	C-Rate	Discharge Time (Hours)	
0.1	10	0.1	10	100
0.2	5	0.211	4.75	105.3
0.5	2	0.588	1.7	117.6
1	1	1.538	0.65	153.8

In Table 21 we can see the original manufacturer's discharge rates (C-rates) and compare them to the actual discharge rates (C-rates) experienced by the cell. The actual discharge rates are found to be larger than the manufacturer's discharge rates which results in a shorter discharge period. This takes the same form as the actual C-rates calculated for the lithium-ion cell. It is noted that while the 0.2C discharge C-rate is found to be better than the lithium-ion's, the 0.5C and the 1C rates are found to be increasingly worse.

The simulation results for the power discharged by the cell for discharge rates (C-rates) of 0.1C, 0.2C, 0.5Cand 1C are displayed below in Figure 51.

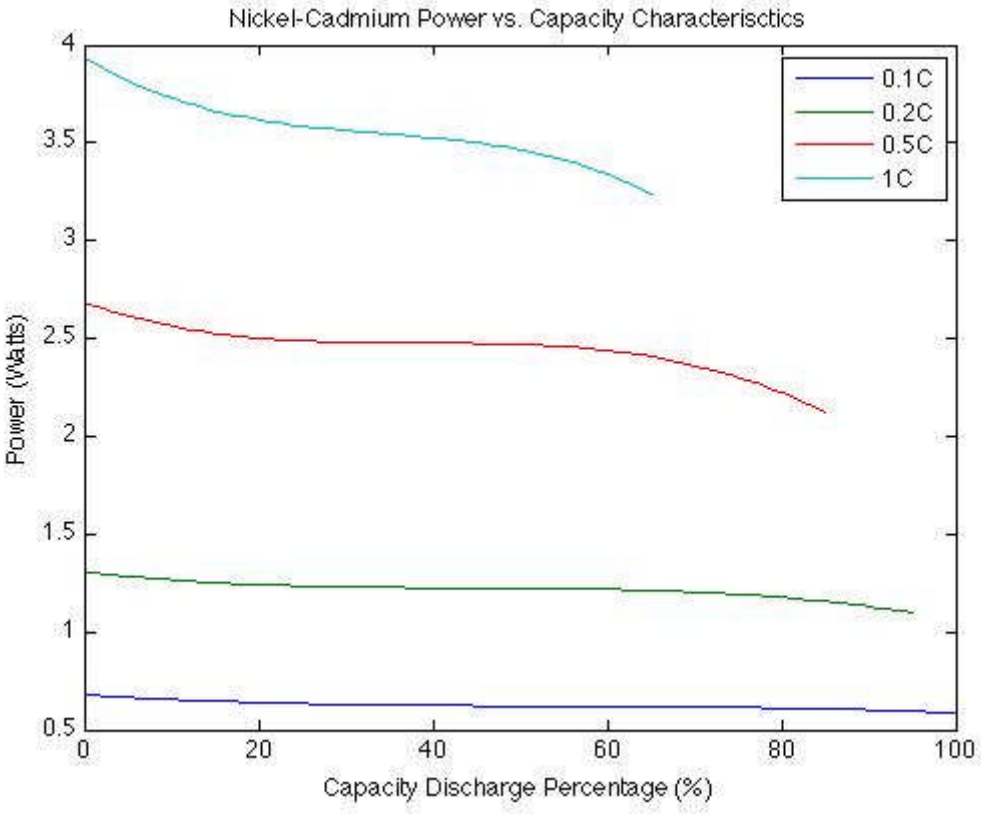

Figure 51: Nickel-Cadmium cell discharge power against depth of discharge (DOD)

The results of the simulation are summarised below in Table 21.

Table 21: Result summary of nickel-cadmium cell discharge power characteristics

C-Rate	Discharge Time (Hours)	Discharge Power at 0% DOD (Watts)	Discharge Power Final (Watts)	Δ Discharge Power (%)
0.1	10	0.6782	0.586	86.4
0.2	5	1.3056	1.0979	84.1
0.5	2	2.6796	2.1185	79.1
1	1	3.9273	3.2386	82.5

It can be seen that the results obtained for the Matlab simulations and from Figure 51 agree. It is seen that the only difference between the lithium-ion and nickel-cadmium discharge power characteristics are the Δ Discharge Power's. The percentage values found for nickel-cadmium were found to be higher than the corresponding lithium-ion percentages. This can be seen in the discharge voltage graph. The nickel-cadmium curves are noted as being flatter which results in a smaller change in voltage, and as the current remains constant the power is directly proportional to the voltage form. Unlike the lithium-ion, the percentage decreases with increasing discharge rate (C-rate). The 0.5C rate is seen as having a greater difference in power as the 1C rate. This can be a result of the 0.5C rate having been cut-off at a higher depth of discharge then 1C. As the depth of discharge (DOD) increases, it is noted that the voltages drop at a higher rate, this shows the 1C discharge did not discharge for much of its depth of discharge

The nickel-cadmium battery cell was simulated into a module by connecting cells in series and parallel to produce a desired output. The parameters were as follows:

Ns = 383 cells;

Np = 5 cells.

This resulted in the discharge curves shown in Figure 52 and Figure 53 for discharge rates (C-rates) of 0.1C, 0.2C, 0.5C and 1C.

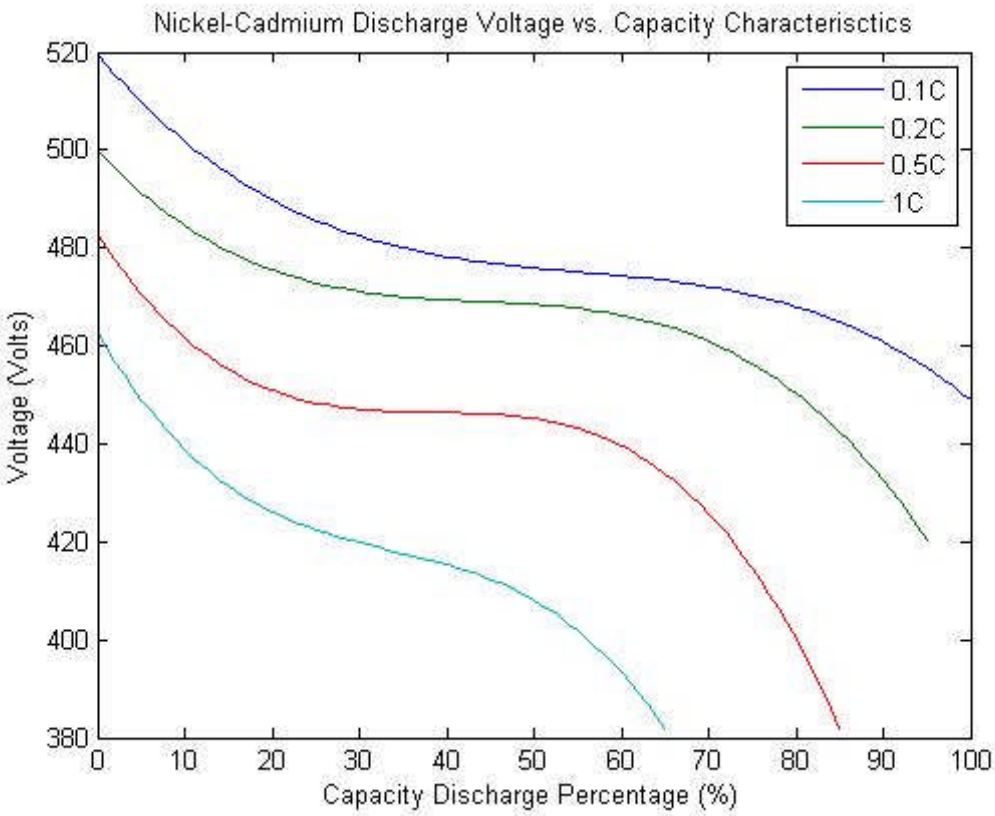

Figure 52: Nickel-Cadmium module discharge voltage against depth of discharge (DOD)

The results of the simulation were summarized in the following Table 22.

Table 22: Result summary of nickel-cadmium module discharge voltage characteristics

C-Rate	Discharge Time (Hours)	Discharge Voltage at 0% DOD (Volts)	Discharge Current (Ampere)	Maximum Capacity at cut-off (Ampere Hours)	Maximum Capacity (% of Full)
0.1	10	519.5	2.5	12.50	100
0.2	5	500	5	11.875	95
0.5	2	482.9	10.625	10.605	85
1	1	462.8	16.25	8.125	65

It can be seen that the results obtained for the Matlab simulations and from Figure 22 agree. The results for the module are scaled values of the results for the cell. The discharge voltage has increased in proportion to Ns (cells in series) and the discharge current and maximum capacity has increased in proportion to Np (cells in parallel). The new actual C-rates are found to be the same as those for the cell simulation.

The simulation results for the power discharged by the module for discharge rates (C-rates) of 0.2C, 0.5C, 1C and 2C are displayed below in Figure 53.

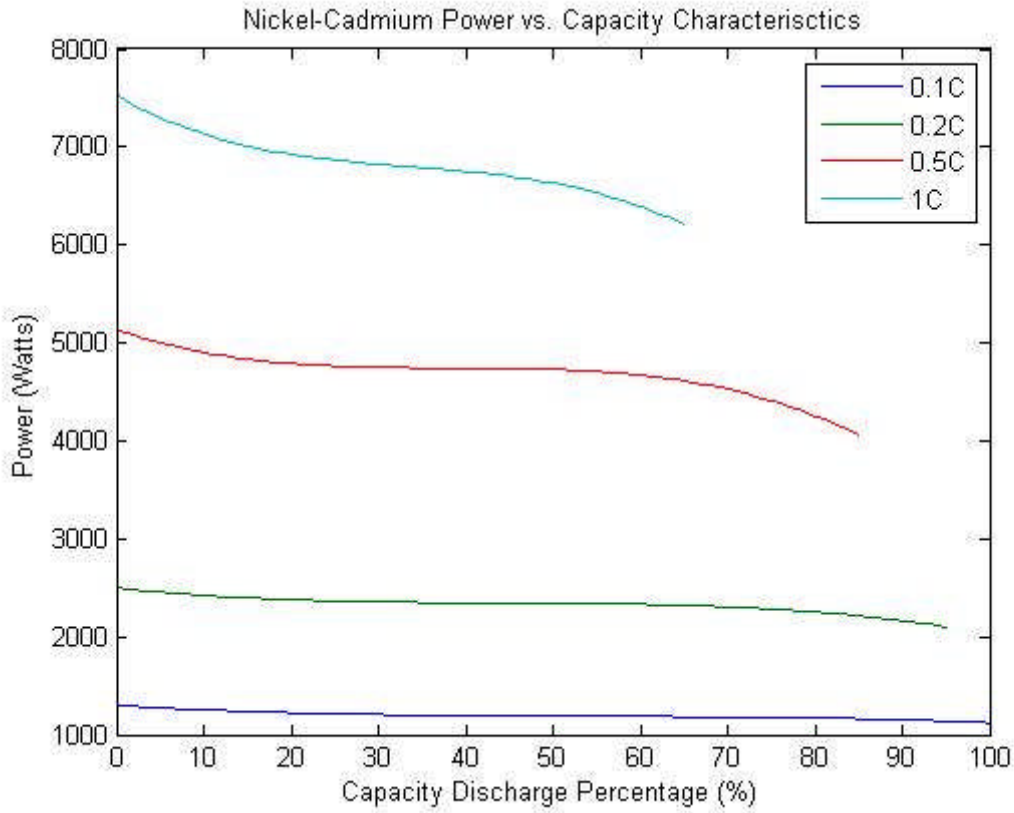

Figure 53: Lithium-Ion module discharge power against depth of discharge (DOD)

The results for the simulation have been summarized in Table 23.

Table 23: Result summary of nickel-cadmium module discharge power characteristics

C-Rate	Discharge Time (Hours)	Discharge Power at 0% DOD (Watts)	Discharge Power Final (Watts)	Δ Discharge Power (%)
0.1	10	1298.8	1122.3	86.4
0.2	5	2500.2	2102.5	84.1
0.5	2	5131.5	4056.9	79.1
1	1	7520.8	6201.9	82.5

By comparing Table 22 and Table 23, we can see that the power has increased in proportion to the product of the number of cells connected in series and parallel. The power discharged in 0.1C is seen as having the smallest actual power change (176.5W) for the different rates of discharge (C-rates) but produces the least quantity of instantaneous power to the system.

The nickel-cadmium module is seen as having the same characteristics as that of the nickel-cadmium cell, while increasing the voltage and currents discharged results in an increased power discharge.

Charge Characteristics

The nickel-cadmium cell charging characteristics were investigated for the charging protocol of CC (constant current) charging. The influence the charging has on the voltage is determined.

The CC charging protocol charges the cell at a constant current of 20A/100Ah. The voltage is charged from 1.4V up to 1.683V which is taken as fully charged.

The voltage result obtained for the simulation of a 7 hour CC charging protocol on the nickel-cadmium cell is displayed below.

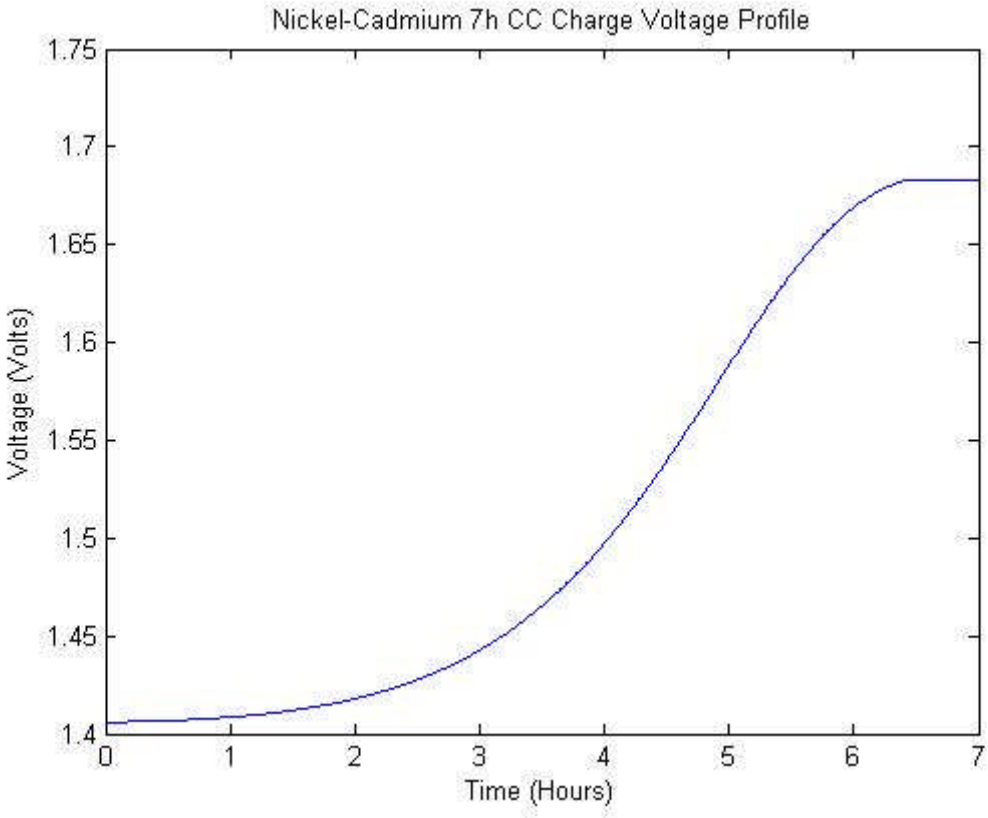

Figure 54: Nickel-Cadmium 7 hour CC charging protocol for voltage

5.3.5 Lead-Acid

In this section we will explore the discharge and charging characteristics that define the lead-acid battery. The battery is modelled as a single cell and then as a module made up of cells connected in series and parallel. The section takes the same form as the two previous sections.

Discharge Characteristics

The single lead-acid cell was tested for various discharge rates (C-rates) and their influence on the discharge voltage, current and power was investigated. The cells were discharged until they reached their cut-off voltage of 3V.

The simulation results for cell voltage at discharge rates of 0.1C, 0.2C, 0.3C and 1C are plotted against depth of discharge (DOD) and displayed below in Figure 58.

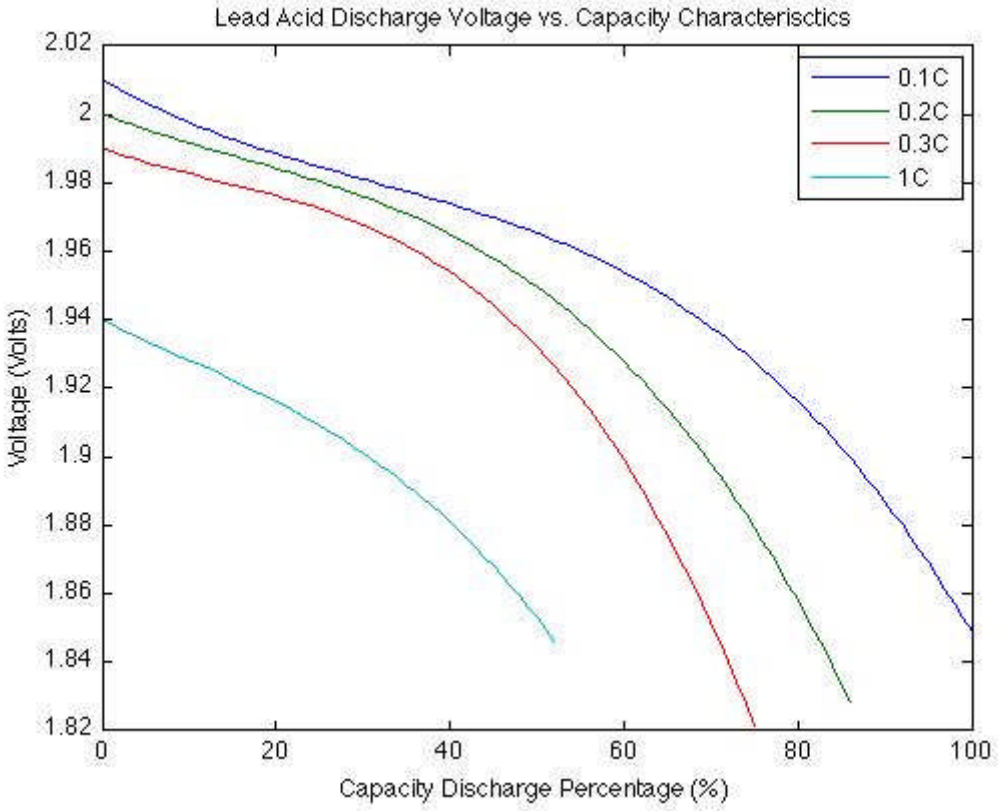

Figure 55: Lead-Acid cell discharge voltage against depth of discharge (DOD)

The results of the simulations are summarised below in Table 24.

Table 24: Result summary of lead-acid cell discharge voltage characteristics

C-Rate	Discharge Time	Discharge Voltage at 0% DOD (Volts)	Discharge Current	Maximum Capacity (at cut-off)	Maximum Capacity (% of Full)
0.1	10	2.01	250	2500	100
0.2	5	2	430	2150	86
0.3	3	1.99	625	1875	75
1	1	1.94	1300	1300	52

It can be seen that the results obtained for the Matlab simulations and from Figure 55 agree.

The lead-acid characteristics are similar to those of the lithium-ion and the nickel-cadmium batteries. As the C-rate increases, a decrease in the discharge voltage and the maximum capacity is experienced. The depth of discharge (DOD) of the battery is decreased as the discharge rate (C-rate) increases and the discharge current is increased with a faster C-rate. A new maximum capacity, which can be seen in column 5 of Table 24, decreases as the discharge current is increased.

A new, practical C-rate which accurately accounts for the discharge time is presented in Table 25.

Table 25: Actual lead-acid C-rate

Original Data		New Data		ΔC-Rate (%)
C-Rate	Discharge Time (Hours)	C-Rate	Discharge Time (Hours)	
0.1	10	0.1	10	100
0.2	5	0.233	4.3	116.5
0.3	3	0.444	2.25	148
1	1	1.923	0.52	192.3

The simulation results for the power discharged by the cell for discharge rates (C-rates) of 0.1C, 0.2C, 0.3C and 1C are displayed in Figure 56.

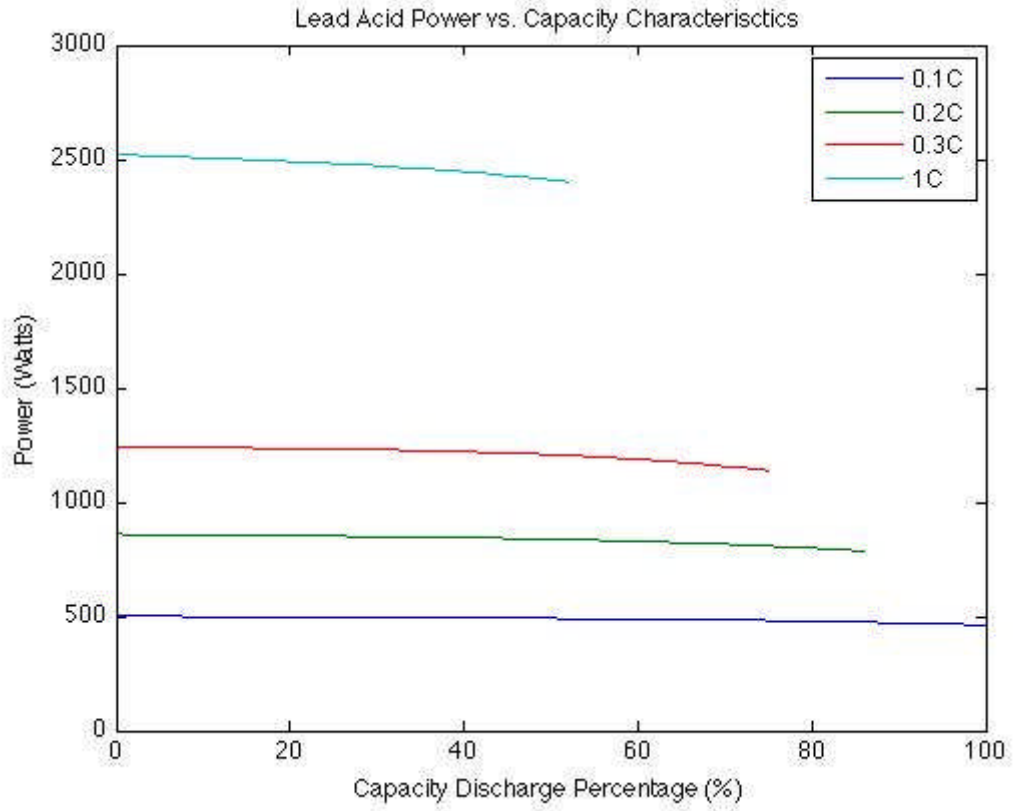

Figure 56: Lead-Acid cell discharge power against depth of discharge (DOD)

The results of the simulation are summarised below in Table 26.

Table 26: Result summary of lead-acid cell discharge power characteristics

C-Rate	Discharge Time (Hours)	Discharge Power at 0% DOD (Watts)	Discharge Power Final (Watts)	Δ Discharge Power (%)
0.1	10	502.5	462.25	92
0.2	5	860	786.35	91.44
0.3	3	1243.8	1138.6	91.54
1	1	2522	2400.1	95.17

It can be seen that the results obtained for the Matlab simulations and from Figure 56 agree. The characteristics of the lead-acid differ from the lithium-ion and the nickel-cadmium in the discharge power percentage. The discharge power percentage is seen as being higher and will result in a smaller fluctuation of the power provided.

The lead-acid battery cell was simulated into a module by connecting cells in series and parallel to produce a desired output. The parameters were as follows:

Ns = 3 cells;

Np = 1 cells.

This resulted in the discharge curves shown in Figure 57 and Figure 58 for discharge rates (C-rates) of 0.1C, 0.2C, 0.3C and 1C.

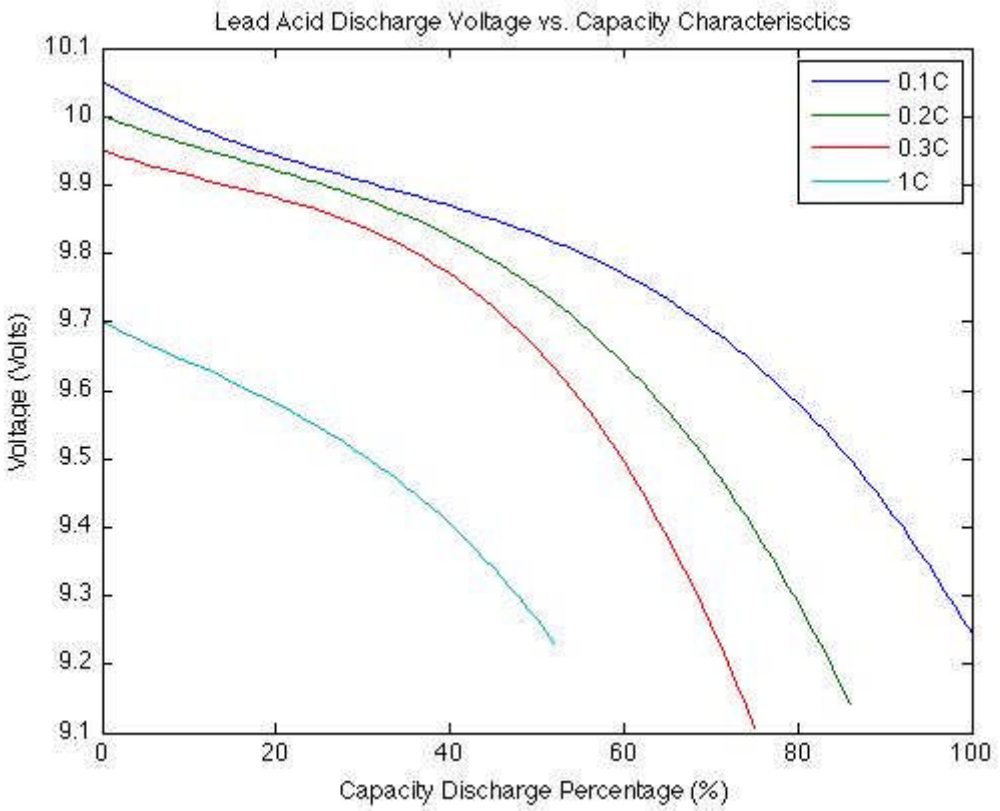

Figure 57: Lead-Acid module discharge voltage against depth of discharge (DOD)

The results of the simulation were summarized in the following Table 27.

Table 27: Result summary of lead-acid module discharge voltage characteristics

C-Rate	Discharge Time	Discharge Voltage at 0% DOD (Volts)	Discharge Current	Maximum Capacity (at cut-off)	Maximum Capacity (% of Full)
0.1	10	6.03	250	2500	100
0.2	5	6	430	2150	86
0.3	3	5.97	625	1875	75
1	1	5.82	1300	1300	52

It can be seen that the results obtained for the Matlab simulations and from Figure 57 agree. The discharge voltage has increased in proportion to Ns (cells in series) and the discharge current and maximum capacity has increased in proportion to Np (cells in parallel). The new actual C-rates are found to be the same as those for the cell simulation.

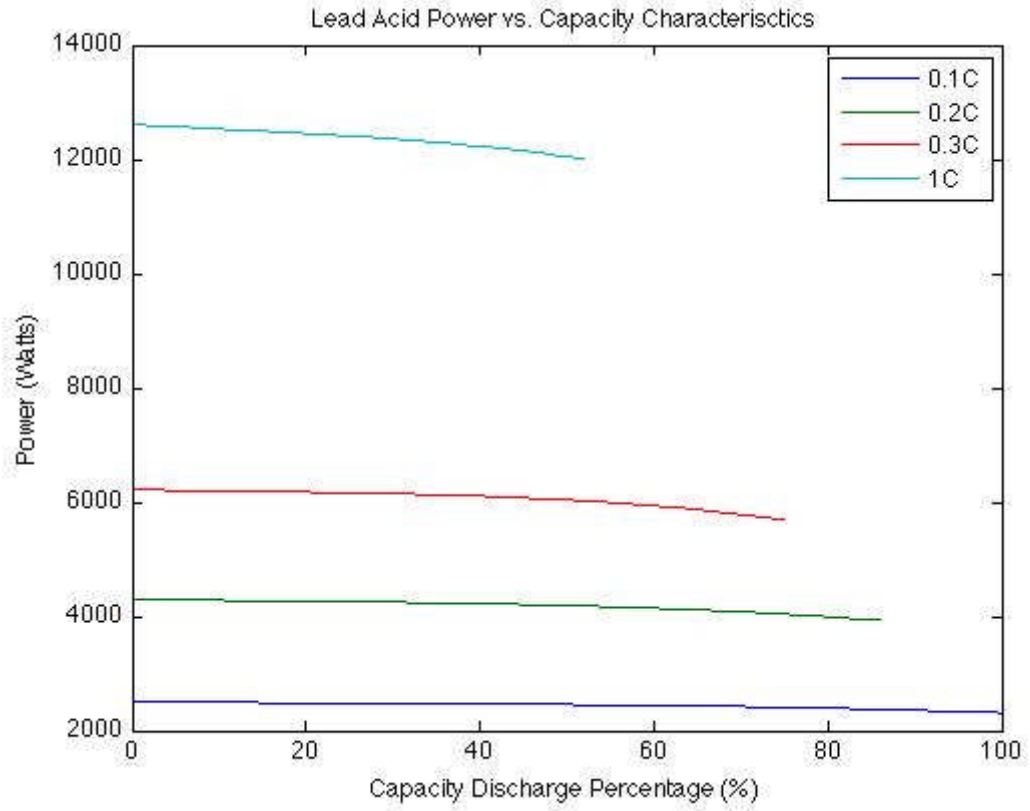

Figure 58: Lead-Acid module discharge power against depth of discharge (DOD)

The results for the simulation have been summarized in Table 28.

Table 28: Result summary of lead-acid module discharge power characteristics

C-Rate	Discharge Time (Hours)	Discharge Power at 0% DOD (Watts)	Discharge Power Final (Watts)	Δ Discharge Power (%)
0.1	10	1507.5	1386.7	92
0.2	5	2580	2359.1	91.44
0.3	3	3731.3	3415.7	91.54
1	1	7566	7200.4	95.17

The power has increased in proportion to the product of the number of cells connected in series and parallel. The power discharged in 0.1C is seen as having the smallest actual power change (120.8W) for the different rates of discharge (C-rates) but produces the least quantity of instantaneous power to the system.

The lead-acid module is seen as having the same characteristics as that of the lead-acid cell, while increasing the voltage and currents discharged resulting in an increased power discharge.

Charge Characteristics

The lead-acid charging characteristics were investigated for the charging protocol of CV (constant voltage) charging. The influence charging has on the current of the cell are determined.

The CV charging protocol charges the cell by applying a constant voltage of 2.45V while the current, initially constant at 2A, decreases exponentially until the cell is fully charged.

The results obtained for the simulation of a 7 hour CV charging protocol for a 2.5Ah lead-acid cell are displayed below.

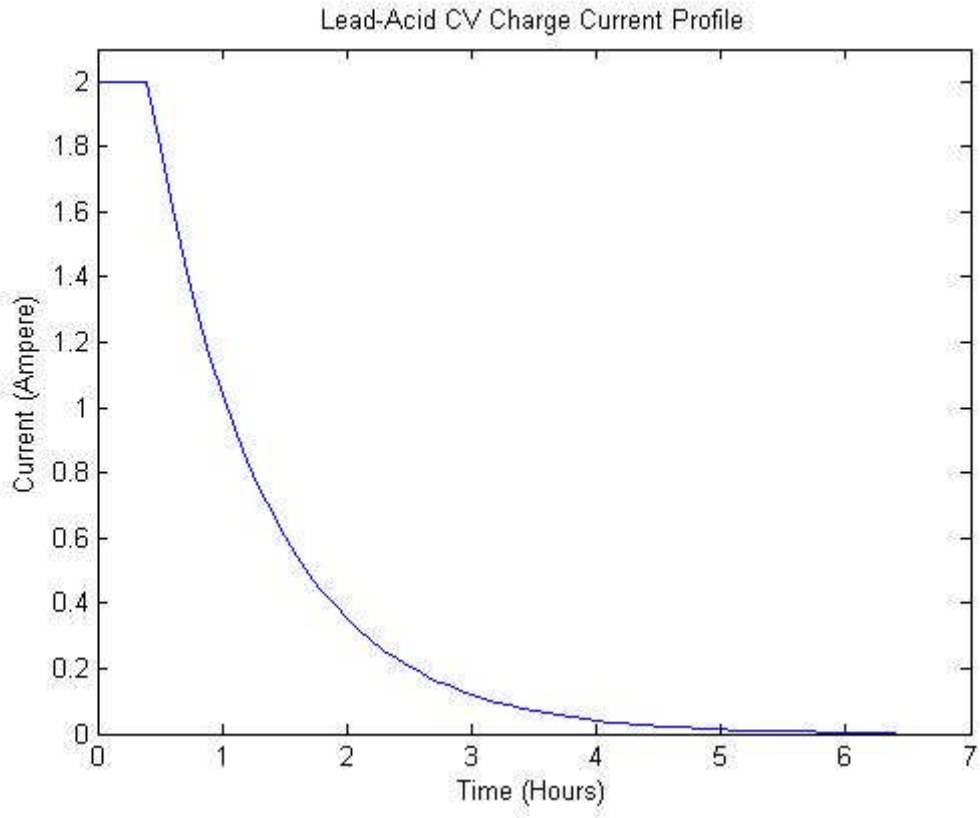

Figure 59: Lead-Acid 7 hour CV charging protocol for current

It can be seen in Figure 59 that the current is initially at 2A and then starts decreasing exponentially in the first hour until the cell is fully charged.

5.4 *Super-capacitor Validation*

The aim of this section is to validate the super-capacitor model proposed in Section 3.3.4. This section contains results obtained from the super-capacitor model simulation. It explores the charging and discharging characteristics of the super-capacitor.

5.4.1 Charging

The super-capacitor charging characteristics were investigated for a CC (constant-current) charging protocol. The capacitor was charged at 10A until fully charged. The time period for the charge was 3.7 minutes.

Figure 60 displays the voltage characteristics against time (minutes) of the super-capacitor for the above CC charging protocol.

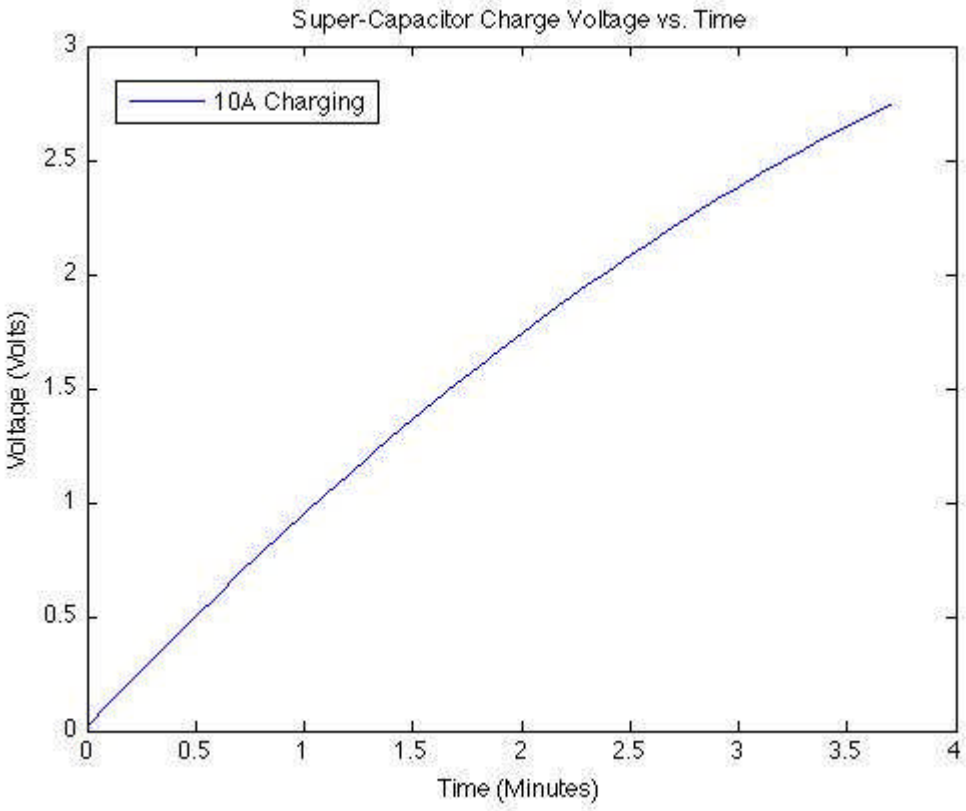

Figure 60: Super-Capacitor voltage profile for 10A CC charging protocol

5.4.2 Discharging

Discharging characteristics of the super-capacitor were then investigated. The super-capacitor was designed and set to be discharged at a constant current of 5A. The Figure 61 displays the results obtained for the voltage profile of the discharge. The voltage is plotted against time and it is seen that the full discharge occurs in 7.136 minutes.

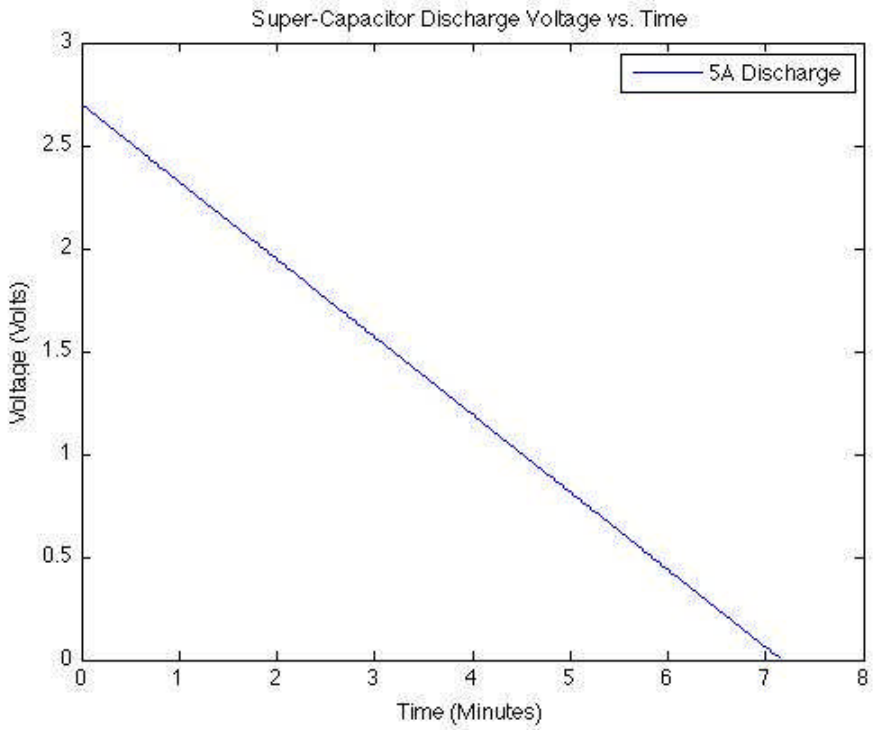

Figure 61: Super-Capacitor voltage profile for 5A CC discharging protocol

The power provided by the discharging super-capacitor is displayed in Figure 62.

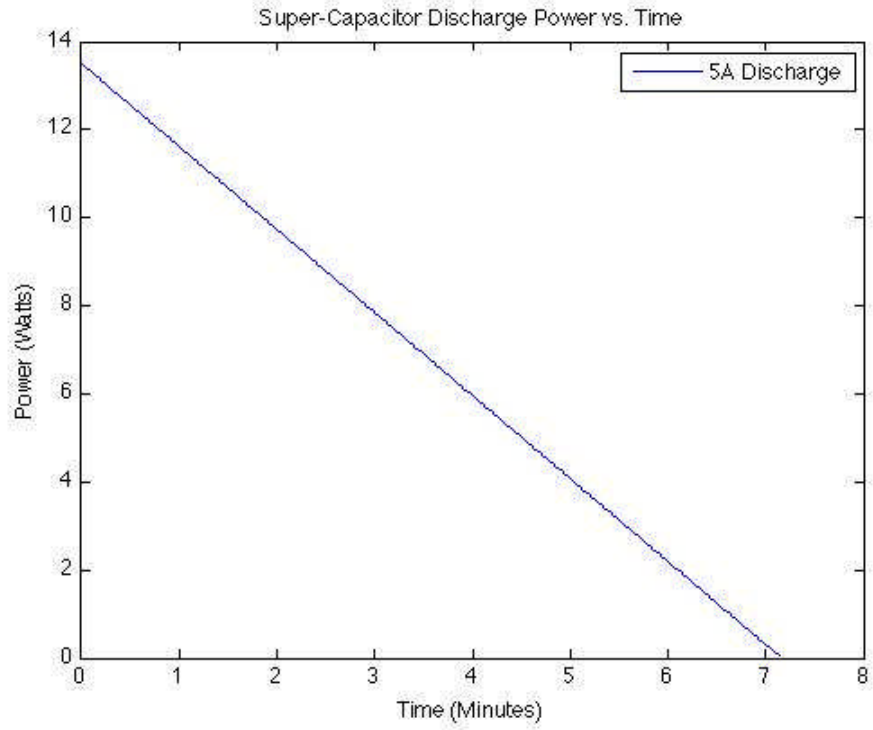

Figure 62: Super-Capacitor power provided for 5A CC discharging protocol

The cumulative power provided by the super-capacitor discharge is displayed in Figure 63.

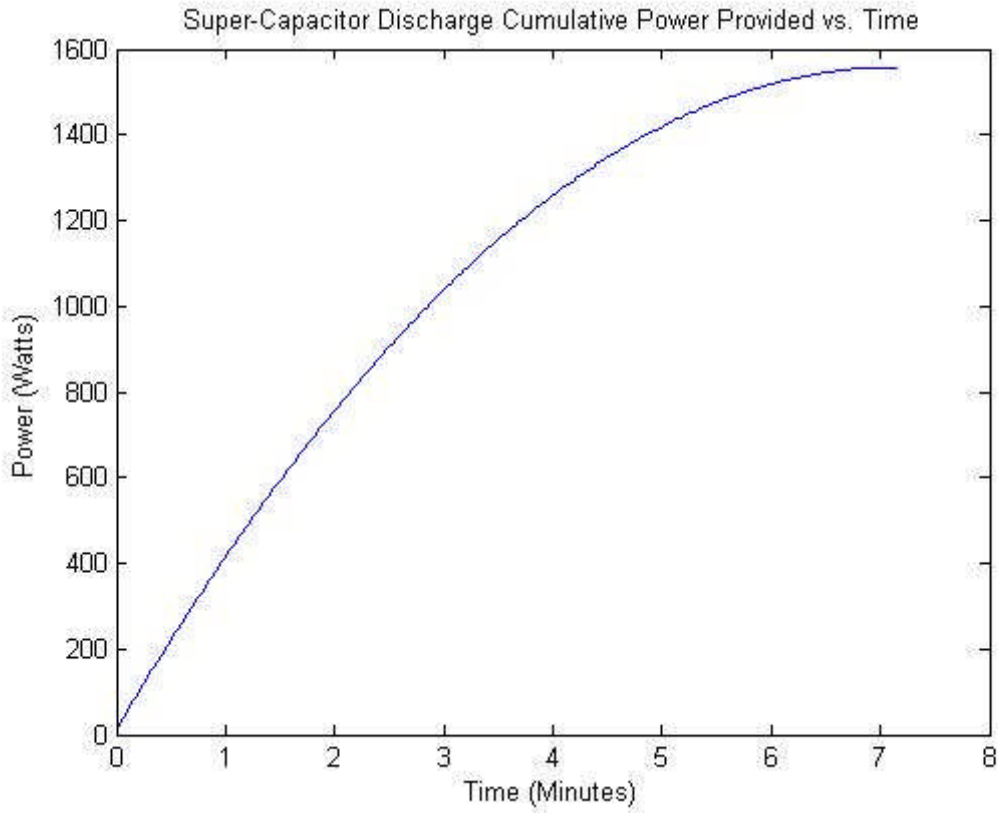

Figure 63: Super-capacitor cumulative power discharged over time

5.5 *PV Power Provided*

This section investigates the power provided by the PV for daily irradiance levels. The irradiance profile is simulated for the worst-case scenario daily irradiance values and plotted over a day. The PV power provided is then simulated using these irradiance values and the power output of the PV over a day can determined.

5.5.1 Irradiation Profile

The daily irradiance values are used to simulate the model. Figure 64 displays the irradiance over a time period of 24 hours for averaged worst-case scenarios values obtained in summer months and winter months.

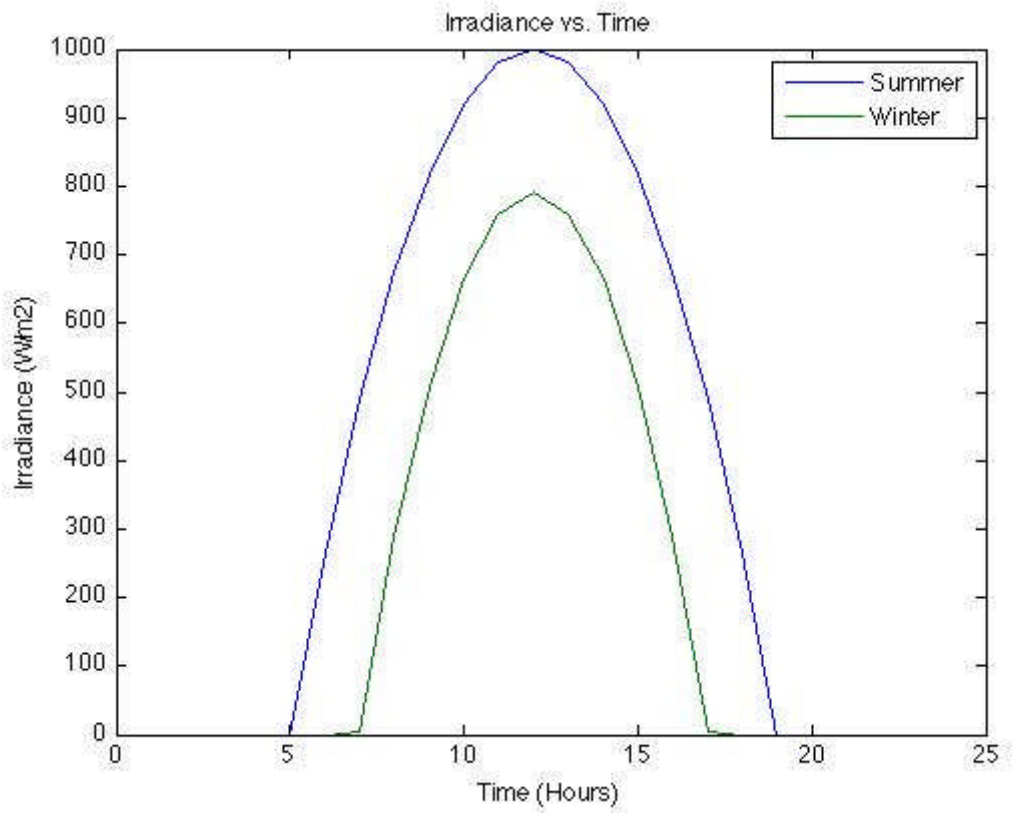

Figure 64: Daily irradiance averages for summer and winter

From Figure 64 we can see that the maximum irradiance values occur at 12h00 (mid-day).

$E_{Summer,max}$ = 1000 W/m^2

$E_{Winter,max}$ = 800 W/m^2

The irradiance in summer is seen as starting at 5h00 and ending at 19h00 while the winter irradiance starts at 7h00 and ends at 17h00. This together with the maximum irradiance values results in the PV providing more power for a longer period in summer than in winter.

5.5.2 PV power provided (Summer)

The PV module was simulated over the irradiance levels of a worst-case scenario averaged summer day. The power provided by the PV module is displayed in Figure 65.

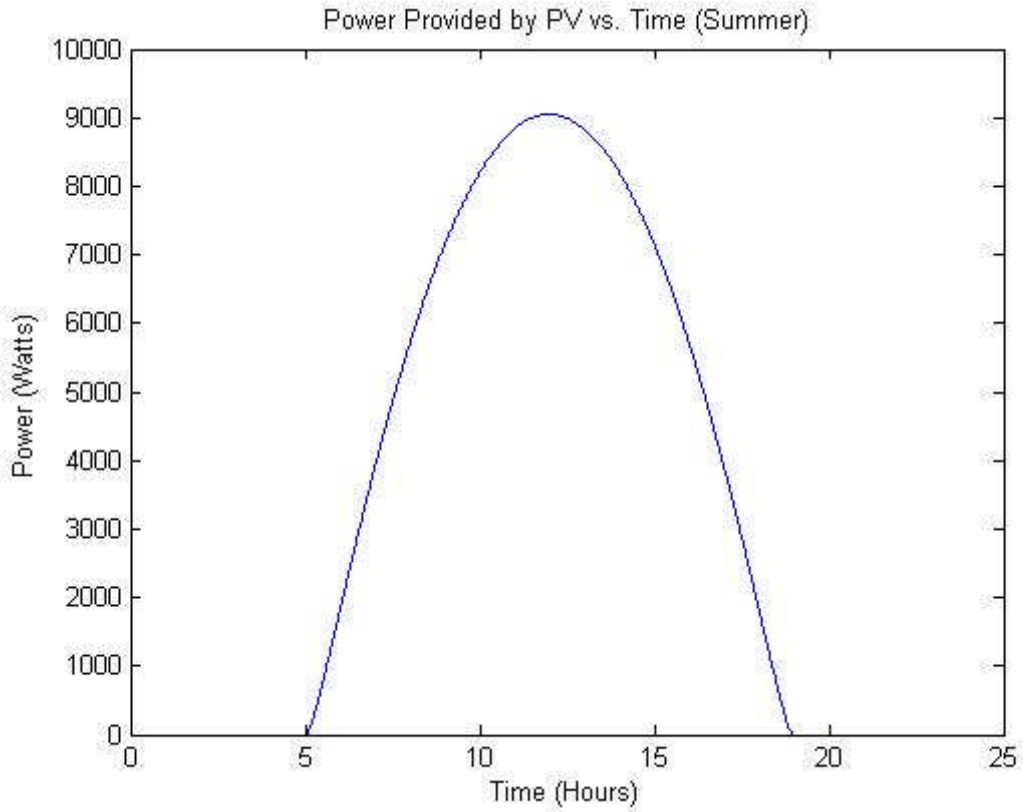

Figure 65: Power provided by the PV for a worst-case scenario averaged summer day

It can be seen from Figure 65 that the maximum power the PV provides over the 24 hours is at 12h00.

$P_{PV,max}$ = 9048.6 W

The power provided follows the form of the irradiance. The output data of the PV is taken for the maximum power point (MPP) of each step over the 24 hours. No power is provided by the PV between 19h00 and 5h00 as this simulates a period of no irradiation or night-time.

The cumulative power provided by the PV is displayed in Figure 66 and plotted against time.

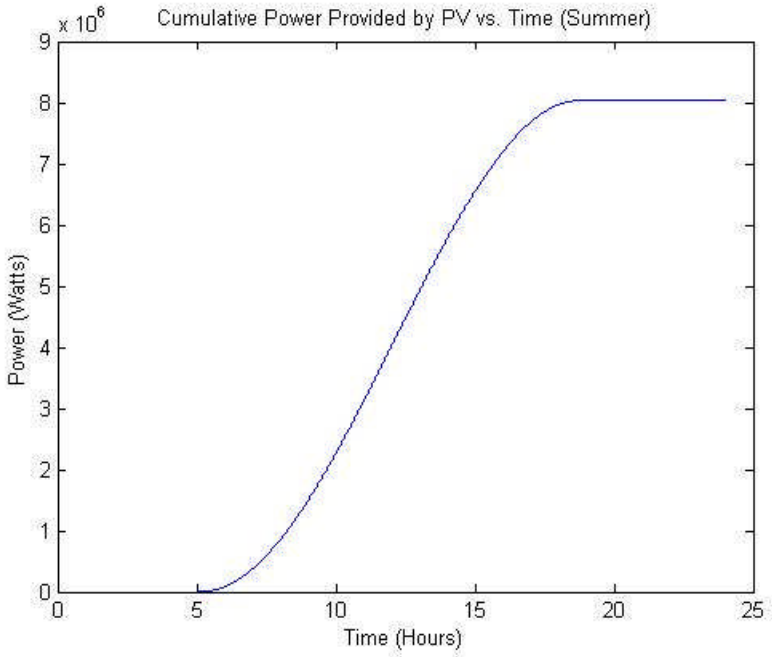

Figure 66: Cumulative power provided by PV against time for worst case summer irradiation

The cumulative power provided by the PV for summer is:

$P_{pv,summer}$= 8.0405X10^{6}W

5.5.3 PV power provided (Winter)

The PV module was simulated over the irradiance levels of a worst-case scenario averaged winter day. The power provided by the PV module is displayed in Figure 67.

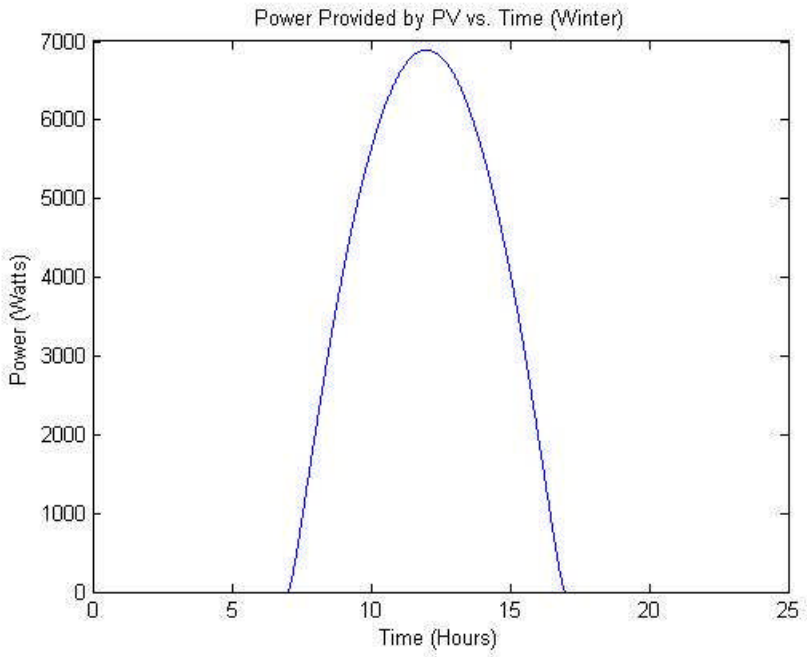

Figure 67: Power provided by the PV for worst-case scenario averaged winter day

It can be seen from Figure 67 that the maximum power the PV provides over the 24 hours is at 12h00.

$P_{PV,max}$ = 6891.5 W

The power provided follows the form of the irradiance. The output data of the PV is taken for the maximum power point (MPP) of each step over the 24 hours. No power is provided by the PV between 17h00 and 7h00 as this simulates a period of no irradiation or night-time.

The cumulative power provided by the PV is displayed in Figure 68 and plotted against time.

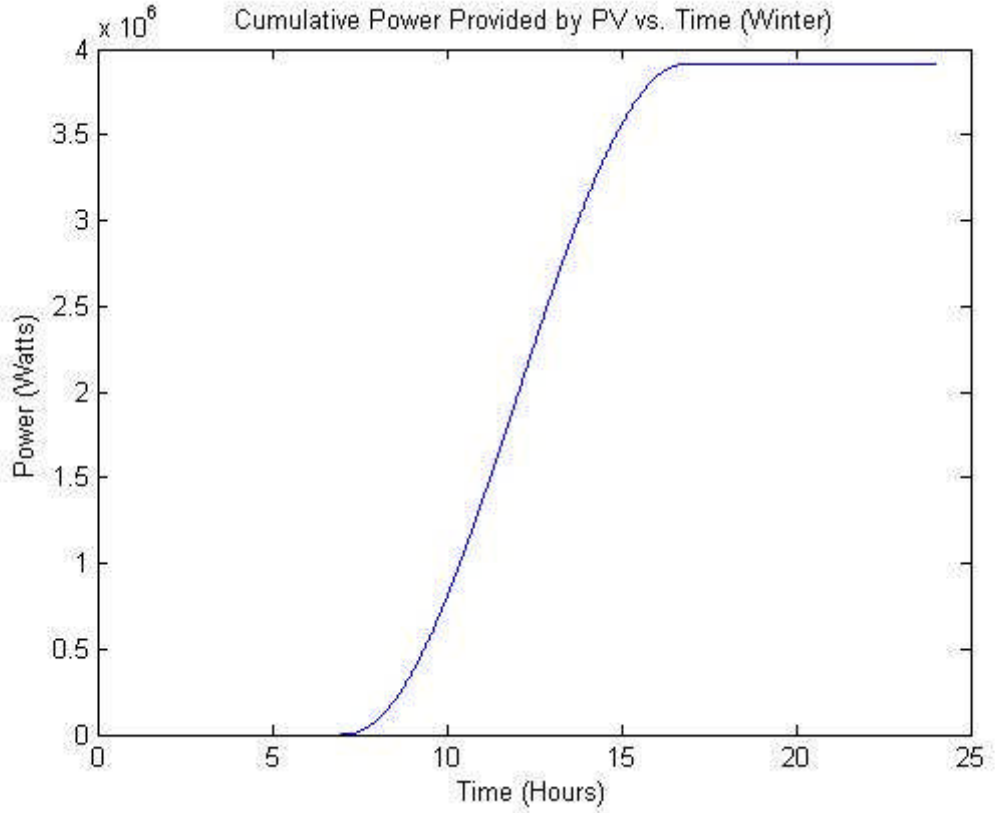

Figure 68: Cumulative power provided by PV against time for worst case winter irradiation

The cumulative power provided by the PV for winter is:

$P_{pv,winterr}$= 4.3621X10^{6}W

5.6 *Battery Energy Storage System (BESS) Power Provided*

This section aims to investigate the power provided to the system by the different battery chemistries. Each of the chemistries is explored and simulated for various discharge rates (C-Rates). The power provided is plotted against time; then the cumulative power provided by batteries is plotted against time.

5.6.1 Lithium-ion

The lithium-ion discharge power was plotted against time for discharge rates (C-rates) of 0.2C, 0.5C, 1C and 2C. The results obtained for this simulation are shown in Figure 69.

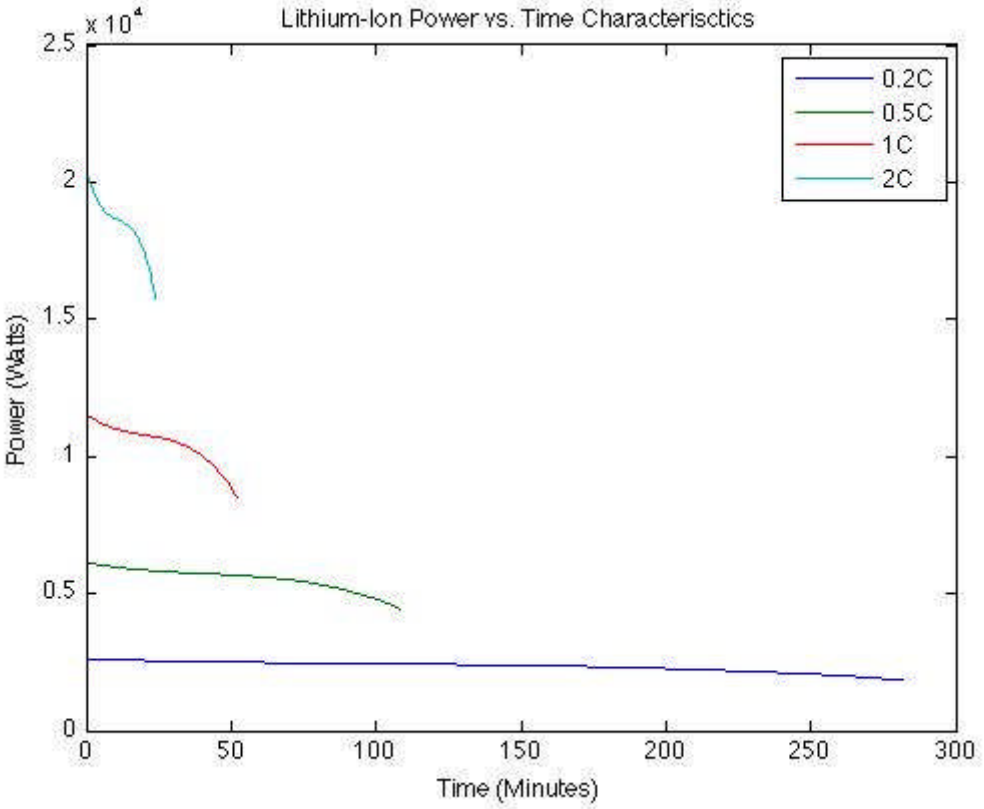

Figure 69: Lithium-ion power provided against time

The results of the power provided are given in Table 18. The discharge times for the different C-rates are given below.

$T_{0.2C}$ = 4h42;

$T_{0.5C}$ = 2h48;

T_{1C} = 0h52;

T_{2C} = 0h24.

The cumulative power provided by the different C-rates against time is presented in Figure 70.

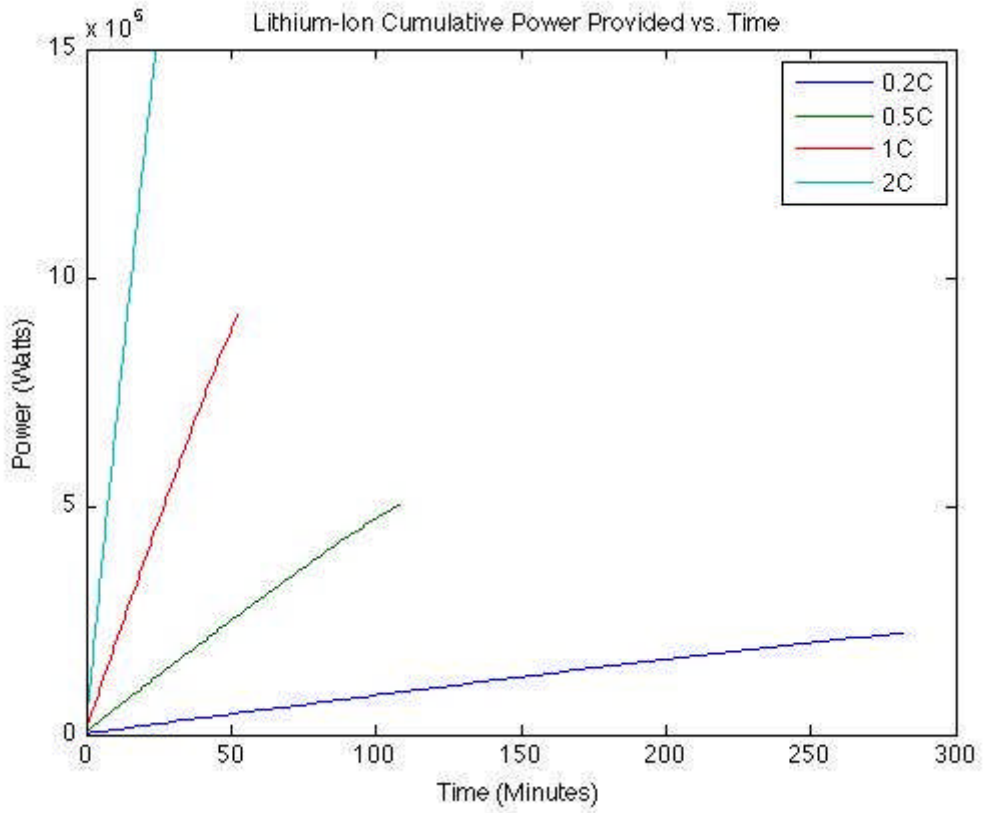

Figure 70: Lithium-ion cumulative power provided against time

The results of the simulation for cumulative power are given below:

$P_{0.2C}$ = 2.2213X10^{5}W;

$P_{0.5C}$ = 5.0309X10^{5}W;

P_{1C} = 9.2004X10^{5}W;

P_{2C} = 1.4929X10^{6}W.

5.6.2 Nickel-cadmium

The nickel-cadmium discharge power was plotted against time for discharge rates (C-rates) of 0.1C, 0.2C, 0.5C and 1C. The results obtained for this simulation are shown in Figure 71.

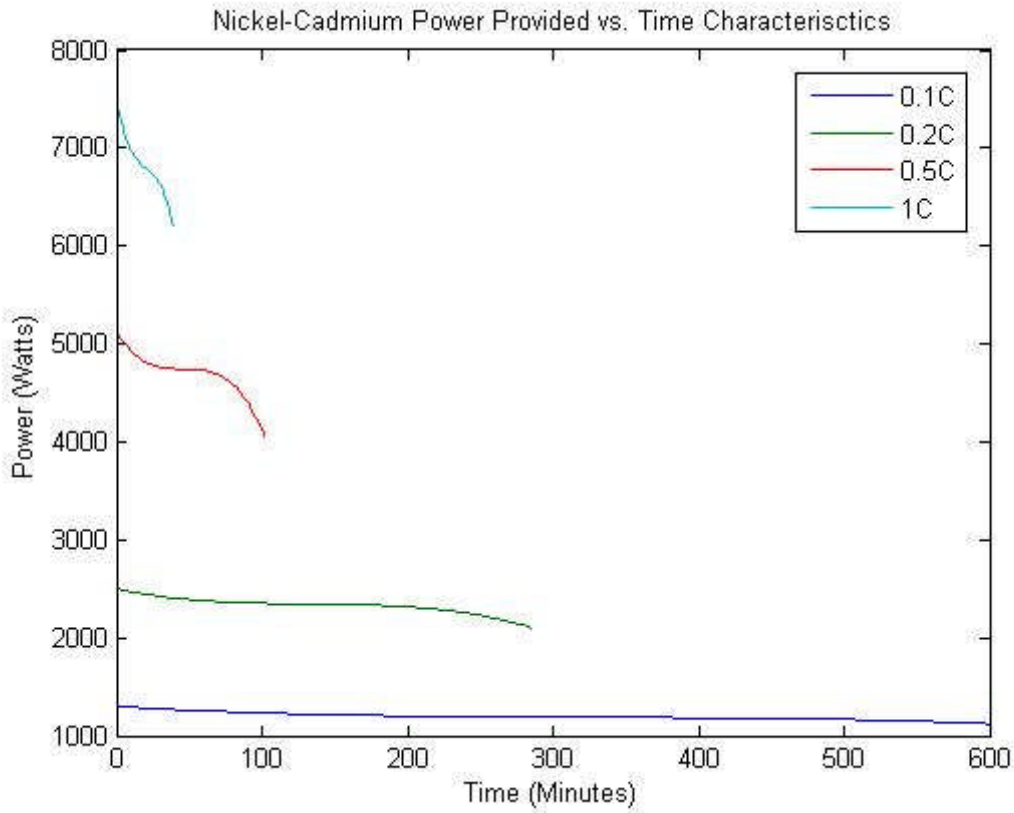

Figure 71: Nickel-cadmium power provided against time

The results of the power provided are given in Table 23. The discharge times for the different C-rates are given below.

$T_{0.1C}$ = 10h00;

$T_{0.2C}$ = 4h45;

$T_{0.5C}$ = 1h42;

T_{1C} = 0h39.

The cumulative power provided by the different C-rates against time is presented in Figure 72.

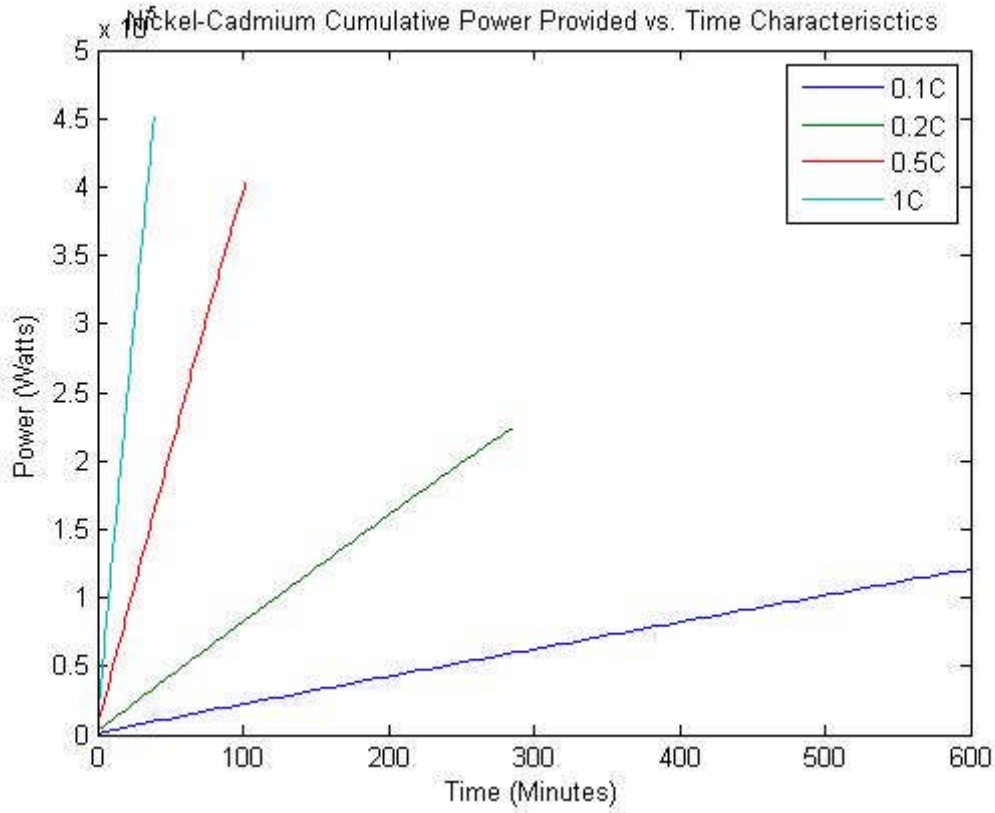

Figure 72: Nickel-cadmium cumulative power provided against time

The results of the simulation for cumulative power are given below:

$P_{0.1C} = 1.20887X10^5W$;

$P_{0.2C} = 2.361X10^5W$;

$P_{0.5C} = 4.0346X10^5W$;

$P_{1C} = 4.5034X10^5W$.

5.6.3 Lead-acid

The lead-acid discharge power was plotted against time for discharge rates (C-rates) of 0.1C, 0.2C, 0.3C and 1C. The results obtained for this simulation are shown in Figure 73.

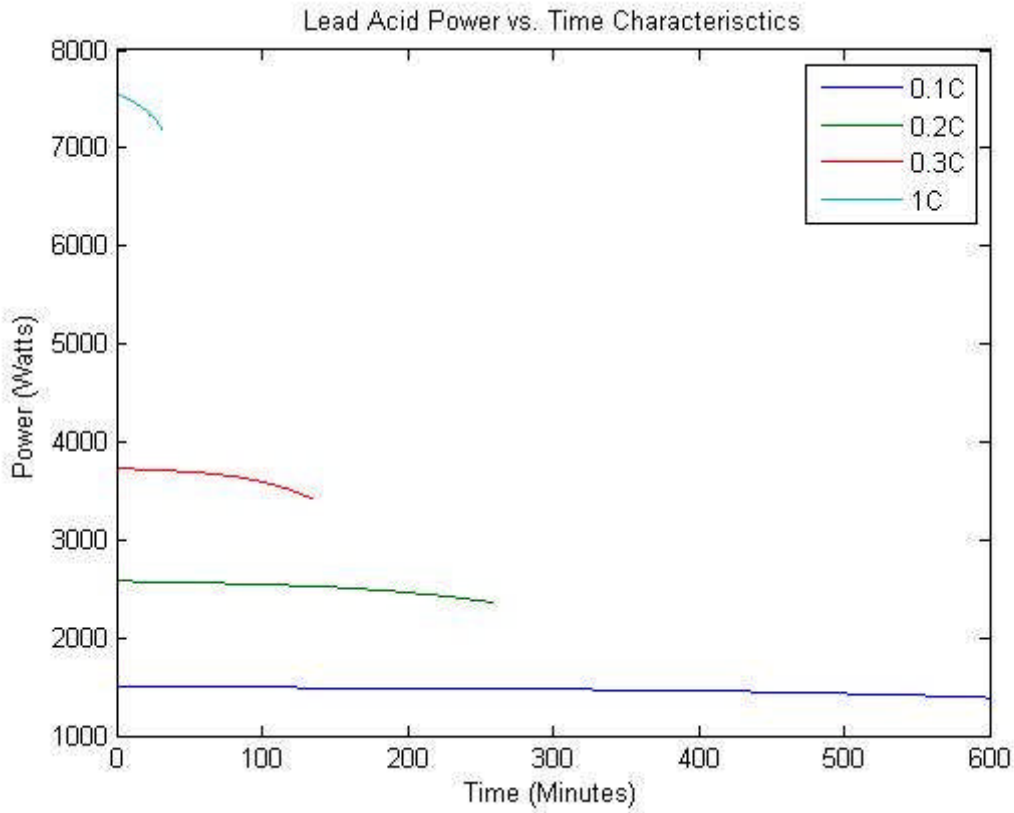

Figure 73: Lead-acid power provided against time

The results of the power provided are given in Table 28. The discharge times for the different C-rates are given below.

$T_{0.1C}$ = 10h00;

$T_{0.2C}$ = 4h18;

$T_{0.3C}$ = 2h15;

T_{1C} = 0h31.

The cumulative power provided by the different C-rates against time is presented in Figure 74.

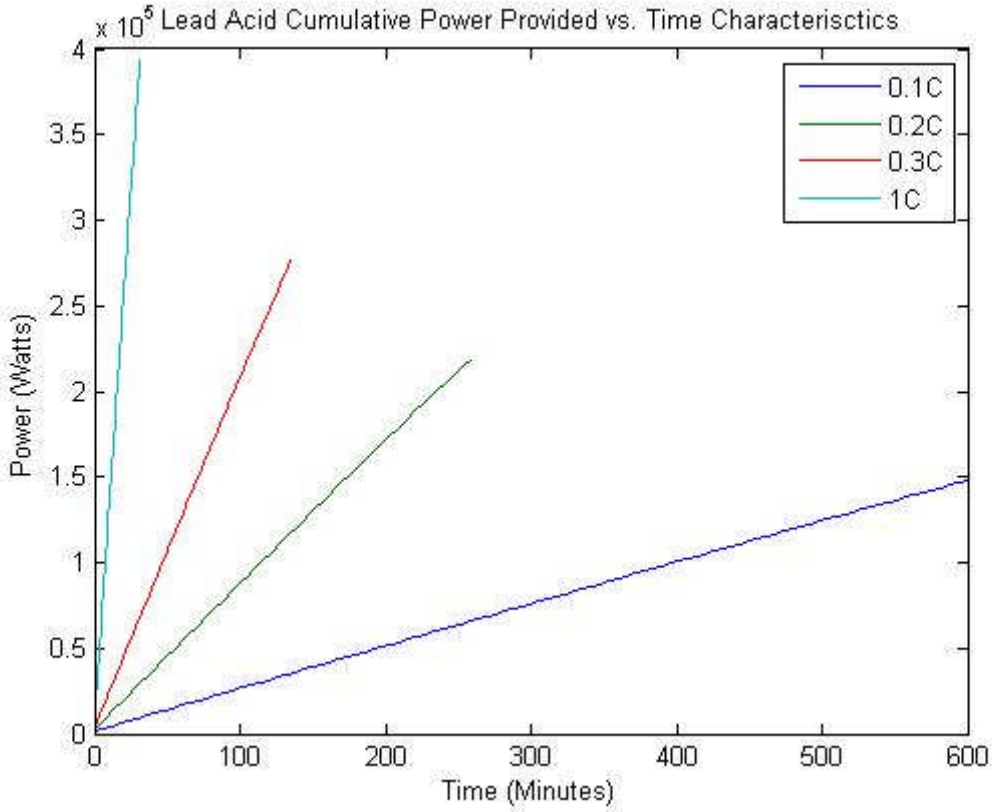

Figure 74: Lead-acid cumulative power provided against time

The results of the simulation for cumulative power are given below:

$P_{0.1C}$ = 1.4795 X10^5W;

$P_{0.2C}$ = 2.1829X10^5W;

$P_{0.3C}$ = 2.7647X10^5W;

P_{1C} = 3.9327X10^5W.

5.7 *Power Provided by the System*

This section focuses on the results obtained from the power provided by the PV system and the Battery Energy Storage System (BESS). The three battery chemistries are simulated with the PV in order to determine the total power that can be supplied to a load over 24 hours. The discharge rate of 0.2C was chosen as the common C-rate for all three chemistries however, the lithium-ion module was discharged over two depth of discharges (DOD) and the nickel-cadmium was discharged at 0.5C as well in order to gain a better

understanding of the relationship between the depth of discharge (DOD) and the C-rate in terms of the power provided

The batteries were chosen to discharge to a depth of discharge (DOD) of 50% as the common case across the three chemistries. This is to simulate practical conditions where the batteries need stored charge in case of emergencies such as another battery failing or heavy cloud cover for a day resulting in minimal irradiation and the batteries not being able to charge.

The lithium-ion was then discharged to a depth of discharge (DOD) of 70% in order to simulate a deep discharging battery.

The nickel-cadmium was also discharged at a rate of 0.1C in order to compare discharge rate performance.

The batteries were arranged to start discharging in a cascaded manner. Once a battery is depleted, the next battery immediately begins discharging.

The batteries are taken as fully charged and the cycle begins at 12h00 till 12h00 the next day in a worse-case scenario summer irradiation.

5.7.1 Lithium-ion

The lithium-ion battery was discharged under two conditions. The first being at a C-rate of 0.2 to a depth of discharge (DOD) of 50%, the second was at the same C-rate to a depth of discharge (DOD) of 70%.

0.2C Discharge to a depth of discharge (DOD) of 50%

Seeing as the battery is discharged to 50%, the time the battery can supply a load was calculated as follows:

$Time_{0.2C,\ 50\%}$ = DOD X Battery Discharge Time (0.2C)

= 50% X 4h42

= 2h21

The battery discharge start times are shown below:

$Battery_1$ = 17h24

$Battery_2$ = 19h46

$Battery_3$ = 22h08

$Battery_4$ = 00h29

$Battery_5$ = 02h50

$Battery_6$ = 05h12

The results for the above conditions yield the following result where:

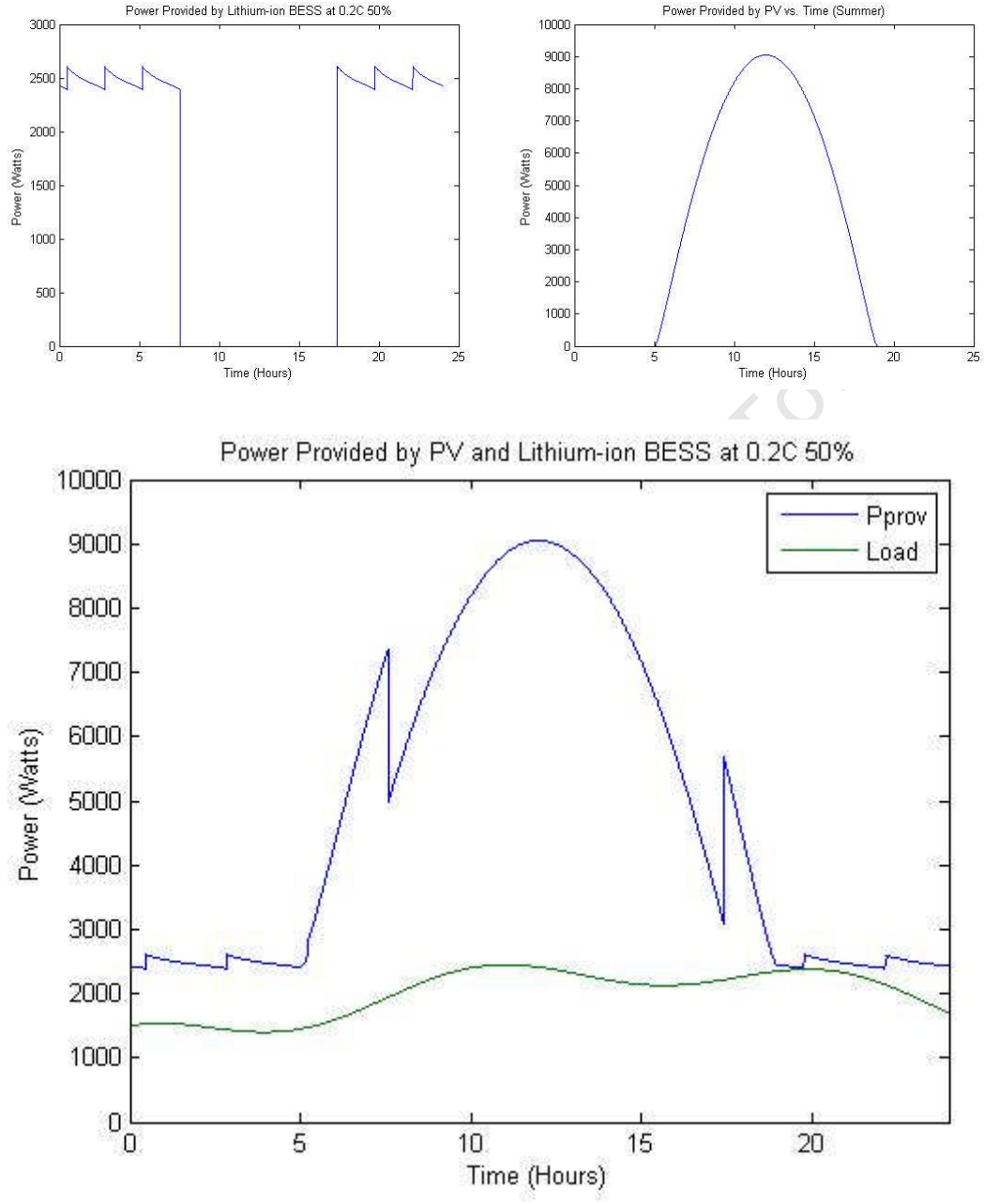

Figure 75: a). BESS power provided b). PV power provided c). System power provided with load demand for lithium-ion 0.2C 50%

$P_{prov} = P_{batt} + P_{pv} = 6.6639 \text{ X } 10^5 + 8.0405\text{X}10^6 = 8.7068 \text{ X } 10^6\text{W}$ over 24 hours;

$P_{prov,hour} = 3.6278 \text{ X } 10^5\text{W/hour}$

0.2C Discharge to a depth of discharge (DOD) of 70%

Seeing as the battery is discharged to 70%, the time the battery can supply a load was calculated as follows:

$Time_{0.2C,\ 70\%}$ = DOD X Battery Discharge Time (0.2C)

= 70% X 4h42

= 3h17

The battery discharge start times are shown below:

$Battery_1$ = 17h24

$Battery_2$ = 21h07

$Battery_3$ = 00h25

$Battery_4$ = 03h44

The results for the above conditions yield the following result where:

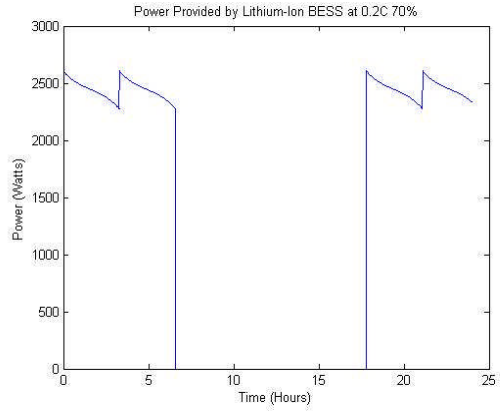

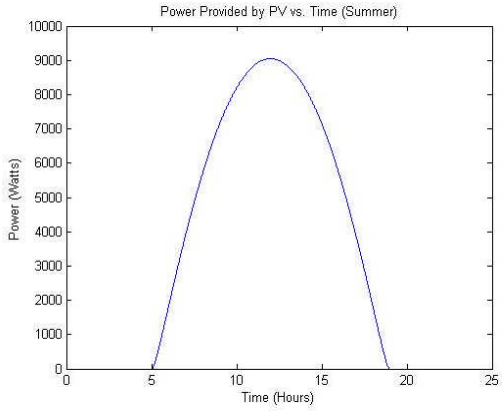

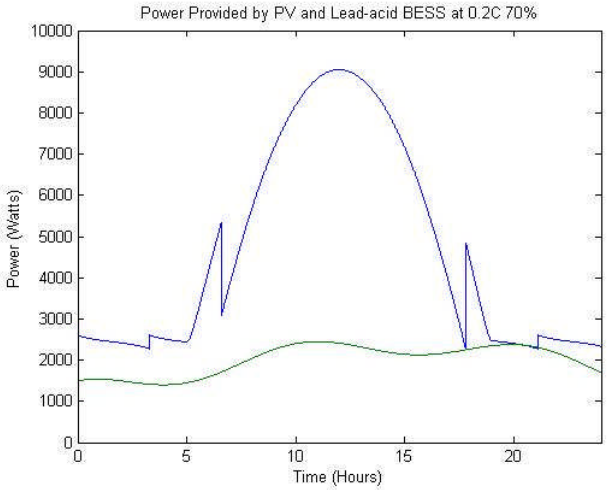

Figure 76: a). BESS power provided b). PV power provided c). System power provided with load demand for lithium-ion 0.2C 70%

$P_{prov} = P_{batt} + P_{pv} = 6.2196 \text{ X } 10^5 + 8.0405 \text{ X } 10^6 = 8.6624 \text{ X } 10^6$W over 24 hours;

$P_{prov,hour} = 3.6093 \text{ X } 10^5$W/hour

5.7.2 Nickel-cadmium

The nickel-cadmium battery was discharged under two conditions. The first being at a C-rate of 0.2C and the second at a C-rate of 0.1C. Both were discharged to a depth of discharge (DOD) of 50%.

0.2C Discharge to a depth of discharge (DOD) of 50%

Seeing as the battery is discharged to 50%, the time the battery can supply a load was calculated as follows:

$Time_{0.2C, 50\%}$ = DOD X Battery Discharge Time (0.2C)

= 50% X 4h45

= 2h22

The battery discharge start times are shown below:

$Battery_1$ = 17h24

$Battery_2$ = 19h46

$Battery_3$ = 22h08

$Battery_4$ = 00h29

$Battery_5$ = 02h50

$Battery_6$ = 05h12

The results for the above conditions yield the following result where:

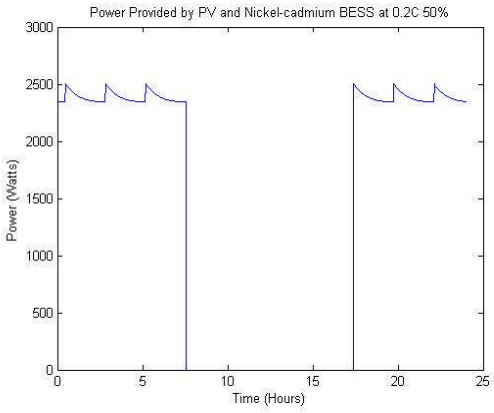

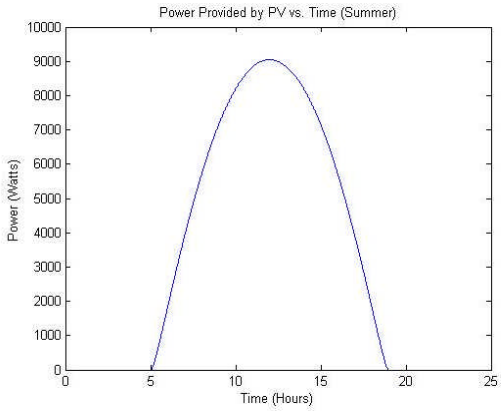

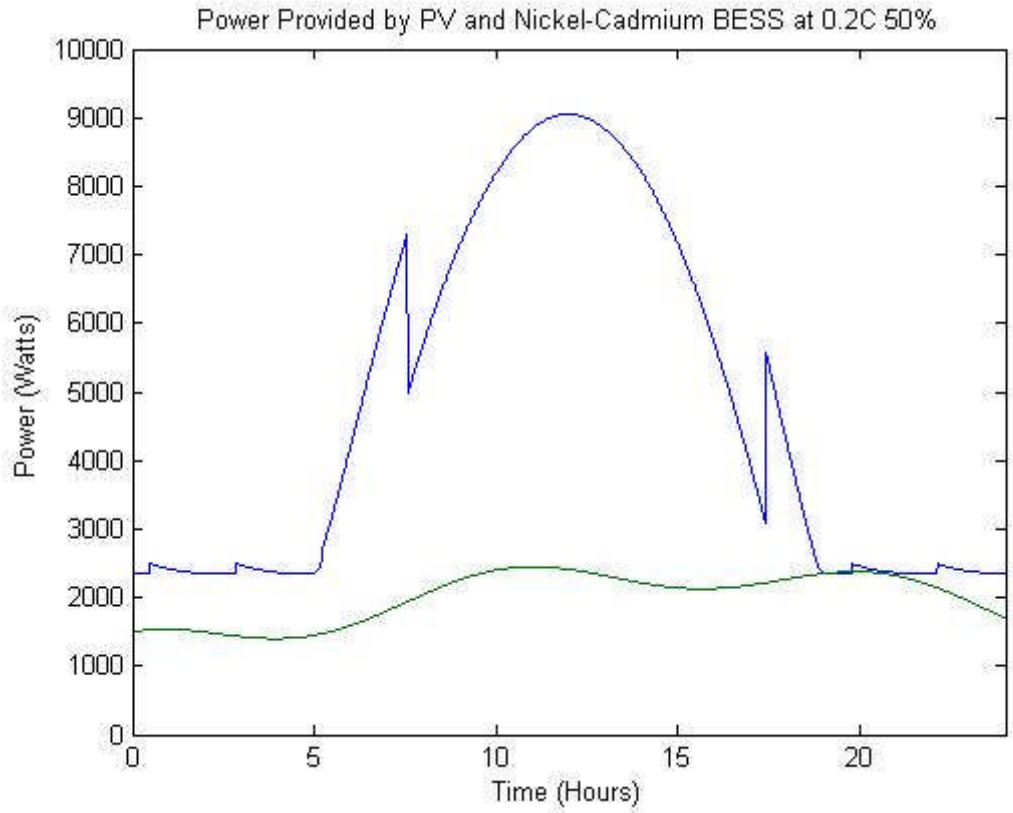

Figure 77: a). BESS power provided b). PV power provided c). System power provided with load demand for nickel-cadmium 0.2C 50%

$P_{prov} = P_{batt} + P_{pv} = 7.083 \text{ X } 10^5 + 8.0405 \text{ X } 10^6 = 8.7488 \text{ X } 10^6$W over 24 hours;

$P_{prov,hour} = 3.6453\text{X } 10^5$W/hour

0.1C Discharge to a depth of discharge (DOD) of 50%

Seeing as the battery is discharged to 50%, the time the battery can supply a load was calculated as follows:

$Time_{0.1C,\ 50\%}$ = DOD X Battery Discharge Time (0.2C)

= 50% X 10h00

= 5h00

The battery discharge start times are shown below:

$Battery_1$ = 17h24

$Battery_2$ = 22h25

$Battery_3$ = 03h25

The results for the above conditions yield the following result where:

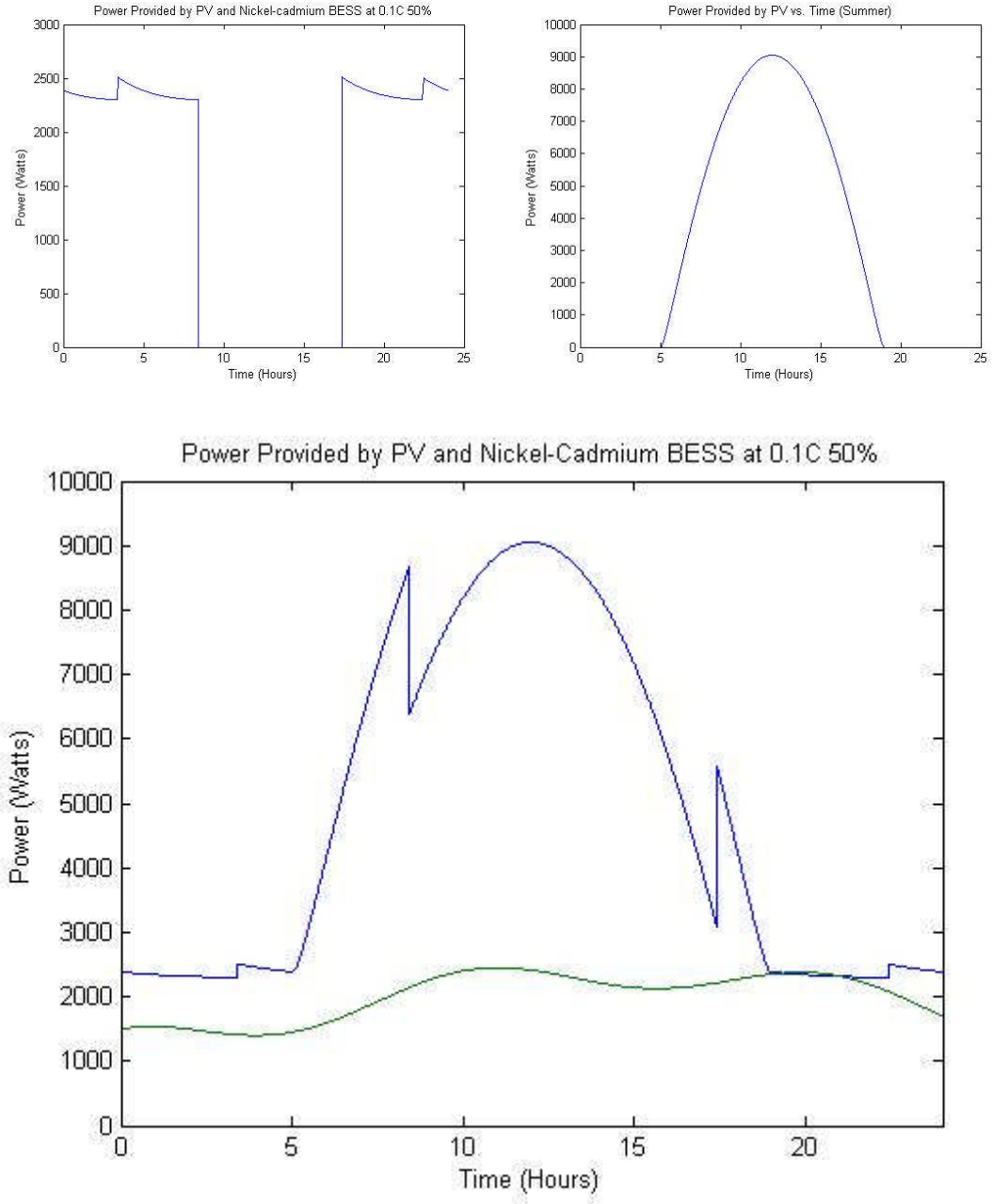

Figure 78: a). BESS power provided b). PV power provided c). System power provided with load demand for lithium-ion 0.1C 50%

$P_{prov} = P_{batt} + P_{pv} = 6.7551X\ 10^5 + 8.0405\ X\ 10^6 = 8.7160\ X\ 10^6 W$ over 24 hours;

$P_{prov,hour} = 3.6317\ X\ 10^5 W/hour$

5.7.3 Lead-acid

The lead-acid battery was discharged at a C-rate of 0.2C to a depth of discharge of 50%.

0.2C Discharge to a depth of discharge (DOD) of 50%

Seeing as the battery is discharged to 50%, the time the battery can supply a load was calculated as follows:

$Time_{0.2C,\ 50\%}$ = DOD X Battery Discharge Time (0.2C)

= 50% X 4h18

= 2h09

The battery discharge start times are shown below:

$Battery_1$ = 17h24

$Battery_2$ = 19h34

$Battery_3$ = 21h44

$Battery_4$ = 23h58

$Battery_5$ = 02h03

$Battery_6$ = 04h12

The results for the above conditions yield the following result where:

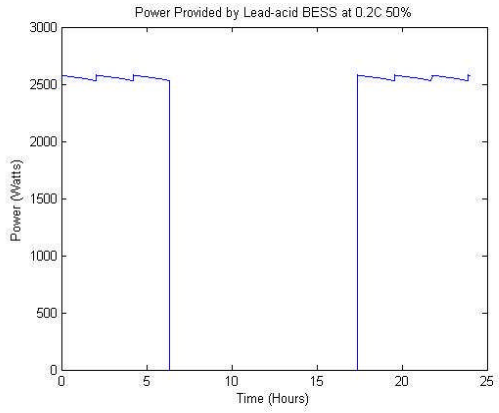

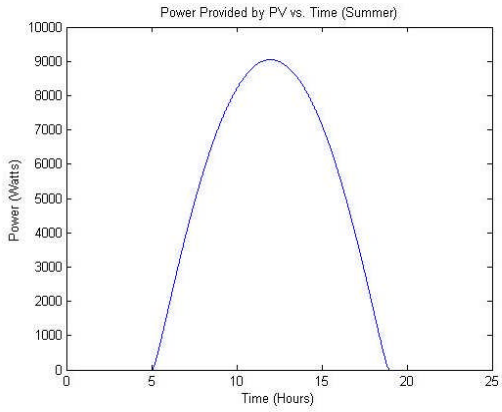

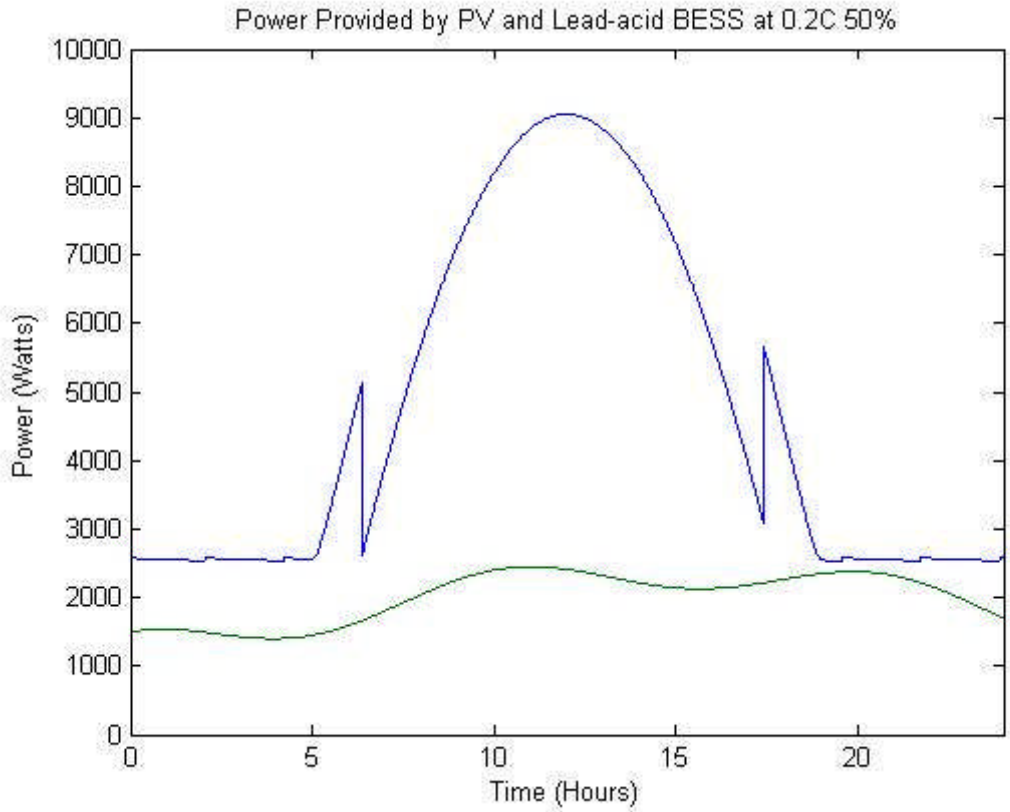

Figure 79: a). BESS power provided b). PV power provided c). System power provided with load demand for lead-acid 0.2C 50%

$P_{prov} = P_{batt} + P_{pv} = 6.5487 \text{ X } 10^5 + 8.0405 \text{ X } 10^6 = 8.69537 \text{ X } 10^6$W over 24 hours;

$P_{prov,hour} = 3.623\text{X } 10^5$W/hour

5.7.4 Result summary for power provided by the system

The results obtained were summarized in the following table:

Table 29: Summary of results for system power provided

Battery Chemistry	C-Rate	DOD (%)	P_{Batt} (Watts)	P_{PV} (Watts)	P_{Prov} (Watts)	$P_{Hour,avg}$ (Watts)	P_{Batt} vs. P_{PV} (%)
Lithium-Ion	0.2	50	$6.6639\text{X}10^5$	$8.0405\text{X}10^6$	$8.7068\text{X}10^6$	$6.6278\text{X}10^5$	8.288
	0.2	70	$6.2196\text{X}10^5$	$8.0405\text{X}10^6$	$8.6624\text{X}10^6$	$6.6093\text{X}10^5$	7.735
Nickel-Cadmium	0.1	50	$6.7551\text{X}10^5$	$8.0405\text{X}10^6$	$8.7160\text{X}10^6$	$6.6317\text{X}10^5$	8.401
	0.2	50	$7.0830\text{X}10^5$	$8.0405\text{X}10^6$	$8.7488\text{X}10^6$	$6.6453\text{X}10^5$	8.809
Lead-Acid	0.2	50	$6.5487\text{X}10^5$	$8.0405\text{X}10^6$	$8.6953\text{X}10^6$	$6.6230\text{X}10^5$	8.145

The lithium-ion 0.2C 70% DOD used 4 battery banks rated at 2.5kWh each while the Nickel-Cadmium 0.1C 50% DOD used 3 at 2.5kWh. All the other battery conditions used 6 battery banks rated at 2.5kWh each.

Table 30: Summary of results for BESS sizes

Battery Chemistry	C-Rate	DOD (%)	No. Banks Used	No. Cells in Bank	No. Cells in BESS
Lithium-Ion	0.2	50	6	1320	7920
	0.2	70	4	1320	5280
Nickel-Cadmium	0.1	50	3	3700	11100
	0.2	50	6	1915	11490
Lead-Acid	0.2	50	6	3	18

5.8 *PV and BESS (Lithium-ion) Complete*

The lithium ion model was used to simulate a complete cycle of the system including the battery charging. The batteries were split into 6 banks in order to cover the load demand throughout the day. In order to charge the 6 banks, they were split into two for lower peak power consumption resulting in 12 banks of half power, needing to be charged.

The lithium-ion batteries were chosen to discharge at a rate of 0.2C until 50% DOD. They were incorporated with the PV power provided for worse-case scenario summer irradiation.

We want to determine the power provided that wasn't used by the load or the charging of the batteries. This power can be sold back to the grid.

The additional power is the difference between the power providing modules and the power requiring modules. The providing modules consist of the PV module and the BESS discharge state. The requiring modules consist of the load and the BESS charging state.

$P_{prov} = P_{pv} + P_{batt,discharge}$

$P_{req} = P_{load} + P_{batt,charge}$

$P_{additional} = P_{rov} - P_{req}$

If the additional power is positive, the power provided is greater than the power required and can be sold back to the grid. If the additional power is negative, the power provided does not meet the power required and grid power must be bought.

Power provided

The power required is represented in the following Figure 80.

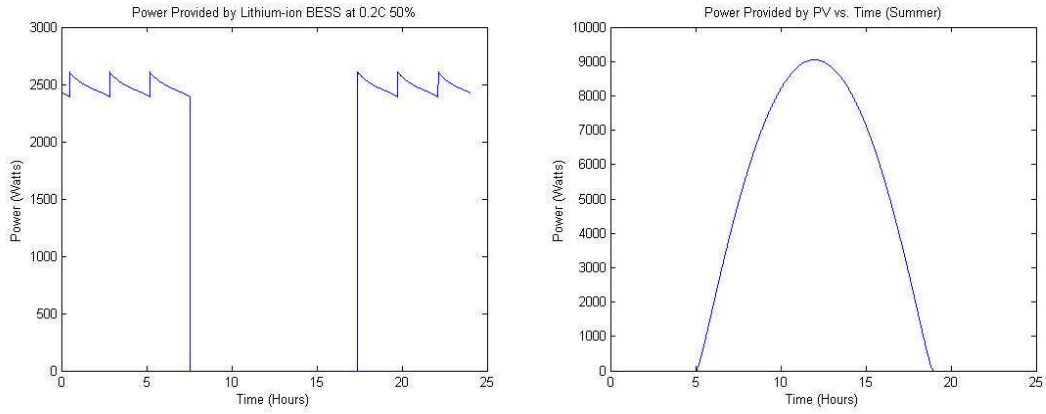

Figure 80: Power provided by system a). BESS b). PV

Power required

The power required is displayed in the following Figure 81.

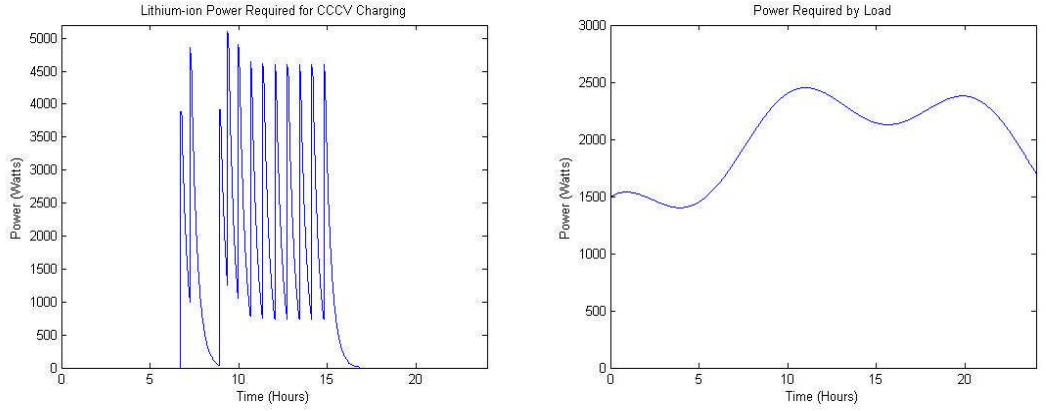

Figure 81: Power required by system a). BESS b). Load

Power additional

The power required (blue) and provided (green) is displayed in the following Figure 82.

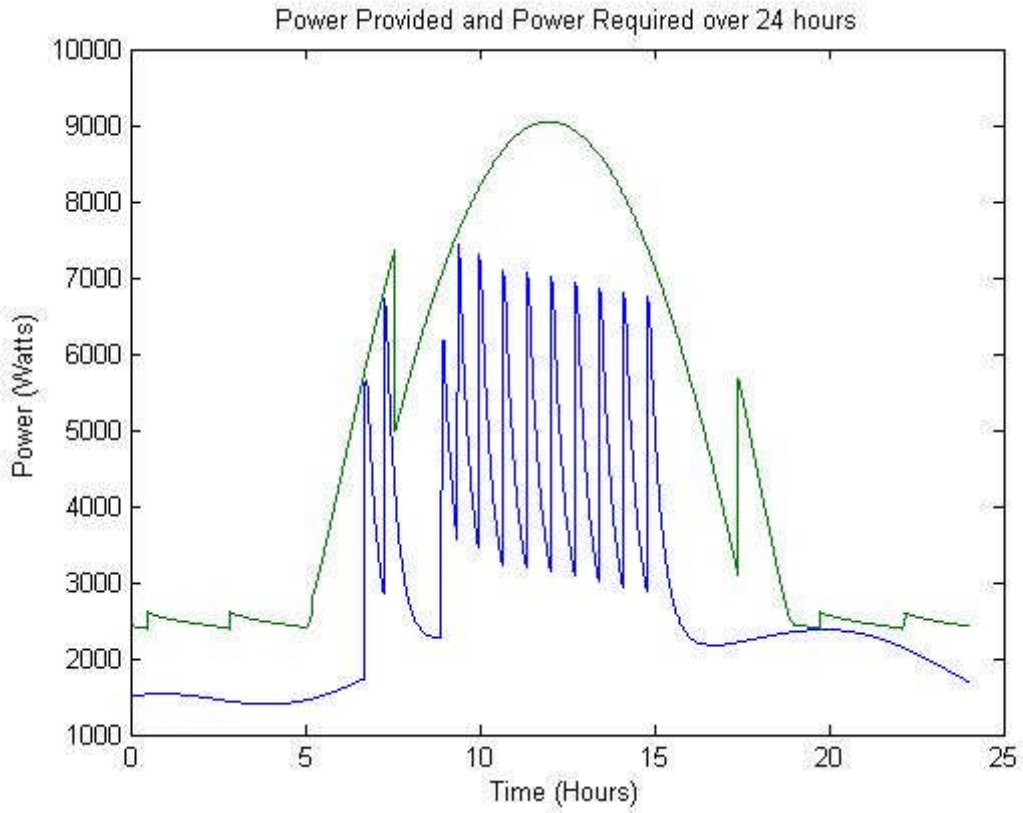

Figure 82: Power provided and power required over 24 hours

The additional power is represented by Figure 83.

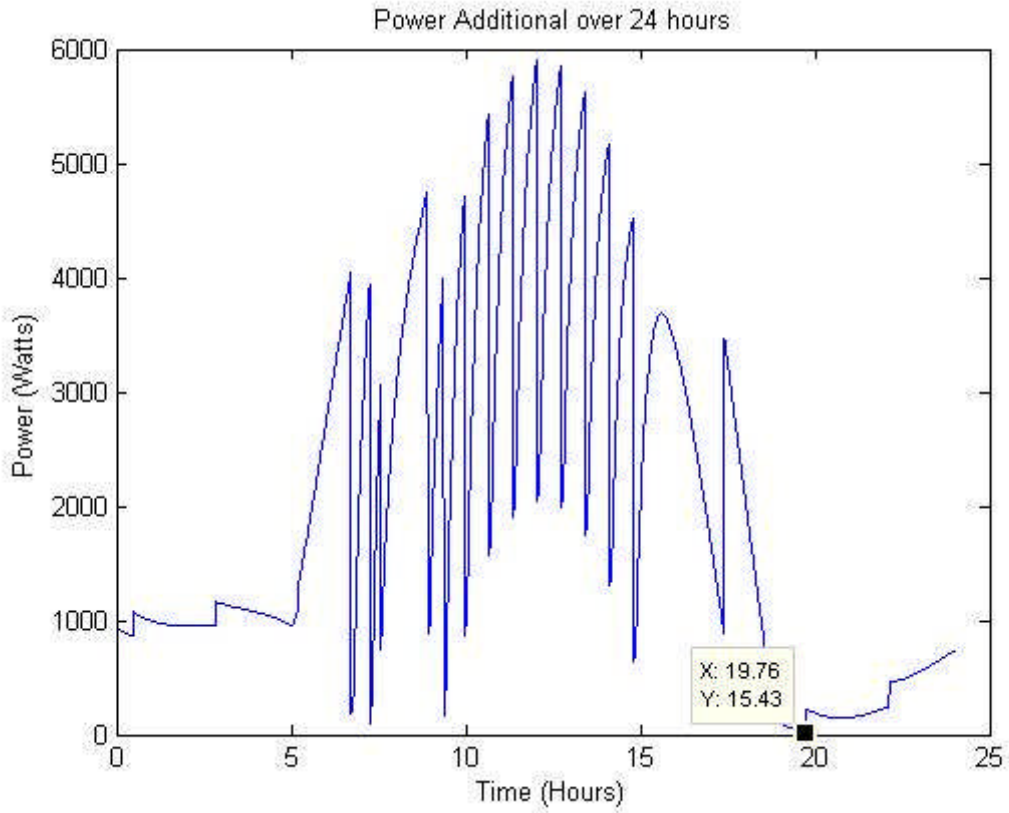

Figure 83: Additional power provided over 24 hours

As can be seen from the above figures, the provided power by the system is always greater than the required power by the system. The minimum amount for the additional power is seen to be 15.43 W at 19h46. This is 46 minutes after the PV is providing no power and falls on a secondary load peak.

The PV system with the dedicated BESS can supply the load over 24 hours and still have additional power to sell to the grid.

6 Conclusions

The aim of this thesis was to provide insight into the modelling and simulation of a stand-alone photovoltaic system with dedicated hybrid battery energy storage system. The thesis produce results for the output voltage, current and power of the PV module and the BESS. Provided power by the PV and the BESS and required power by the BESS and the load were also provided. Models were developed for each element of the stand-alone system. These models are suitable tools for further PV system and dedicated BESS supplied studies.

Each of the components was validated to theory and has concluded the following remarks.

6.1 *Photovoltaic Model*

The Double-Exponential Model proved to be the most accurate and efficient PV cell model over the various reviewed cell models.

The developed PV model reflected properly the I-V and P-V characteristics of a photovoltaic module. It was able to take into account variances in the environmental variable such as temperature and irradiance. This was found to be useful as datasheets only predict expected performance under standard test conditions (STC).

The effect of series and parallel connections of cells to form PV modules was investigated and proved. The model did not take into account the temperature of the cell; it just used the environment temperature.

The model was implemented in Matlab but was thought to be a general model for PV simulations. The results obtained from the model were very satisfying and proved to be an accurate simulation of a real PV module.

It can be concluded that this work can be used as a practical design guide for stand-alone solar electricity systems.

6.2 *MPPT model*

The MPPT model that was developed performed a search for the MPP and outputted the values of power, voltage and current at this point. It worked well for all values of the PV module that were inserted into it.

It was found to be a much simpler and quicker alternative to the initial perturb-and-observe technique. It utilized the maximum power indexing technique.

6.3 *Battery model*

The BESS was modelled for three different chemistry types. The most popular and readily available chemistries, namely lead-acid, nickel-cadmium and lithium-ion were investigated.

The battery was initially developed as a Kinetic Battery Model (KiBaM), but due to its complexity of intricate internal characteristics of the cell, another model was developed. This was due to the fact that the work performed in this thesis did not require intricate internal characteristics in order to produce the desired BESS results.

The model developed for this thesis provided phenomenological results such as the charge and discharge characteristic voltage, power and currents as well as examining the depth of discharge and C-rates for these characteristics.

Forming a battery bank or module out of series- and parallel-connected cells was investigated and validated on the obtained results. Instantaneous and cumulative power provided by the different batteries was investigated for different chemistries and size modules.

The BESS is termed a hybrid system due to the inclusion of the super-capacitor model. The model of the super-capacitor was found to be accurate. This allowed short term high currents to be provided by the super-capacitor instead of the battery bank, allowing the battery bank to solely provide the load demand and negating the increased destruction of the battery bank associated with high start-up currents.

When compared to manufacturer's results, the model was found to produce very accurate and satisfying results. The lithium-ion chemistry was found to exhibit the best characteristics for this application shortly followed by the nickel-cadmium chemistry and as the ageing lead-acid chemistry produced fair performance results, it was not considered in load simulations due to it being a fading technology.

6.4 *Controller model*

The control logic proposed in this thesis was implemented and found to have satisfying results. It could determine the time at which the BESS would need to be charged and discharged in respect to the load demand and PV power provided. The discharging of the BESS performance of the controller was very successful as it managed to discharge the BESS banks so that power was provided over the whole day. The controller managed to

handle a full charging and discharging cycle for a lithium-ion 0.2C 50% DOD BESS including the PV and load demand. It managed to fully charge and discharge the BESS to predetermined set points and ensuring the load demand is met throughout the day.

6.5 *Load model*

The load profile proposed in this thesis was found to be of a generic form. The profile was modified by scaling it in order to meet the load requirements for the investigations.

Power provided by the PV system and the BESS discharge state was modelled against the power required of the load demand and the BESS charge state. The stand-alone system managed to supply a sufficient amount power and the remaining available power over 24 hours was displayed.

It can be said that the 9kW PV system together with the 2.5kWh BESS can safely supply a 2.4kW load profile demand with excess power available. A peak excess power of almost 6kW is experienced at roughly 12h00 and it is thought that a grid connected stand-alone system of this size would be able to provide this power to the grid for grid peak load levelling.

7 Recommendations

On the basis of the above conclusions the following recommendations are made in order to better the model:

7.1 *Recommendations to improve the PV module model*

7.1.1 Conduct further studies into cell temperature modelling

Research and implement a method for determining the cell temperature from the environment temperature. This will lead to more accurate characteristic results for the PV module.

7.1.2 Increase test data resources

In order for a more accurate simulation of the PV module, test the model against real data as well as more simulated results.

7.2 *Recommendations to improve the MPPT model*

7.2.1 Implement control theory

Control theory will allow for a technique which performs the MPPT in the shortest time and will also have the benefit of having the least oscillations.

7.3 *Recommendations to improve the battery model*

7.3.1 Implement a model that includes intricate internal characteristics

Implementing a physics based model will allow for simulation of the intricate internal characteristics of a BESS. This will allow for more accurate simulation results and the effects of these internal characteristics on output power and charging can be investigated.

7.3.2 Investigate additional battery technologies

An investigation into additional battery technologies and feasibility is also advised in order to determine the optimum sizing of the BESS that yields the best performance at the lowest cost.

7.3.3 Implement the simulation of the voltage source inverter (VSI)

Simulation of the VSI would allow for more accurate results in terms of real world applications and should be considered in future work.

7.4 *Recommendations to improve the controller*

7.4.1 Research protection to be implemented in the controller

Inserting protection methods into the controller will create a longer lasting model. This will prevent damaging voltages and currents from reaching components in the system.

7.5 *Recommendations to include the inverters*

7.5.1 Implement DC-DC converters

The design and inclusion of a DC-DC inverter model will allow for more accurate results in the load studies.

7.5.2 Implement DC-AC inverters

The design and inclusion of a DC-AC inverter will allow for investigations of the AC power provided to loads.

7.6 *Recommendations to improve the load*

7.6.1 Investigate specific load conditions

Investigation of specific loads to be supplied by the stand-alone system will allow for the design and simulation of specific stand-alone systems and their performances.

7.6.2 Investigate peak load levelling capabilities

This will result in the stand-alone system being able to supply excess power to the grid for peak load levelling. This also introduces a monetary factor and feasibility can be studied. An investigation concerning the cost of the stand-alone system operation opposed to the earnings of the stand-alone system can determine whether the system is a more feasible option opposed to grid provided power.

7.7 *Recommendations to improve the practicality and implementation of the system*

Further work is urged to include greater considerations into the practical application of the system. Implementing the system to be supplied on practical industry voltages will allow for a better understanding of the system operation in a real-world environment. This would include implementing a voltage source inverter (VSI) in place of the current source inverter (CSI) as it is seen to be more practical approach.

8 references

[1] J. Li, H. Wang, "A Novel Stand-alone PV Generation System Based on Variable Step Size INC MPPT and SVPWM Control," *IEEE, 2009*

[2] M.G. Villalva, J.R. Gazoli, E.R. Filho, "Comprehensive Approach to Modelling and Simulation of Photovoltaic Arrays," *IEEE Transactions on Power Electronics, vol. 24, no. 5, 2009*

[3] A. Jager-Waldau, "Photovoltaics and Renewable Energies in Europe," *European Commision, Renewable Energy Unit,2005*

[4] J.H. So, Y.S. Jung, G.J. Yu, J.Y. Choi, J.H. Choi, "Performance Results and Analysis of 3kW Grid-connected PV Systems, *"Renewable Energy 32, pp. 1858-1872, 2007*

[5] L. Mendez, L. Narvarte, A.G. Marsinach, P. Izquierdo, L.M. Carrasco, R. Eyras, "Centralized Stand Alone PV System in Micro Grid In Morocco," *3rd World Conference on Photovoltaic Energy Conversion, 2003*

[6] R. Chenni, M. Makhlouf, T. Kerbache, A. Bouzid, "A Detailed Modelling Method for Photovoltaic Cells," *Energy 32, pp. 1724-1730, 2007*

[7] A.D. Hansen, P. Sorenson, L.H. Hansen, H. Bindner, "Models For a Stand-alone PV System," *Riso-R-1219(EN), 2001*

[8] D.D. Nguyen, B. Lehman, "Modelling and Simulating of Solar PV Arrays Under Changing Illumination Conditions," *IEEE COMPEL Workshop, 2006*

[9] Y.T. Tan, D.S. Kirschen, N. Jenkins, "A Model of PV Generation Suitable for Stability Analysis," *IEEE Transactions on Energy Conversion, vol. 19, no. 4, 2004*

[10] J.A. Gow, C.D. Manning, "Development of a Model for Photovoltaic Arrays Suitable for Use in Simulation Studies of Solar Energy Conversion Systems," *Power Electronics and Variable Speed Drives, Conference Publication, no. 429, 1996*

[11] K. Nishioka, N. Sakitani, Y. Uraoka, and T. Fuyuki, "Analysis of multi-crystalline silicon solar cells by modified 3-diod equivalent circuit model taking leakage current through periphery into consideration," *Solar Energy Mater. Solar Cells, vol. 91, no. 13, pp. 1222-1227, 2007.*

[12] E. Lorenzo, "Solar Electricity of Photovoltaic Systems," 2004

[13] Bosch el al, "ITE-Boss – A new software tool for photovoltaic system design,"10th European Solar Photovoltaic Energy Conference, 2005

[14] J.F Manwell, J.G McGowan, "Extension of the Kinetic Battery Model for Wind/Hybrid Power Systems," *In Proceedings of EWEC, pp. 284-289, 1994*

[15] J.M Enrique, E. Duran, M. Sidrach-de-Cardona, J.M. Andujar, "Theoretical Assessment of Maximum Power Point Tracking Efficiency of Photovoltaic Facilities with Different Converter Topologies," *Solar Energy, vol. 81, pp. 31-38, 2007*

[16] D.P. Hohm, M.E Ropp, "Comparative Study of Maximum Power Point Tracking Algorithms Using an Experimental, Programmable, Maximum Power Point Tracking Test Bed," *Photovoltaic Specialist Conference, 2000. Conference Record of the Twenty-Eighth IEEE, pp. 1699-1702, 2000*

[17] S. Chowdhury, S.P. Chowdhury, G.A. Taylor, Y.H. Song, "Mathematical Modelling and Performance Evaluation of a Stand-alone Polycrystalline PV Plant with MPPT Facility," *IEEE*

[18] N. Veissid, A.M Andrade, "The I/V Silicon Solar Cell Characteristic Temperature Dependence – An Experimental Study Using the Standard Deviation Method," *10th European Photovoltaic Solar Energy Conference, 1991.*

[19] *http://solarfornow.com/images/diagram_solar_power.gif*

[20] M.G Villalva, J.R Gazoli, E.R Filho, "Comprehensive Approach to Modelling and Simulation of Photovoltaic Arrays," *IEEE Transactions on Power Electronics, vol. 24, no. 5, 2009.*

[21] I. Papic, "Simulation Model for Discharging a Lead-Acid Battery Energy Storage System for Load Leveling," *IEEE Transactions on Energy Conversion, vol. 21, no. 2, 2006.*

[22] M. Dubarry, N. Vuillaume, B.Y Liaw, "From Li-ion Single Cell Model to Battery Pack Simulation," *17th IEEE International Conference on Control Applications, 2008.*

[23] L. Gao, S. Liu, R.A. Dougal, "Dynamic Lithium-Ion Battery Model for System Simulation," *IEEE Transactions on Components and Packing Technologies, vol. 25, no. 3, 2002.*

[24] S. Buller, M. Thele, R. W De Doncker, E. Karden, "Impedance-Based Simulation Models of Super-capacitors and Li-ion Batteries for Power Electronic Applications," *IEEE Transactions of Industry Applications, vol. 41, no. 3,2005.*

[25] S. X Chen, K. J Tseng, S. S Choi, "Modeling of Lithium-Ion Battery for Energy Storage System Simulation," *IEEE Power & Energy Society (PES).*

[26] D. Linden, A.J. Salkind, A.G Cannone,"Battery Handbook," *Digital Engineering Library, McGraw-Hill, 2004.*

[27] N. K Medora, A. Kusko, "An Enhanced Dynamic Battery Model of Lead-Acid Batteries Using Manufacturer's Data," *IEEE, vol. 21, no. 1.*

[28] M. E Glavin, P. K Chan, S. Armstrong, W. G Hurley, "A Stand-alone Photovoltaic Super-capacitor Battery Hybrid Energy Storage System," *IEEE, 2008.*

[29] C. J Rydh, B. A Sanden, "Energy Analysis of Batteries in Photovoltaic Systems. Part I: Performance and Energy Requirements," *Science Direct, Energy Conversion and Management, no. 46, 2005.*

[30] P. Arun, R. Banerjee, S. Bandyopadhyay, "Optimum Sizing of Photovoltaic Battery Systems Incorporating Uncertainty Through Design Space Approach," *Science Direct, Solar Energy, no. 83, 2009.*